

Drug Research Program
Division of Pharmaceutical Chemistry and Technology
Faculty of Pharmacy
University of Helsinki
Finland

**MINIATURIZED DEVICES FOR REACTION
MONITORING USING ONLINE MASS
SPECTROMETRY AND DEVELOPMENTS
TOWARDS REACTION CONTROL**

Sofia M. E. Nilsson

ACADEMIC DISSERTATION

To be presented, with the permission of the Faculty of Pharmacy of
the University of Helsinki, for public examination in Auditorium 1041,
Viikki Biocenter 2, on 29 November 2019, at 12 noon.

Helsinki 2019

© Sofia Nilsson

ISBN 978-951-51-5674-7 (paperback)

ISBN 978-951-51-5675-4 (PDF, <http://ethesis.helsinki.fi>)

Unigrafia, Helsinki, Finland 2019

Published in the DSHealth series '*Dissertationes Scholae Doctoralis Ad Sanitatem Investigandam Universitatis Helsinkiensis*'

ISSN 2342-3161 (paperback); ISSN 2342-317X (PDF)

The Faculty of Pharmacy (University of Helsinki) uses the Urkund system (plagiarism recognition) to examine all doctoral dissertations.

Supervisors

Professor Tapio Kotiaho
Drug Research Program
Division of Pharmaceutical
Chemistry and Technology
Faculty of Pharmacy
and
Department of Chemistry
Faculty of Science
University of Helsinki
Finland

Professor Jari Yli-Kauhaluoma
Drug Research Program
Division of Pharmaceutical
Chemistry and Technology
Faculty of Pharmacy
University of Helsinki
Finland

Dr. Gustav Boije af Gennäs
Drug Research Program
Division of Pharmaceutical
Chemistry and Technology
Faculty of Pharmacy
University of Helsinki
Finland

Professor Sami Franssila
Department of Chemistry and Materials Science
Aalto University
Finland

Reviewers

Professor Carita Kvarnström
Materials Chemistry group
University of Turku
Finland

Professor Sabeth Verpoorte
Faculty of Science and Engineering
University of Groningen
The Netherlands

Opponent

Professor Åsa Emmer
Department of Chemistry
KTH Royal Institute of Technology
Sweden

ABSTRACT

Understanding the mechanism of chemical reactions brings possibilities to optimization of reaction conditions to e.g. improving the yield of reaction product(s), modification of reaction conditions to become more environmentally friendly, or steering the reaction outcome towards certain products. Microreactors coupled online to mass spectrometric detection provide a system highly suitable for mechanistic studies, enabling sensitive, selective, and rapid detection of often small amounts of samples. By combining the information obtained with this experimental system with theoretical density functional theory investigations of the potential energy surface of the system, detailed information about the mechanism of a reaction can be obtained. On the other hand, molecularly imprinted polymers are useful tools for facilitating chemo-, regio-, or stereoselective synthesis. This is achieved by formation of cavities within the polymer matrix, which are able to stabilize the transition state of the desired reaction.

In this thesis, three different miniaturized reactors fabricated with additive manufacturing were combined online with electrospray ionization mass spectrometry for monitoring chemical reactions (Studies I-IV). The different miniaturized reactors were found to be variably suitable for this task. Overall, three different reactions were studied using miniaturized reactors coupled to a mass spectrometer – an inverse electron-demand Diels-Alder, followed by a retro Diels-Alder reaction (Studies I and II), an oxidation of a heptafulvene into the corresponding tropone by *meta*-chloroperoxybenzoic acid (Study III), and an acetylation reaction yielding the antibiotic drug linezolid (Study IV). Identification of reaction species was aided by e.g. MSⁿ experiments, fragmentation schemes, the detected ions' relative intensities at different reaction times, and accurate mass spectrometry measurements. The online mass spectrometry results obtained for the heptafulvene oxidation reaction were furthermore used as a basis for density functional theory studies of said reaction (Study III). Nine reaction pathways were investigated. The key step of the mechanism with the lowest energy barrier for oxidation of the studied heptafulvene into its corresponding tropone was identified as a Criegee-like rearrangement, while the overall reaction follows a Hock-like mechanism.

Furthermore, highly porous molecularly imprinted polymer systems, which in flow injection quartz crystal microbalance studies exhibited enantioselectivity for a proposed transition state analogue of a transamination reaction, were developed and assessed (Study V). The molecularly imprinted systems prepared with *n*-heptane as porogen, and polystyrene beads, which, when extracted out, formed pores in the polymers that were imprinted with a molecule having either a D- or L-conformation of a proposed transition state analogue of a transaminase reaction, showed a clear selectivity for the transition state analogue enantiomer that they were imprinted with in flow

injection quartz crystal microbalance studies. Otherwise these systems exhibited similar selectivity for the other analytes screened.

The results presented in this thesis demonstrate that online combination of additively manufactured miniaturized reactors and mass spectrometry provides a convenient system for monitoring reactions online. At the same time, the results highlight limitations of the system such as memory effects arising from rough surfaces of the miniaturized reactors in combination with (from a mass spectrometry viewpoint) high concentrations of reactants used. However, the results from the oxidation study show that combinations of several methods can aid in overcoming limitations that one single approach may present. Finally, the developed hyperporous molecularly imprinted systems for enantioselective transamination reaction are promising for introduction into miniaturized reactors in the future.

ACKNOWLEDGEMENTS

First and foremost, my sincere gratitude is owed to my supervisors who have guided and directed this thesis and the research it is based on. I am very grateful to my main supervisor Tapio Kotiaho for accepting me as a doctoral candidate, and for transferring his comprehensive skills in mass spectrometry. My gratitude to my co-supervisors Gustav Boije af Gennäs and Jari Yli-Kauhaloma goes even further back in time than my time as a doctoral student; The fact that you accepted me as a project student in your research project during my master's studies both contributed to spark my interest for research, as well as helped to integrate me into the community of the Division of Pharmaceutical Chemistry and Technology at the University of Helsinki. I am thankful to my co-supervisor Sami Franssila, who during my years as doctoral student repeatedly provided useful input on my research from a microfluidics perspective.

Furthermore, I am grateful to a number of funding entities for allowing me to live not merely on air and grit while pursuing my doctoral degree, as well as for enabling me to participate in a number of interesting conferences and schools all over the world. The organizations which provided me funding include the Academy of Finland, the Doctoral Program in Drug Research (University of Helsinki), Magnus Ehrnrooth's foundation, the Finnish Cultural Foundation, the Kordelin Foundation (Gust. Komppa division), the Finnish Pharmaceutical Society, the Swedish Cultural Foundation in Finland, FinPharma Doctoral Program, Oscar Öflunds stiftelse, the Finnish Mass Spectrometry Foundation, the Brazilian Mass Spectrometry Society, and the International Mass Spectrometry Foundation.

Many bright minds, in addition to the ones mentioned above, were involved in the research presented in this thesis. Three engineers are extra noteworthy: the microfluidics experts Gianmario Scotti and Ville Jokinen, and Markus Haapala - who can render anything from chilli to a microfluidic set-up to be palatable. The synthesis masterminds Alexandros Kiriazis and Subban Kathiravan are acknowledged for providing me analytes to work with in my experiments. I am grateful to Päivi Pöhö for teaching me how to harness the power that accurate mass spectrometers offer. Jukka Saarinen is acknowledged both for being a pleasant office mate, always ready to discuss music or running, as well as for providing Raman data for one of my publications. Ville-Pekka Matilainen, Anti Salminen, Eran Gal-Or, and Yaniv Gershoni (and once more Gianmario Scotti and Markus Haapala) are kindly acknowledged for fabricating miniaturized reactors for me to utilize in my doctoral research. I am highly grateful to Subramanian (Subbu) Suriyanarayanan and Ian Nicholls for being flexible and accommodating co-operation partners, who allowed me to escape to the picturesque Swedish city of Kalmar for a couple of months during my doctoral studies. Furthermore, I

am very grateful to Subbu for always working with a "can do" mindset and teaching me the practices and theory of quartz crystal theory. Ian, I have very much appreciated your and your family's hospitality during my stays in Kalmar.

In addition to co-authoring one of the publications presented in this thesis, Clare Stachan is warmly acknowledged for acting in my steering group, and offering me support and advice on both research and career matters. Mikael Ehn is also thanked for acting in my steering group and offering me yet another (more physicist oriented) perspective on my research.

Considering later stages of my thesis and doctoral project renders me indebted to my opponent, Åsa Emmer, as well as my pre-examiners Carita Kvarnström and Sabeth Verpoorte for ensuring the scientific standard of my work.

During my time as doctoral student, I was privileged to work at the Division of Pharmaceutical Chemistry and Technology, which in practice meant that friendly and helpful colleagues with great know-how skills always were around and for a chat or support. I especially wish to thank the people I have had lots of exciting adventures with in conferences. Thanks to you, I have survived both being lost in the South Korean mountains during a North Korean attack, discovered mesmerizing spheres in a sphere and tried to (unsuccessfully, as usually...) fish for research results in Dublin, and explored Florence with the best guides possible. Finally, my colleagues and friends Sari and J-P played a crucial role both for making me feel as home in Finland, as well as to help me escape from Finland.

Shifting the focus from Finland, I dearly wish to thank all my friends residing in Sweden – it has always been a blast meeting you, no matter how long time has passed since last time. Specifically, I am grateful to Angie and Tobbe, who tuned my research visits (as well as casual visits) to Sweden into great reunions and outings. Considering people living in Sweden, I also wish to acknowledge Marcia and Dan, who greatly facilitated my master's studies thanks to their hospitality, but more importantly made my stays in Stockholm highly enjoyable. If it weren't for you, I would had been significantly less likely to pursue master's studies, and thus the existence of this PhD thesis would had been considerably less probable.

Moving the focus a bit further South, I am very grateful to my friends Henning (congratulations - you managed to become a PhD before me!) and Wiebke, and (the other) J-P for all enjoyable festival memories, and for keeping me well supplied with cherry mead during my first day at a new job, as well as for explaining the life and world to me (and everyone else...).

Marlene, I am happy to have you as a friend, no matter how geographically afar we are (I am, though, not sure if I am happy that you introduced me to mämmi...).

My dearest, dearest wife Marina, I am eternally grateful to you for so much; thank you for always finding time for me, for supporting me no matter if it concerns a rejected manuscript or post-holiday blues, as well as always being

ready to celebrate any achievement! Also, thank you for daring to (repeatedly!) join me to a festival camping!

Karro, Ida, Mams, Paps, and Farmor, I am happy and grateful to have you as my family. Thank you for always making me feeling close to you and welcome when I visit you, no matter how long it has been since we last met. Thank you for making the effort to keep in touch by letters, parcels with chocolate or tea, and electronically even though I sometimes have been a "thesis hermit". I am furthermore very grateful to have a bonus family on the other side of the Ostsee. I especially wish to express my gratitude to Lilith and Levin for accompanying me to activities as diverse as Wikingertage, zoo visits and running.

Finally I have reached the point which can no longer be avoided; A significant reason that you actually are reading this thesis after all (thus, someone to blame) – Henning. Henning, thank you thousand fold for simply everything. Thank you for accompanying me through this Kafkaesque experience. Thank you for always questioning everything and being so frustratingly logical. Thank you for caring for me, always, even when my pneumonic coughing robbed you of your well needed sleep. Thank you for being prepared to provide me with chocolate (or food in general) when my mood dips (or simply always). Thank you for, after dreaming to go there for years, brought me to Summer Breeze. Thank you for facilitating my fascination for Seehunde. Thank you for never stopping experiencing new things (such as biking 300 km as one race or getting a house) together with me. Thank you for joining me to even Flogsta (and letting me joining you to Kontula). Thank you for being a great co-author. Thank you for putting the idea of pursuing doctoral studies in my head to start with, and then, over and over again throughout the process making me believing that it was (even remotely) possible (...yes, you were eventually right. Again.).

"...Fülle mich mit Leben
Komm und fülle mich mit Dir
Heute will ich mich hingeben
Ich ist tot, es lebe Wir..."

Jopli Wilson

Uppsala, 6th November 2019

CONTENTS

Abstract	4
Acknowledgements.....	6
Contents	9
List of original publications	11
Abbreviations.....	13
1 Introduction	14
2 State-of-the-art	18
2.1 Miniaturized reactors for mass spectrometric online monitoring of chemical reactions	18
2.1.1 Characteristics of electrospray, critical points for integration on miniaturized devices, and use in reaction mechanism studies	30
2.2 Density functional theory combined with mass spectrometry for organic chemistry reaction mechanism studies	32
2.3 Molecularly imprinted polymers and quartz crystal microbalance	34
3 Aims of the study	36
4 Experimental.....	37
4.1 Chemicals and materials	37
4.2 Analytical methods and instrumentation	40
4.3 Miniaturized reactors coupled online to mass spectrometry.....	43
4.3.1 Fabrication of miniaturized reactors.....	43
4.3.2 Reactions studied and experimental designs	45
4.3.2.1 Inverse electron-demand Diels-Alder and subsequent retro Diels-Alder reaction (Studies I and II). 45	

4.3.2.2	<i>meta</i> -Chloroperoxybenzoic acid oxidation of heptafulvenes to tropones (Study III).....	46
4.3.2.3	Acetylation reaction (Study IV).....	47
4.4	Computational details.....	47
4.5	Molecularly imprinted polymers	48
4.5.1	Preparation of molecularly imprinted polymers	48
4.5.2	Quartz crystal microbalance experiments.....	50
5	Results and discussion.....	51
5.1	Coupling of miniaturized devices to mass spectrometry and reaction mechanism studies	51
5.1.1	A 3D printed miniaturized polypropylene reactor and stainless steel reactor for online study of an inverse electron-demand Diels-Alder and retro Diels-Alder reaction	51
5.1.1.1	Identification of reaction-related ions.....	55
5.1.2	A 3D printed miniaturized polypropylene reactor for online study of the <i>meta</i> -chloroperoxybenzoic acid oxidation of a heptafulvene into a tropone and complementary density functional theory investigations	61
5.1.3	A 3D printed miniaturized glass reactor for online study of an acetylation reaction	66
5.2	Comparison of miniaturized reactors and their suitability for coupling to mass spectrometry for reaction monitoring.....	70
5.3	Development of molecularly imprinted polymers for enantioselective transamination	72
6	Summary, assessment of limitations, and outlook.....	77
	References	81

LIST OF ORIGINAL PUBLICATIONS

This thesis is based on the following publications:

- I Gianmario Scotti*, **Sofia M. E. Nilsson***, Markus Haapala, Päivi Pöhö, Gustav Boije af Gennäs, Jari Yli-Kauhaluoma, and Tapio Kotiaho. A miniaturised 3D printed polypropylene reactor for online reaction analysis by mass spectrometry. *React. Chem. Eng.*, 2017, 2, 299-303. DOI: 10.1039/C7RE00015D, and *React. Chem. Eng.*, 2017, 2, 811-811. DOI: 10.1039/C7RE90018J (correction)
- II Gianmario Scotti*, **Sofia M. E. Nilsson***, Ville-Pekka Matilainen, Markus Haapala, Gustav Boije af Gennäs, Jari Yli-Kauhaluoma, Antti Salminen, and Tapio Kotiaho. Simple 3D printed stainless steel microreactors for online mass spectrometric analysis. *Heliyon*, 2019, 5, e02002. DOI: 10.1016/j.heliyon.2019.e02002
- III **Sofia M. E. Nilsson**, Henning Henschel, Gianmario Scotti, Markus Haapala, Alexandros Kiriazis, Gustav Boije af Gennäs, Tapio Kotiaho, and Jari Yli-Kauhaluoma. Mechanism of the Oxidation of Heptafulvenes to Tropones Studied by Online Mass Spectrometry and Density Functional Theory Calculations. *J. Org. Chem.* 2019, 84, 13975–13982. DOI: 10.1021/acs.joc.9b02078
- IV Eran Gal-Or, Yaniv Gershoni, Gianmario Scotti, **Sofia M. E. Nilsson**, Jukka Saarinen, Ville Jokinen, Clare J. Strachan, Gustav Boije af Gennäs, Jari Yli-Kauhaluoma, and Tapio Kotiaho. Chemical analysis using 3D printed glass microfluidics. *Anal. Methods*, 2019, 11, 1802-1810. DOI: 10.1039/c8ay01934g
- V **Sofia M. E. Nilsson**, Subramanian Suriyanarayanan, Subban Kathiravan, Jari Yli-Kauhaluoma, Tapio Kotiaho, and Ian A. Nicholls. Enantioselective hyperporous molecularly imprinted thin film polymers. *RSC Adv.*, 2019, 9, 33653-33656. DOI: 10.1039/C9RA07425B

These publications are referred to in the text by their Roman numerals and have been reprinted with the permission of their copyright holders. In addition, some unpublished material is presented.

* Equal contributions.

Author's contribution to the above publications:

Publication I

The experimental design for coupling the reactor online to an ion trap MS was outlined by the author, GS, and MH. The reaction and MS conditions were designed by the author. The online ion trap MS experiments were conducted by the author. The accurate mass orbitrap MS measurements were done by the author and PP. The study was planned by all co-authors. The manuscript was written by all co-authors.

Publication II

The experimental set-up for coupling the reactor online to MS was designed by the author, GS, and MH. The reaction and MS conditions were designed by the author. The online microreactor-MS reaction studies were conducted by the author. The study was planned by all co-authors. The manuscript was written by all co-authors.

Publication III

The experimental set-up for coupling the reactor online to MS was designed by the author. The reaction and MS conditions were designed by the author. The online microreactor-MS reaction studies were performed by the author. Novel reaction pathways were suggested by the author and HH. DFT calculations of isolated structures were performed and analyzed by the author with assistance from HH. Structures of molecular complexes and transition states were calculated and analyzed by HH with aid from the author. The study was planned by all co-authors. The manuscript was written by the author with contributions from co-authors.

Publication IV

The interfacing of miniaturized devices with MS, reaction conditions for the MS studies, and MS conditions were designed by the author, as were the offline ion trap and MS experiments and NMR spectroscopy experiment. These experiments were also conducted by the author. The offline quadrupole MS experiments were designed and conducted by the author and GBaG. Characterization of the miniaturized devices was done by the author, GS, and VJ. The study was planned by all co-authors. The manuscript was written by all co-authors.

Publication V

The QCM, borosilicate, and silicon substrates were prepared by the author. The MIP systems were designed by the author, SS, and IAN and prepared by the author. The QCM experiments were conducted by the author. The FTIR experiments were performed by the author and SS. The study was planned by all co-authors. The first draft of the manuscript was prepared by the author, and later versions were written jointly by all co-authors.

ABBREVIATIONS

AIBN	azobisisobutyronitrile
APCI	atmospheric pressure chemical ionization
APPI	atmospheric pressure photo ionization
CAD	computer-aided design
DFT	density functional theory
EGDMA	ethylene glycol dimethacrylate
ESI	electrospray ionization
FDM	fused deposition modeling
FIA	flow injection analysis
FTIR	Fourier transform infrared
HPLC	high-pressure liquid chromatography
HV	high voltage
i.d.	internal diameter
IEFPCM	integral equation formalism polarizable continuum model
IR	infrared
LAM	laser additive manufacturing
LC-MS	liquid chromatography-mass spectrometry
MAA	methacrylic acid
MALDI	matrix-assisted laser desorption/ionization
<i>m</i> CB	<i>meta</i> -chlorobenzoate
<i>m</i> CBA	<i>meta</i> -chlorobenzoic acid
<i>m</i> CPBA	<i>meta</i> -chloroperoxybenzoic acid
MIP	molecularly imprinted polymer
MS	mass spectrometry
MS ⁿ	multiple-stage mass spectrometry
<i>m/z</i>	mass-to-charge ratio
o.d.	outer diameter
PCM	polarizable continuum model
PS	polystyrene
QCM	quartz crystal microbalance
R _a	average roughness
RAFT	reversible addition-fragmentation chain transfer
RMS	root mean square
R _q	root mean square roughness
RSD	relative standard deviation
SEM	scanning electron microscope
S _N 2	bimolecular nucleophilic substitution
TLC	thin-layer chromatography
TS	transition state
TSA	transition state analogue
UV	ultraviolet

1 INTRODUCTION

Improving the yields in synthesis of compounds is a constant goal for both the individual synthetic chemist and companies manufacturing the compounds. By understanding the mechanism through which a reaction progresses, the reaction conditions can be optimized and the chemo-, regio-, and stereoselectivity of the reaction can be controlled to a larger extent, which results in a possibility to maximize the yield of reaction product(s). Improved reaction yields bring less reagent consumption, more streamlined synthesis, and, through this, production of less waste in the process. When the reaction mechanism is understood, it can also be possible to modify the reaction conditions to become more environmentally friendly without compromising the yield of the reaction. In order to determine a reaction mechanism, it is necessary to find and identify the intermediates of the reaction. A good experimental method to obtain this knowledge is to use microreactors with online mass spectrometric (MS) detection^[1].

Microreactors (also called microchips) are miniaturized systems, typically having reactor channel dimensions narrower than 1 mm^[2], wherein numerous functional components (e.g. catalytic surfaces, mixing structures, heating)^[3] can be integrated. Integration of several functionalities directly on the chip might bring possibilities for automation of the synthesis and work-up procedure, and thus optimization of synthesis may be achieved. Additionally, miniaturized reactors bring a number of other advantages: only small amounts of reactants/samples are required, and they have improved heat transfer and a high surface area to volume ratio compared with macroscale systems.^[4] This brings improved yields and selectivity with respect to reaction products, safer usage of toxic chemicals, increased environmental friendliness, and better control of reactions.^[5] These characteristics and the suitability of microreactors as a platform for conducting reactions in a controlled manner, in combination with synthesis by microreactor methods being highly suitable for scale-up by simply using several microreactors in parallel^[6], make development and use of microreactors highly attractive for the pharmaceutical industry and chemists in general. Additionally, microreactors can beneficially be used for high-throughput screening of drug candidates.^[7-9]

MS as a detection method has unsurpassed selectivity (the mass-to-charge, m/z , ratio of the analyte is detected) and sensitivity^[10] with rapid response time^[11] and an applicability on a very broad spectrum of analytes. The possibility to choose from several different ionization techniques makes it easy to find an ionization technique that is optimal for the analytes of interest.^[12] Electrospray ionization (ESI), for example, is suitable for analyzing polar analytes, while atmospheric pressure photo ionization (APPI) and atmospheric pressure chemical ionization (APCI) are ideal for non-polar compounds. By investigating the fragmentation pattern of the analytes, with

tandem and multiple-stage MS (MS^n) analysis, MS gives additional valuable structural information that cannot be obtained with the same sensitivity with other detection methods. As MS furthermore tends to use analyte flow rates that are in the same range ($\mu\text{L}/\text{min}$) as the ones used for miniaturized reactors, these two systems can be easily combined. Furthermore, flow chemistry systems have numerous times been demonstrated to be useful for detecting short-lived reaction intermediates, highly supporting their applicability for reaction mechanism studies.^[13,14] Other detection techniques that have been coupled to miniaturized systems for reaction monitoring include NMR spectroscopy, Raman spectroscopy, ultraviolet (UV)/visible/near infrared (IR) spectroscopy, attenuated total reflectance–Fourier transform IR spectroscopy, and X-ray absorption spectroscopy.^[15] However, as these techniques require analytes to have specific properties (e.g. presence of nuclei with suitable spin characteristics or chromophores), this limits their usefulness relative to MS, which does not require any of these characteristics, but only that the analyte is ionizable.^[10]

The devastating case of thalidomide, a drug frequently used in the 1950s and 1960s against pregnancy sickness, which caused birth abnormalities in tens of thousands of babies due to the drug being administered as a racemic mixture (one of the enantiomers is teratogen),^[16] illustrates the integral importance of chirality and enantioselective synthesis in pharmacology and chemistry. One useful tool for the augmentation of the selectivity of chemical reactions is molecularly imprinted polymers (MIPs). MIPs have historically been useful for improving work-up processes by functioning as a highly selective solid phase in solid-phase extraction.^[17] However, their use in synthetic chemistry has not yet been widely exploited. Nevertheless, MIPs have proven to be useful for obtaining reaction products in a regio^[18–20]-, diastereo^[21]-, and enantioselective^[22–24] manner, as well as in a number of catalytic reactions by producing MIPs with catalytic properties^[22,25,26].

In this work, miniaturized reactors, fabricated with different additively manufacturing (3D printing) techniques, have been coupled to MS detection for studying chemical reactions online. At present, only one study, in addition to the work presented in Studies I^[27], II^[28], III^[29], and IV^[30] in this thesis, has been published using 3D printing for fabricating a miniaturized reactor for coupling to MS for reaction monitoring^[31], demonstrating the novelty of this approach.

The reactions chosen for studying were an inverse electron-demand Diels-Alder and subsequent retro Diels-Alder reaction (Studies I and II), an oxidation of a heptafulvene into the corresponding tropone with *meta*-chloroperoxybenzoic acid (Study III), and an acetylation reaction (Study IV).

The Diels-Alder reaction is one of the most important organic reactions for selective formation of carbon-carbon bonds.^[32] The reaction concertedly forms two carbon-carbon bonds through a cyclic transition state, and involves a conjugated electron-rich diene, which typically reacts with an electron-poor alkene (dienophile), to form a cyclohexene-like structure.^[33] However, the

corresponding reaction may also occur when the diene is electron-poor and the dienophile electron-rich, as is the case in the reaction studied in Studies I and II. This reaction is called an inverse electron-demand Diels–Alder reaction, and the formed cycloadduct subsequently participates in a retro Diels–Alder reaction, yielding the final reaction product. More specifically, a *trans*-cyclooctene derivative was used as the dienophile in Studies I and II. The rationale behind this is that the double-bond strain of the *trans*-cyclooctene is released during the Diels–Alder reaction, which makes the reaction energetically favored and rapid^[34]. As a consequence, the reaction can be expected to be fast enough, even at relatively low reactant concentrations, to be conducted in microreactor systems that typically entail short reaction times. Furthermore, in the second step of the reaction, elemental nitrogen is eliminated from the system, making the reaction essentially irreversible, which eliminates any possible ambiguity that may arise when approaching equilibrium.

Some tropones and troponoid compounds are medicinally relevant owing to their anti-cancer effects^[35,36], antimicrobial properties^[37,38], and antifungal activities^[39]. Chemically, the oxidation of the *exo*-cyclic double bond of a heptafulvene by *meta*-chloroperoxybenzoic acid (*m*CPBA) is an unusually mild method to form a troponone structure^[40]. The *m*CPBA-mediated oxidation of a heptafulvene resembling the one investigated in this work has previously been studied offline using a micropillar array electrospray set-up.^[41] In this work (Study III), the study of *m*CPBA-initiated oxidation of heptafulvenes to yield tropones is taken further by investigating the reaction continuously over a longer time with a miniaturized reactor coupled online to MS, allowing concentration profiles of the reaction species to be obtained, and complementing the experimental studies with theoretical density functional theory (DFT) calculations.

Synthesis of the antibiotic linezolid (**16**) is of high clinical importance, as it is one of the most powerful last-resort drugs available to treat infections caused by Gram-positive bacteria.^[42,43] A convenient method to obtain linezolid is to allow (5*S*)-5-(aminomethyl)-3-[3-fluoro-4-(4-morpholinyl)phenyl]-1,3-oxazolidin-2-one, also called linezolid-related compound C (**14**), to react with an acylating agent, in the case of Study IV with acetic anhydride (**15**). This reaction has been studied online with MS in Study IV.

In Study V, molecularly imprinted polymer systems for enantioselective synthesis of D- and L-phenylalanine, respectively, were developed and investigated with Fourier transform infrared (FTIR) spectroscopy, scanning electron microscopy (SEM), and quartz crystal microbalance (QCM). In the flow injection analysis (FIA)-QCM experiments, it was noted that the polymer imprinted with the L-TSA exhibited a selectivity for L-TSA over the D-TSA, while the polymer imprinted with D-TSA showed the corresponding selectivity for D-TSA over L-TSA. Otherwise, these two polymers demonstrated similar selectivities for the other analytes screened. Additionally, the effect of a

porogen (*n*-heptane) and polystyrene (PS) beads (to form pores when extracted out) on the polymers was investigated.

2 STATE-OF-THE-ART

This section reviews the state-of-the-art of miniaturized reactors coupled online to MS detection, the principle of ESI, and relevant aspects of the ionization technique with regard to integration on miniaturized devices and use in MS-reaction monitoring, and use of density functional theory (DFT) in combination with MS for investigating organic reaction mechanisms. It continues by describing the theory behind MIPs, presents techniques for preparing them, and details their usefulness to date. Additionally, the use of QCM technology in evaluation of MIP performance is covered.

2.1 MINIATURIZED REACTORS FOR MASS SPECTROMETRIC ONLINE MONITORING OF CHEMICAL REACTIONS

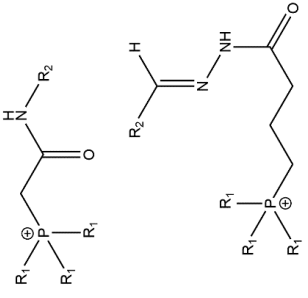
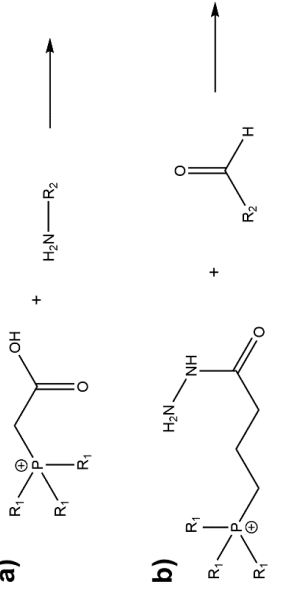
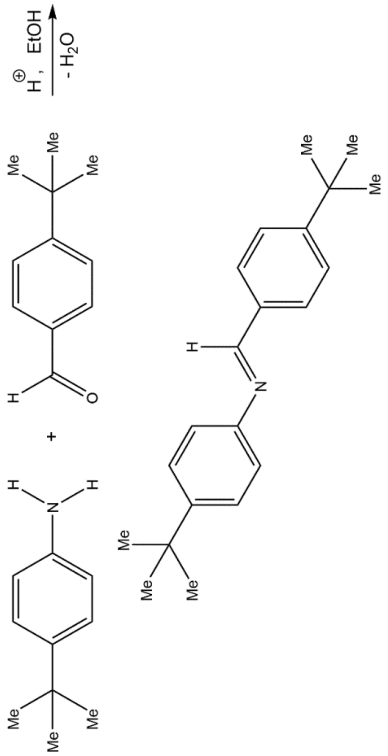
Encouraged by the advantages (outlined in Ch. 1) that miniaturized reactor systems coupled online to MS detection bring and the suitability of these systems for reaction monitoring, efforts have been made to use this set-up for examining various organic reactions^[1,44]. Also microfluidic droplets can in principle be considered as microreactors, in their most minimalistic form, and microdroplet-generating systems have been interfaced with mass spectrometry for monitoring synthetic^[45,46], as well as bio^[47]-chemical reactions. Other fluidic systems, consisting of a T-junction or a tubular coil, coupled directly to a commercial ionization source have been described as “microreactors”^[1] (see Table 1 for an overview of original publications describing organic reactions studied with miniaturized devices coupled to MS), and provide some of the benefits associated with miniaturized systems (high surface-to-volume ratio and possibilities for automatization) and online detection.

Noteworthy examples of more conventional miniaturized reactors (microchips) coupled to MS include immobilized enzyme reactors for studying (the kinetics of) enzymatic reactions^[48] and proteomics reactions^[49], and microfluidic electrochemical cells for conducting electrochemical reactions online^[50]. Miniaturized reactors (microchips) have also been coupled to MS for monitoring a number of organic reactions.^[1] A summary of organic reactions, studied with miniaturized devices (reactors, T-junction systems, or tubular coils) coupled directly to MS is given in Table 1. Based on the results summarized in Table 1, the systems consisting of T-junctions or tubular coils coupled online to MS seem to be efficient for obtaining new information about reaction mechanisms. For example, previously undetected reaction intermediates have been observed using T-junctions coupled to MS^[51–56], which in some cases has provided support for a previously suggested

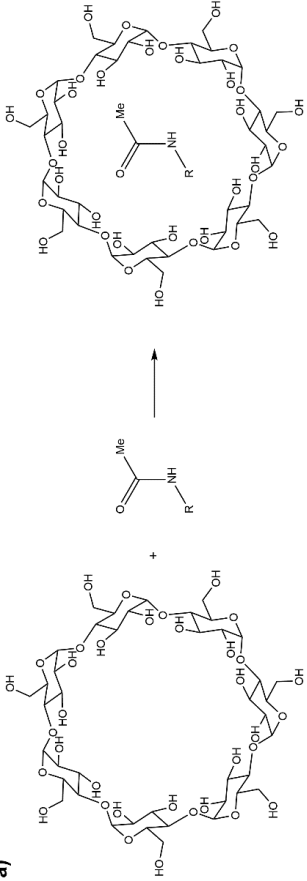
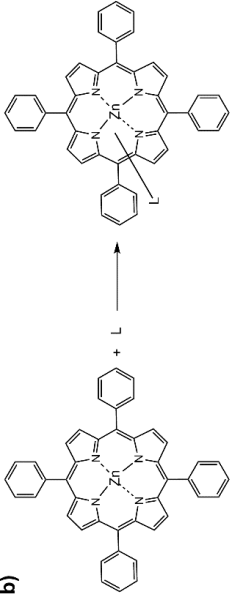
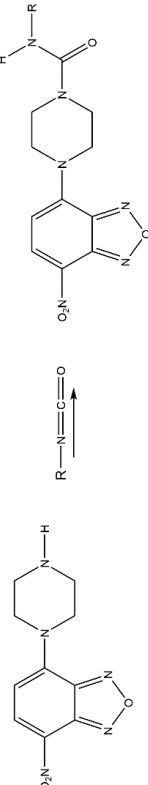
mechanism, while in other cases has allowed previously discussed mechanisms to be discarded. Concerning tubular coils coupled online to MS, the automatization that these systems enable has been used for optimizing reaction conditions in terms of temperature, concentration of reactants, and reaction time.^[57,58] When it comes to miniaturized reactors interfaced with MS, most of the studies presenting miniaturized reactors coupled online to MS have typically been used for a proof-of-concept type reaction, for investigating the suitability of the experimental system. However, the observation of a key reaction intermediate provided support for the proposed mechanism of a Prins-type cyclization^[59], and this experimental system has been used to study the kinetics of various reactions^[60,61]. Thus, the advantages of combining miniaturized reactors online with MS for reaction studies presented in Ch. 1 seem to not have yet been fully realized. However, as the advantages of miniaturized systems coupled online to MS that are translatable to T-junctions or tubular coils have been efficiently exploited for reaction studies, this indicates that the use of miniaturized reactors coupled to MS for reaction studies might emerge in the future when the system has become more established.

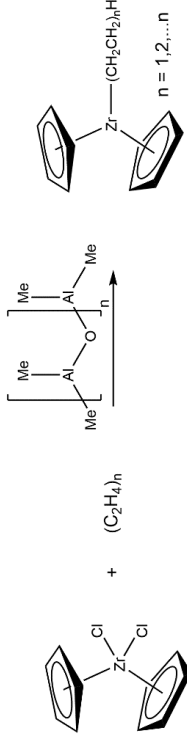
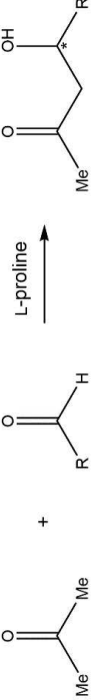
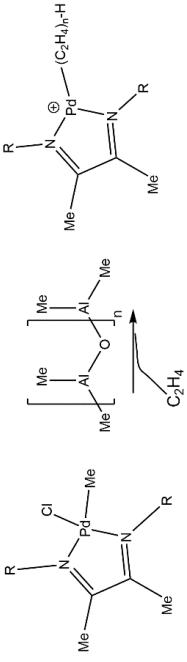
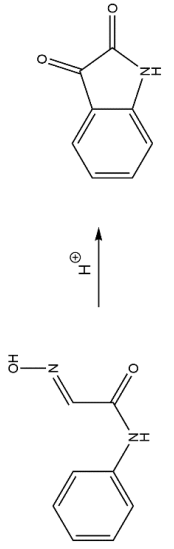
Table 1 Organic reactions studied with miniaturized devices coupled online to MS detection.

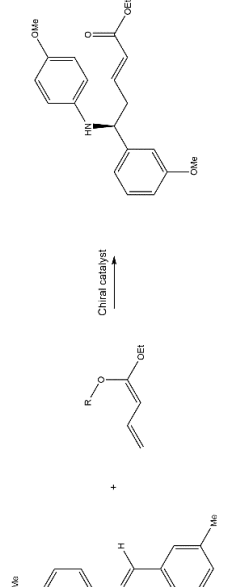
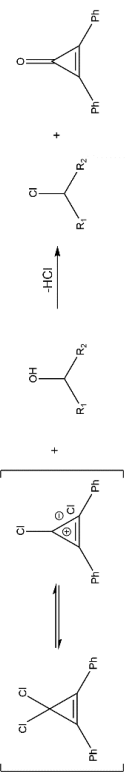
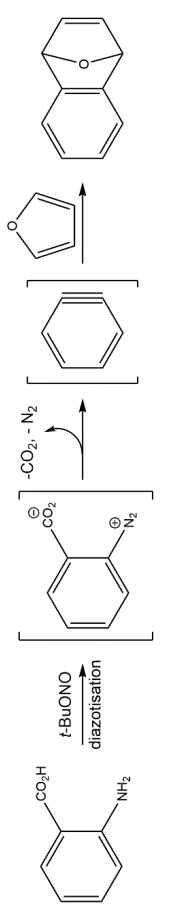
Reaction name	Reaction scheme showing the most important components of the reaction	Miniaturized device	Ionization technique	Year
Reaction of Fe(III)-bleomycin with iodossylbenzene		T-junction coupled to a commercial ion source	ESI	1995 ^[62]
Subreactions of the Ugi multicomponent reaction		Glass silicon microreactor coupled to a commercial ion source	ESI	2001 ^[63]
Lactam hydrolysis		T-junction coupled to a commercial ion source	ESI	2001 ^[64]

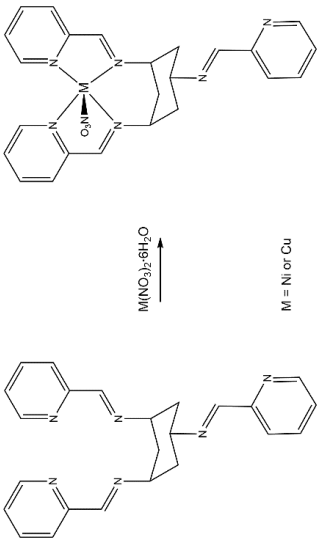
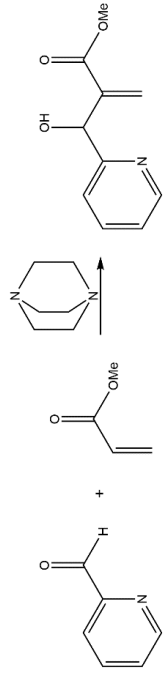
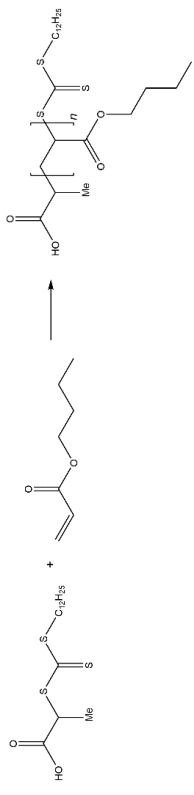
<p>Amide (a) and imine (b) formation</p>	<p>a)</p>  <p>b)</p> 	<p>Glass microreactor coupled to a commercial ion source</p>	<p>ESI</p>	<p>2002^[65]</p>
<p>Schiff base formation</p>		<p>Glass silicon microreactor interfaced with a commercial MALDI source (within the vacuum chamber)</p>	<p>MALDI</p>	<p>2002^[66] and 2005^[67]</p>

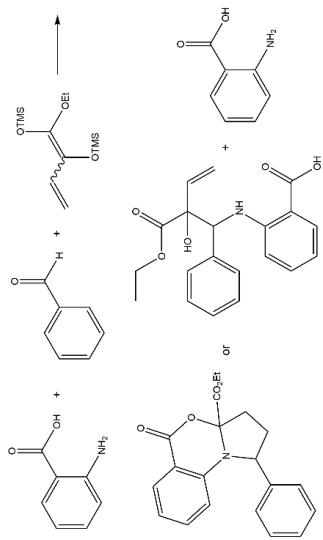
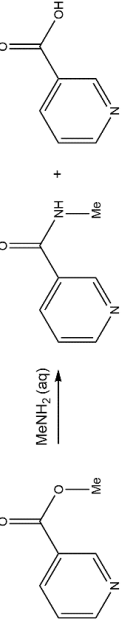
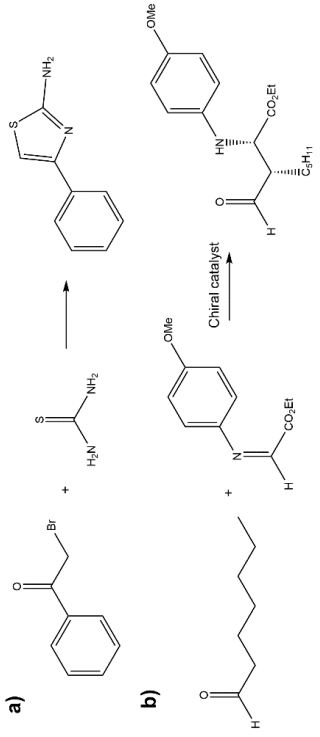
<p>[2+2] cycloaddition</p>		<p>T-junction coupled to a commercial ion source</p>	<p>APCI and ESI</p>	<p>2003^[51,52]</p>
<p>Electron transfer-initiated Diels-Alder</p>		<p>T-junction coupled to a commercial ion source</p>	<p>APCI and ESI</p>	<p>2004^[53]</p>

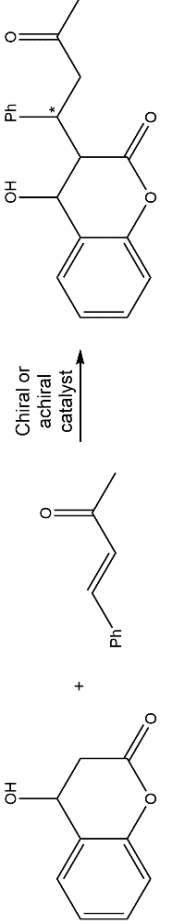
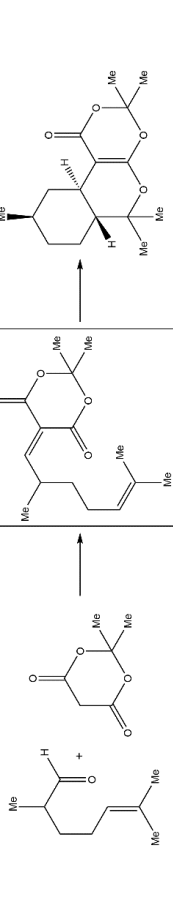
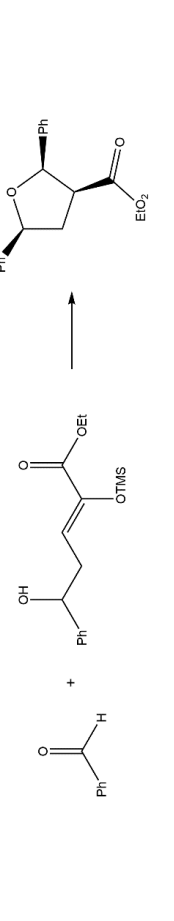
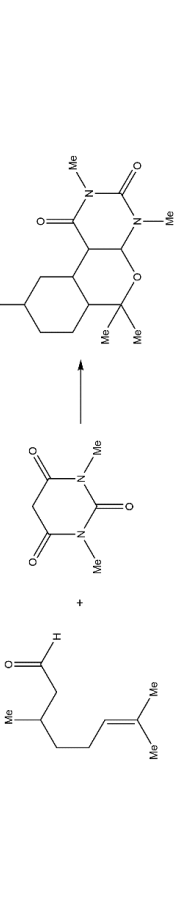
<p>Complexation of β-cyclodextrin and small molecules (a) and (b) coordination of Zn-porphyrin and nitrogen-containing heterocyclic ligands (L in scheme)</p>	<p>a)</p>  <p>b)</p> 	<p>Glass microreactor with integrated nano-ESI needle</p>	<p>ESI</p>	<p>2005^[65]</p>
<p>Urea formation</p>		<p>Glass microreactor with integrated nano-ESI needle</p>	<p>ESI</p>	<p>2005^[60]</p>

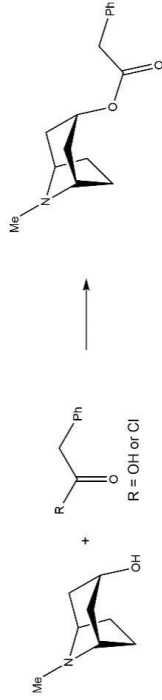
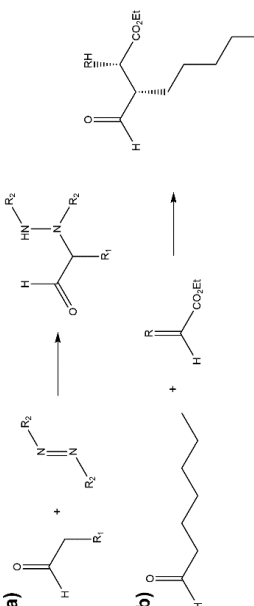
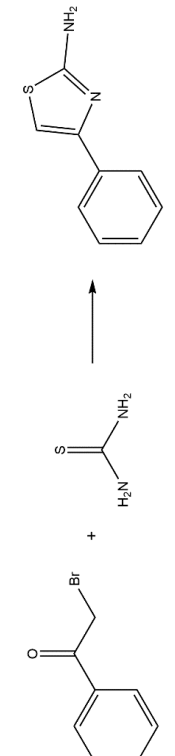
<p>Ziegler-Natta polymerization</p>		<p>T-junction coupled to a commercial ion source</p>	<p>ESI</p>	<p>2006^[54]</p>
<p>L-proline catalyzed aldol reaction</p>		<p>T-junction coupled to a commercial ion source</p>	<p>ESI</p>	<p>2006^[55]</p>
<p>Brookhart polymerization</p>		<p>T-junction coupled to a commercial ion source</p>	<p>ESI</p>	<p>2008^[59]</p>
<p>Sandmeyer cyclization</p>		<p>T-junction coupled to a commercial ion source</p>	<p>ESI</p>	<p>2011^[60]</p>

<p>Mannich reaction</p>		<p>Glass microreactor with integrated nano-ESI needle</p>	<p>ESI</p>	<p>2011^[70]</p>
<p>Chlorination</p>		<p>T-junction coupled to a commercial ion source</p>	<p>ESI</p>	<p>2011^[71]</p>
<p>Diels-Alder reaction, benzyne as a dienophile</p>		<p>Tubular coil coupled to a commercial ion source</p>	<p>ESI</p>	<p>2012^[57]</p>

<p>Complexation of <i>cis,trans</i>-1,3,5-tris[pyridin-2-ylmethylene]cyclohexane-1,3,5-triamine and metal-salt complexes</p>		<p>3D printed reactor coupled to a commercial ion source</p>	<p>ESI</p>	<p>2013^[31]</p>
<p>Morita-Baylis-Hillman reaction</p>		<p>Polyimide glass digital microfluidics device with folded integrated nano-ESI needle</p>	<p>ESI</p>	<p>2013^[72]</p>
<p>Reversible addition-fragmentation chain transfer (RAFT) polymerization</p>		<p>Glass microreactor coupled to a commercial ion source</p>	<p>ESI</p>	<p>2015^[73]</p>

<p>Multicomponent [3+2]-cycloannulation</p>		<p>Glass microreactor with integrated nano-ESI needle</p>	<p>ESI</p>	<p>2015^[74]</p>
<p>Amide formation</p>		<p>Tubular coil coupled to a commercial ion source</p>	<p>APCI</p>	<p>2016^[68]</p>
<p>Hantzsch cyclization (a) and Mannich reaction (b)</p>		<p>Glass-polymer microreactor with integrated nano-ESI needle</p>	<p>ESI</p>	<p>2016^[75]</p>

<p>Michael reaction</p>	 <p>Chiral or achiral catalyst</p>	<p>Glass microreactor with integrated corner ESI emitter</p>	<p>ESI</p>	<p>2016^[76]</p>
<p>Knoevenagel condensation followed by intramolecular hetero-Diels-Alder reaction</p>		<p>Glass microreactor with integrated corner ESI emitter</p>	<p>ESI</p>	<p>2017^[61]</p>
<p>Vinyllogous aldol reaction and subsequent Prins-type cyclization</p>		<p>Glass microreactor with integrated corner ESI emitter</p>	<p>ESI</p>	<p>2017^[69]</p>
<p>Knoevenagel condensation followed by intramolecular hetero-Diels-Alder reaction</p>		<p>PDMS microreactor with integrated nano-ESI needle</p>	<p>ESI</p>	<p>2017^[71]</p>

<p>Acylation</p>		<p>Glass microreactor coupled to a commercial ion source</p>	<p>ESI</p>	<p>2017^[6]</p>
<p>Hydrazination (a) and Mannich (b) reaction</p>		<p>Glass microreactor with integrated corner ESI emitter</p>	<p>ESI</p>	<p>2018^[7]</p>
<p>Hantzsch cyclization</p>		<p>Glass microreactor with integrated corner ESI emitter</p>	<p>ESI</p>	<p>2019^[9]</p>

2.1.1 CHARACTERISTICS OF ELECTROSPRAY, CRITICAL POINTS FOR INTEGRATION ON MINIATURIZED DEVICES, AND USE IN REACTION MECHANISM STUDIES

Based on the current literature (Table 1), ESI seems to be the primary ionization technique when coupling miniaturized reactors to MS for monitoring reactions. The principle of formation of ions from the solvent phase and their transfer to the gas phase in ESI has been thoroughly described^[80,81]. Briefly, by applying a positive charge on a stainless steel needle conducting a liquid with the analyte(s), positively charged ions are formed (so-called positive mode ESI), while negatively charged ions result from when a negative charge is applied on the needle (negative mode ESI). This ionization mechanism of ESI is inherently different from the one of APCI and APPI, where the species already have been transferred to the gas phase before they are ionized by interactions with electrons, protons, or photons or reagent ions from the dopant or solvent^[82]. This process is, compared with the solution phase ionization in ESI, typically a high-energy process. Due to this, ESI is a relatively “soft” ionization technique (i.e. the probability that the analytes’ structure remains intact upon ionization is high)^[83,84]. Keeping this in mind, it is quite intuitive that ESI seems to be the main ionization technique used for analysis of reactions, as the use of a soft ionization technique that enables transfer of reaction species directly from the reaction mixture to the gas phase increases the likelihood that the species observed in the mass spectrum correspond as closely as possible to the ones present in the reaction mixture^[85]. Furthermore, as ESI typically gives the best sensitivity at low flow rates (a few $\mu\text{L}/\text{min}$), while APCI and APPI generally work best at higher flow rates,^[86] this also justifies the use of ESI as the ionization technique when using miniaturized devices for reaction studies.

Another aspect of ESI, attractive to miniaturized devices and reaction monitoring, is the concept of nano-ESI, as first introduced by Wilm and Mann^[87]. Nano-ESI forms ions by the same mechanism as briefly described above for conventional ESI, but here the voltage is applied on a needle, typically made of stainless steel or glass, (having an i.d. of about $1\ \mu\text{m}$) that transfers the solvent containing the analytes, which is interfaced with a grounded MS (or vice versa regarding the voltage configuration). This results in flow rates usually in the range of a few nL/min up to tens of nL/min , which is controlled by the diameter of the stainless steel needle tip and the applied voltage (and if applied, although not necessary for this technique, the magnitude of the backpressure).^[88] An important advantage of nano-ESI is, though, that it does not require external pumping or backpressure to operate.^[87] A difference in the set-up between conventional ESI and nano-ESI is that a nebulizing gas (typically nitrogen) is usually used to mechanically assist the droplet formation in conventional ESI, while this is not included in a nano-ESI set-up.^[89] The low flow rate obtained in nano-ESI both enables

spraying of small sample volumes over longer times and produces smaller droplets, thus enhancing the ionization efficiency^[90]. The former is of direct interest when working with miniaturized devices, as the sample volumes tend to be small in these scenarios.

Other characteristics of ESI relevant when considering its use with miniaturized devices for reaction studies are that, compared with other ionization techniques, it is relatively prone to ion suppression at higher analyte concentrations^[91] (generally $\geq 10^{-3}$ M^[92]) and also to high salt concentrations in the sample and matrix effects^[12]. However, it seems that use of nano-ESI can alleviate the ion suppression typically experienced with ESI^[90]. Finally, it is important to remember that analytes with different chemical properties are ionized with different efficiency, which will affect their intensities in ESI-MS^[93], and due to the ionization mechanism of ESI, electrochemical reactions have been noted to occur in the ionization process^[94-99].

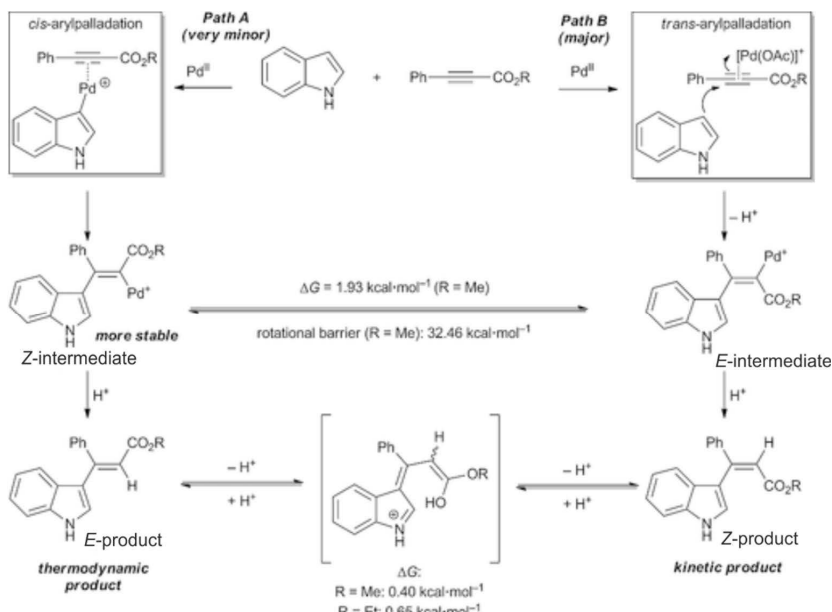
2.2 DENSITY FUNCTIONAL THEORY COMBINED WITH MASS SPECTROMETRY FOR ORGANIC CHEMISTRY REACTION MECHANISM STUDIES

Density functional theory (DFT) is a computational chemistry method that tries to derive the ground state energy of a system from its electron density.^[100] Although it has been shown that this is in principle possible to do exactly,^[101] so far only approximations for a general functional connecting the electron density to the ground state energy have been developed. The electron density of a molecular system can in turn be interpreted in terms of chemical bonds.^[102] With this as a basis, DFT can be used for investigating the potential energy profiles of reaction pathways, and by identifying the reaction mechanism having the lowest energy barrier, the reaction most likely to occur can be proposed.^[100]

When it comes to combining DFT and MS to investigate mechanisms of organic reactions, some examples illustrating its usefulness in various fields of organic chemistry are the Meerwein reaction^[103], the Eberlin reaction^[104], the Biginelli reaction^[105], the Morita-Baylis-Hilman reaction^[106,107], the Dakin-West reaction^[108], hydrogen-mediated coupling of acetylene to carbonyl and imine compounds^[109], coupling of terminal alkynes with carboxylic acids using rhodium catalysis^[110], the Ugi reaction^[111], and Hantzsch and Mannich reactions^[112]. The fact that the Nobel prize in chemistry in 2010 was awarded for palladium-catalyzed cross-coupling reactions^[113] likely contributed to the fact that special effort seems to have been invested in combining MS and DFT for the study of these reactions. Specifically, the mechanisms of palladium-catalyzed synthesis of olefins^[114], aryl amines^[115], aryl ketones^[116], the Heck reaction^[117], and the Fujiwara hydroxylation of alkynes^[118] have been investigated using this approach. Below, two examples are discussed in more detail to demonstrate the advantages gained by combining MS and DFT.

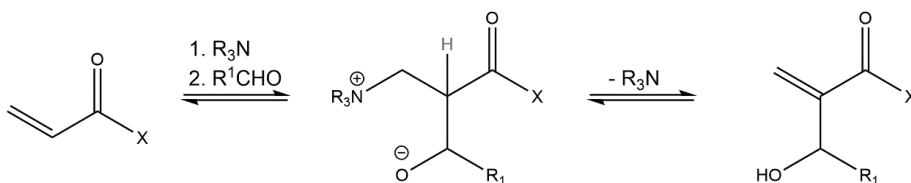
Especially the investigation of the Fujiwara hydroxylation of alkynes is of interest to highlight, as this study, in addition to ESI-MS and tandem MS and DFT, used NMR to probe the mechanism of the reaction. Here two main paths (A and B), yielding the respective thermodynamic and kinetic reaction products were investigated (Scheme 1). Pathway A progressed through a more stable intermediate (*Z*-intermediate, Scheme 1), which was formed through *cis*-arylpalladation, whereas a suggested *anti*-arylpalladation yielded the less stable *E*-intermediate (Scheme 1). Interestingly, the role of electrophilic palladium differs in pathway A and B; in pathway A, it leads to palladation of the arene, while in pathway B it results in Lewis acid activation of the alkene. Previously, palladation of the arene had been suggested as the sole role of the electrophilic palladium in the reaction, but the results of Godoi *et al.*^[118] suggest that palladium may have this role and also activate the alkyne. This is

based on experimental detection of intermediates assigned to belong to both of the respective pathways and on DFT calculations. However, in the systems explored by Godoi *et al.*^[118] – the Pd(OAc)₂-catalyzed indole addition to methyl or ethyl phenylpropionate – alkyne activation seemed to be the predominant mechanism according to NMR and DFT results. This led to a proposed revision of the overall mechanism for the intermolecular reaction between indoles and phenylpropiolates.



Scheme 1 Equilibria of intermediates and products of the Fujiwara hydroxylation of alkenes, *E/Z*-intermediate and *E/Z*-product, respectively. Figure adapted from Godoi *et al.*^[118] with permission from John Wiley & Sons, Inc.

Another interesting combination of experimental and theoretical reaction mechanism investigations was presented by Rodrigues *et al.*^[107], who used an acrylate derivative bearing an imidazolium-ion charge tag to facilitate transfer of the analyte to the gas phase in a study of the Morita-Baylis-Hillman reaction (Scheme 2). More in detail, the effect of a polar protic solvent (methanol), a polar aprotic solvent (acetonitrile), and no solvent (gas phase), both alone and in combination with the anion PF₆⁻, on the mechanism of a rate-limiting hydrogen transfer step of the reaction was investigated. The study concluded that two of the proposed hydrogen transfer pathways are possible based on observed ions and energies obtained from DFT calculations. However, the presence of PF₆⁻ in the systems with methanol or acetonitrile significantly lowered the energy barriers for the transition state of both of the proposed reaction pathways by stabilizing the transition states by a combination of the solvents and PF₆⁻.



Scheme 2 The Morita-Baylis-Hilman reaction studied by Rodrigues *et al.*^[107]. The proton transferred in the rate-limiting step is indicated in red.

2.3 MOLECULARLY IMPRINTED POLYMERS AND QUARTZ CRYSTAL MICROBALANCE

The principle behind MIPs is visualized in Figure 1: firstly, the functional monomers to be utilized are identified and assembled around a template molecule. In the case of preparation of catalytic MIPs, a so-called transition state analogue, (TSA) – a stable molecule resembling the transition state (TS) of the desired reaction – is used as a template. Subsequently, polymerization of these components, together with a suitable cross-linker, yields a polymer matrix where the functional monomers are arranged in specific positions, corresponding to their interactions with the template. Removal of the template by extraction yields a MIP that contains cavities with properties defined by the functional monomers and their interactions with the template. When introducing the reactants of a reaction whose TSA has been used in the MIP preparation, to produce the target molecule, their arrangement corresponding to the TS will be stabilized by the MIP, resulting in selective catalysis of the reaction in question.^[119]

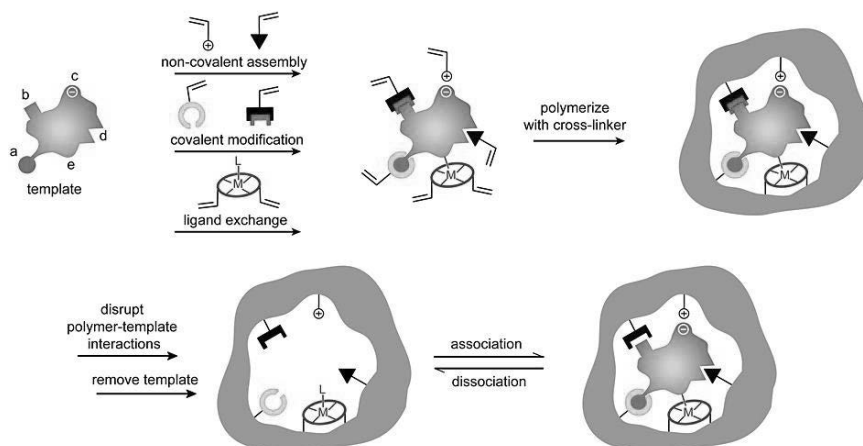


Figure 1 A schematic presentation of the preparation of molecularly imprinted polymers (MIPs). Commonly, only one of the interactions depicted in the assembly step is used to form the MIP, and not in combination as the figure might suggest. Although the procedure represented in this figure describes vinyl polymerization, the principal concept applies to preparation of MIPs in general. Figure reproduced from reference^[119] with permission from John Wiley & Sons, Inc.

In the case of catalytic MIPs, the complex between the template (TSA) or reactants that assemble to form the transition state of the intended reaction and the MIP matrix is typically formed through self-assembly of non-covalent bonds by electrostatic interactions, hydrophobic forces, and van der Waals interactions^[120], or through covalent bonds^[121]. MIPs have been prepared in several different formats, including membranes, monolayers, monoliths, and particles^[122]. Methods typically used to explore the general characteristics of the synthesized MIP include swelling studies and investigation of porosity and surface area.^[123] Fluorometry, IR spectroscopy, NMR spectroscopy, UV spectroscopy, and X-ray crystallography are commonly used to assess the functionality (e.g. selectivity) of the produced MIP.^[124] Additionally, QCM technology has been used for probing the selectivity of MIPs for various substrates.^[125] Advantages of QCM for exploring the selectivity of MIPs include the technique being label-free, robust, relatively cheap, and rapid.^[125] The principle of employing QCM technology in probing the selectivity of MIPs relies on that a quartz crystal will vibrate with a specific frequency when exposed to voltage (Figure 2)^[126]. If something (initially a MIP film, subsequently analytes) is deposited on the surface of the quartz crystal, this will lead to a change in its vibration frequency. By investigating how the frequency of the crystal changes when exposed to an analyte, it is possible to determine whether an analyte is binding to the polymer film deposited on the surface of the crystal.^[127] Based on these determinations, the functionality of the MIP can be validated by applying the template molecule used for fabricating the functional cavity of the polymer film on the QCM chip. If the vibration frequency of the chip upon analyte injection subsequently changes in a way indicating binding, while the same response does not arise when another molecule (e.g. the enantiomer of the analyte) is injected, this indicates selectivity of the polymer film for the template molecule.

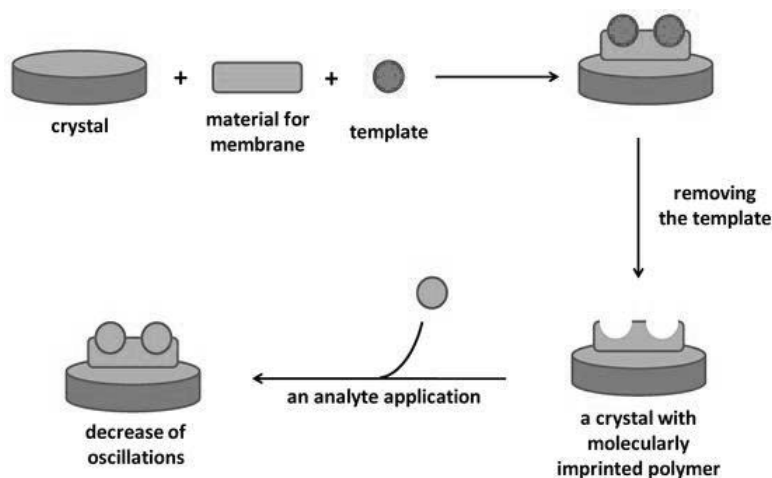


Figure 2 The principle of using a quartz crystal chip for investigating the functionality of a synthesized MIP. The membrane here refers to the MIP. Figure reproduced from reference^[126] with permission from MDPI.

3 AIMS OF THE STUDY

The work conducted focused on the following aims:

- To couple miniaturized additively fabricated devices to MS for reaction monitoring and identification of reaction mixture species, and to evaluate the suitability of this experimental set-up for reaction monitoring (Studies I-IV).
- To investigate the reaction mechanism of the oxidation of a heptafulvene into its corresponding tropone in detail by combining online MS and DFT (Study III).
- To prepare and characterize MIP systems for an enantioselective transamination reaction (Study V).

4 EXPERIMENTAL

This chapter briefly describes the chemicals, materials, instrumentation, experimental set-ups, reaction conditions, and computational details employed in the studies. Further details are given in the respective publications.

4.1 CHEMICALS AND MATERIALS

The reagents, reference compounds, materials, and solvents used in the experiments presented in this work are summarized in Table 2.

Table 2 Chemicals and materials used in the study.

Chemical	Manufacturer/Supplier	Use	Publication
3-[4-(6-Methyl-1,2,4,5-tetrazin-3-yl)phenoxy]propan-1-amine hydrochloride (>95%)	Click Chemistry Tools, Scottsdale, AZ, USA	Reagent	I, II
3-(Trimethoxysilyl)propyl methacrylate (98%)	Sigma-Aldrich, Steinheim, Germany	Reagent	V
(4 <i>E</i>)-Cyclooct-4-en-1-yl <i>N</i> -(3-aminopropyl)carbamate hydrochloride (>95%)	Click Chemistry Tools, Scottsdale, AZ, USA	Reagent	I
(4 <i>E</i>)-Cyclooct-4-en-1-yl <i>N</i> -(3-aminopropyl)carbamate hydrochloride (99%)	Sigma-Aldrich, Steinheim, Germany	Reagent	I, II
4-Methoxy-1-methyl-3-trifluoromethylbenzo[<i>c</i>]azulen-8-one	Synthesized by Dr. A. Kiriazis	Standard	III
(5 <i>S</i>)-5-(Aminomethyl)-3-[3-fluoro-4-(4-morpholinyl)phenyl]-1,3-oxazolidin-2-one (≥97%)	Carbosynth Ltd., Compton, UK	Reagent	IV
8-Isopropylidene-4-methoxy-1-methyl-3-trifluoromethyl-8 <i>H</i> -benzo[<i>c</i>]azulene	Synthesized by Dr. A. Kiriazis	Reagent	III
Acetone, LC-MS grade (99.8%)	VWR International Oy, Helsinki, Finland	Solvent for cleaning miniaturized reactor	II
Acetone, technical grade (≥98.5%)	VWR International Oy, Helsinki, Finland	Solvent	V

Experimental

Acetonitrile, LC-MS Chromasolv®-grade (99.9%)	Honeywell, Morris Plains, NJ, USA	Solvent	II, III, IV
Acetonitrile, HPLC grade (99.9%) [§]	Carlo Erba Reagents, DASH Group, Stockholm, Sweden	Solvent	V
Acetonitrile, LC-MS Chromasolv®-grade (99.9%)	Sigma-Aldrich, Steinheim, Germany	Solvent	I
Acetic anhydride (≥99%)	Sigma-Aldrich, Steinheim, Germany	Reagent	IV
Ammonia solution (25%)	Merck Chemicals GmbH, Darmstadt, Germany	Solvent for cleaning silicon and borosilicate glass substrates	V
Azobisisobutyronitrile* (AIBN, 98%)	Janssen Chimica, Solna, Sweden	Reagent	V
D-2-(5-Hydroxymethyl-8-methyl-3,4-dihydropyridof[4,3-e]-1,3-oxazin-3-yl)phenylalaninamide (D-TSA)	Synthesized by Dr. S. Kathiravan	Analyte and reagent	V
D-Phenylalanine (>98%)	Sigma-Aldrich, Steinheim, Germany	Analyte	V
Dimethyl sulfoxide- <i>d</i> ₆ (DMSO- <i>d</i> ₆ , 100%, 99.96 atom % D)	Sigma-Aldrich, Steinheim, Germany	Solvent	III, IV
Ethanol, analytical grade (99.5%)	Solveco AB, Rosersberg, Sweden	Solvent	V
Ethanol, reagent grade (80%)	Sigma-Aldrich, Steinheim, Germany	Solvent	V
Ethylene glycol dimethacrylate (EGDMA, 98%)	Sigma-Aldrich, Steinheim, Germany	Reagent	V
Formic acid (98-100%)	Merck Chemicals GmbH, Darmstadt, Germany	Additive for MS	I, II, III
<i>n</i> -Heptane, laboratory reagent grade (99%) [§]	Sigma-Aldrich, Steinheim, Germany	Solvent	V
Hydrogen chloride solution (37%, fuming)	Merck Chemicals GmbH, Darmstadt, Germany	Solvent for cleaning silicon and borosilicate glass substrates	V
Hydrogen peroxide (30% w/w in water, stabilized with dipicolinic acid)	Sigma-Aldrich, Steinheim, Germany	Solvent for cleaning QCM chips,	V

Experimental

		silicon, and borosilicate glass substrates	
Hydrogen peroxide (30% w/w in water, stabilized with dipicolinic acid)	Riedel-de Haën, distributed by Honeywell, Morris Plains, NJ, USA	Solvent for cleaning miniaturized reactor	IV
Isopropanol, LC-MS Chromasolv®-grade (99.9%)	VWR International Oy, Helsinki, Finland	Solvent for cleaning miniaturized reactor	II
L-2-(5-Hydroxymethyl-8-methyl-3,4-dihydropyrido[4,3- <i>e</i>]-1,3-oxazin-3-yl)phenylalaninamide (L-TSA)	Synthesized by Dr. S. Kathiravan	Analyte and reactant	V
L-Phenylalanine (≥99.0%)	Sigma-Aldrich, Steinheim, Germany	Analyte	V
Linezolid (≥98%)	Sigma-Aldrich, Steinheim, Germany	Standard	IV
<i>meta</i> -Chloroperoxybenzoic acid (<i>m</i> CPBA, ≤77%)	Sigma-Aldrich, Steinheim, Germany	Reagent	III
Methacrylic acid (MAA, 99%)	Sigma-Aldrich, Steinheim, Germany	Reagent	V
Methanol, reagent Ph. Eur. grade (99.9%)	Carlo Erba Reagents, DASH Group, Stockholm, Sweden	Solvent	V
Nitric acid (10% solution in water)	VWR International Oy, Helsinki, Finland	Solvent for cleaning miniaturized reactor	II
Phenylpyruvic acid (98%)	Sigma-Aldrich, Steinheim, Germany	Analyte	V
Polystyrene (latex) beads, mean diameter 0.3 μm (range: 0.30-0.33 μm, standard deviation 0.03-0.05 μm) in a 10% w/w water suspension	Sigma-Aldrich, Steinheim, Germany	Reagent	V
Pyridoxal hydrochloride (≥99%)	Sigma-Aldrich, Steinheim, Germany	Analyte	V
Pyridoxamine dihydrochloride (≥98%)	Sigma-Aldrich, Steinheim, Germany	Analyte	V
Sodium acetate (99.3%)	VWR International AB, Spånga, Sweden	Reagent used to prepare buffer solution	V

Sulfuric acid (95-98%)	Sigma-Aldrich, Steinheim, Germany	Solvent for cleaning QCM chips, silicon, and borosilicate glass substrates	V
Tetrahydrofuran, Chromasolv®- grade (99.9%) [§]	Sigma-Aldrich, Steinheim, Germany	Solvent	V
Toluene, laboratory reagent grade (99.3%) [§]	Sigma-Aldrich, Steinheim, Germany	Solvent	V
Triethylamine (98%)	Alfa Aesar, Heysham, UK	Reagent	V
Water, purified	Milli-Q Plus purification system, Mohlsheim, France	Solvent	I, II, III, IV, V

[§] Dried with molecular sieves (4 Å, 3.2 mm pellets, Sigma-Aldrich).

* Re-crystallized from methanol before use.

4.2 ANALYTICAL METHODS AND INSTRUMENTATION

An Agilent 6330 ion trap (Agilent Technologies, Santa Clara, CA, USA) was used for the online MS experiments. The MS settings used in these experiments are listed in Table 3. In all MS scan mode experiments presented in this thesis, acquisition of mass spectra was started just before infusion of solvent (which contained analytes or was used without addition of analytes to obtain a background reference spectrum) was initiated, and carried out continuously during the entire experiment.

Table 3 Mass spectrometry conditions used in the experiments.

Parameter	I	II	III	IV
Mass spectrometer	Agilent 6330 (Agilent Technologies, Santa Clara, CA, USA)			
Mode	Positive ESI			
Capillary voltage (kV)	-2.5	-3.0	-2.5	-3.0
MS scan range (<i>m/z</i>)	200-500	50-500	50-600	50-600 or 50-700 [‡]
Product ion scan range (<i>m/z</i>)	50-600	50-500	50-600	50-600 or 50-700 [‡]
Nitrogen drying gas flow (L/min)	6	1	6	4
Drying gas temperature (°C)	200	200	100	300
Product ion isolation width ($\pm m/z$)	1.0	1.0	1.0	1.0

[‡] In some of the online reaction monitoring experiments, the MS and product ion scan range were 50-600 *m/z*, while in other experiments the scan ranges were 50-700 *m/z*.

Other instrumentation was used in the experimental work described in this thesis. Details regarding this instrumentation and software and its use are presented in Table 4.

Table 4 Instrumentation and software used in the experimental work.

Instrument	Manufacturer/supplier	Note	Publication
Agilent Cary 630 FTIR spectrometer	Agilent Technologies, Santa Clara, CA, USA	FTIR experiments	V
Attana Cell 200 QCM instrument	Attana AB, Stockholm, Sweden	QCM experiments	V
Bruker Ascend 400 – Avance III HD NMR spectrometer	Bruker Corporation, Billerica, MA, USA	Verifying purity of reagent	III, IV
Iso-Tech DC power supply	IPS 603, Yleiselektronikka Oyj, Espoo, Finland	Power for the mixer fan	I, III
Leo 1550 Gemini instrument	Zeiss, Oberkochen, Germany	SEM experiments	V
Orbitrap Fusion mass spectrometer	Thermo Fisher Scientific Inc., Waltham, MA, USA	Accurate mass measurements	I
PHD 2000 syringe pump	Harvard Apparatus, Holliston, MA, USA	Infusion of reactants	I, II, III, IV
TM-1000 instrument	Hitachi, Tokyo, Japan	SEM experiments	IV
UV lamp (50 W, wavelength: 365 nm)	Labino AB, Vallentuna, Sweden	Polymerization of polymer films	V
Waters Synapt G2 mass spectrometer, equipped with a Waters Acquity UPLC system	Waters Corporation, Milford, MA, USA	Verifying purity of reagent	III, IV
XYZ-stage	Märzhäuser Wetzlar GmbH & Co. KG, Wetzlar, Germany	Position the reactor in front of the mass spectrometer	I, II, III
<u>Software</u>			
Attaché Evaluation, version 3.3.4	Attana AB, Stockholm, Sweden	Processing of the data obtained with the Attana Cell 200 QCM instrument	V
Attester, version 1.5.3	Attana AB, Stockholm, Sweden	Collect data with the Attana Cell 200 QCM instrument	V
DataAnalysis for 6300 series ion trap	Agilent Technologies, Santa Clara, CA, USA	Processing of data obtained with the	I, II, III, IV

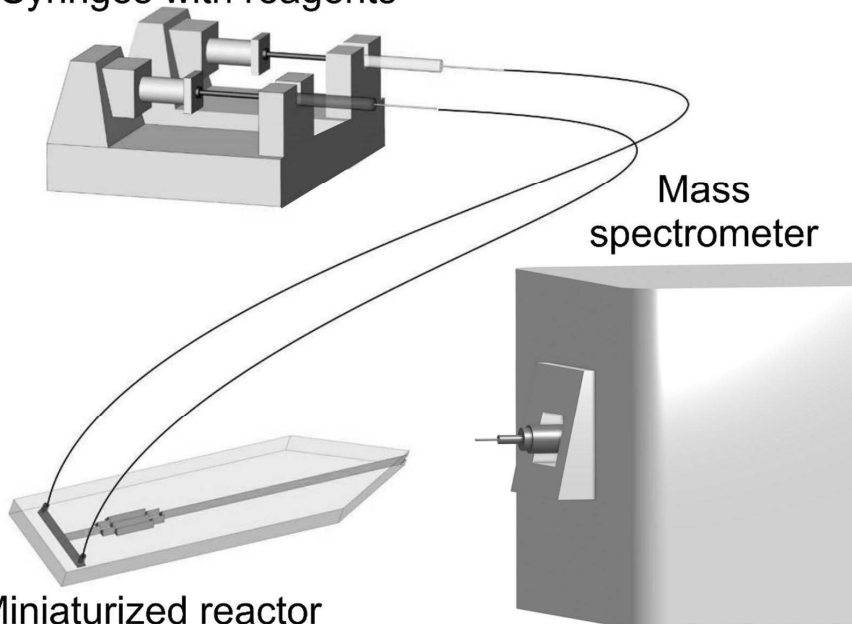
Experimental

LC/MS version 3.4, build 192		Agilent 6330 mass spectrometer	
MassLynx, version 4.0	Waters Corporation, Milford, MA, USA	Processing of the data obtained with the Waters Synapt G2 mass spectrometer	III, IV
MestReNova, version 11.0.3-18688	Mestrelab Research S.L., Bajo, Spain	Processing of the data obtained with the Bruker Avance III 400 MHz NMR spectrometer	III, IV
MoIE Molecular Mass Calculator version 2.02	The RNA Institute, College of Arts and Sciences, State University of New York at Albany, NY, USA	Calculating exact masses of analytes	III, IV
MicroLab PC	Agilent Technologies, Santa Clara, CA, USA	Processing of the data obtained with the Agilent Cary 630 FTIR spectrometer	V
Xcalibur, version 2.2 SP1, build 48	Thermo Fisher Scientific Inc., Waltham, MA, USA	Processing of the data obtained with the Orbitrap Fusion mass spectrometer	I

4.3 MINIATURIZED REACTORS COUPLED ONLINE TO MASS SPECTROMETRY

Schematically, the online reaction monitoring experiments were conducted as shown in Figure 3.

Syringes with reagents



Miniaturized reactor

Figure 3 A schematic illustration of the coupling of a miniaturized reactor to a mass spectrometer for reaction monitoring. Figure adapted from the original publication [128] with permission from Elsevier.

The detailed procedures for coupling miniaturized devices to MS are described for each experiment in Section 4.3.2.

4.3.1 FABRICATION OF MINIATURIZED REACTORS

The miniaturized reactors employed in Studies I–IV were manufactured using different types of additive manufacturing (3D printing) technologies. As Table 1 highlights, the established method for fabricating miniaturized reactors for online coupling to MS for reaction studies has to date been “subtractive fabrication”, which must be carried out in clean rooms^[128].

3D printing typically starts with creation of a computer-aided design (CAD) drawing of the device to be manufactured. Subsequently, the CAD drawing is used to guide the 3D printing machine in manufacturing of the devices.

The polypropylene reactor employed in Studies I and III was fabricated using the 3D printing method fused deposition modeling (FDM), as described

elsewhere^[27]. In FDM, the melted thermoplastic substrate is extruded through a nozzle to produce the desired 3D structure in a layerwise manner.^[129] The reactor chamber of the reactor used in Studies I and III contains a stir bar, which is inserted by pausing, and after insertion resuming, the 3D printing. The volume of the polypropylene reactor's chamber, with the stir bar inserted, was measured to be approximately 250 μL (by filling the reactor with water and comparing the weight of the reactor when filled with water with the weight when empty). A stainless steel nano-ESI needle (also integrated by pausing and resuming the 3D printing) protruding into the reaction chamber enabled pumpless delivery of the species of the reaction mixture directly to the MS. The nano-ESI needle was 50 mm long and had an i.d. of 30 μm and an o.d. of 150 μm (Thermo Fisher Scientific, Vantaa, Finland).

The microreactor used in Study II was fabricated using the technology laser additive manufacturing (LAM, also called selective laser melting or direct metal laser sintering), which operates by depositing metal powder or alloy that is then melted by a laser beam. Once one layer of matter has been melted, the substrate plate is moved downwards, and the next layer of powder or alloy is deposited, and melted. This process is repeated until the whole 3D object is fabricated.^[130–133] After fabrication of the device, the tip of the miniaturized reactor was manually polished to achieve a desired sharpness, i.e. small radius of curvature, to facilitate formation of electrospray. The experimentally determined volume of the stainless steel microreactor was found to be approximately 50 μL (determined by the same method as described above for the reactor used in Studies I and III).

The fabrication of the miniaturized reactor described in Study IV is based on a specialty technology of MICRON₃DP. Molten glass, by extrusion through a nozzle, is deposited on a glass plate (constituting the bottom of the glass device). The whole procedure is carried out in a heated chamber to prevent thermal shock.^[134–136] The volume of the reactor system (microreactor volume and silica capillary connections to syringe pump and MS) used in the online MS experiment presented in Study IV (Figure 4c) was, based on the time it took from start of infusion of analytes until their detection, estimated to be 65–70 μL . The miniaturized devices used are presented in Figure 4.

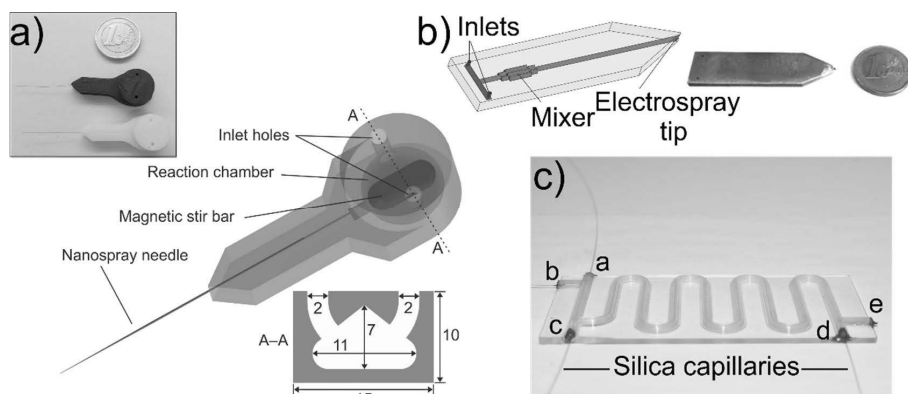


Figure 4 Miniaturized fluidic devices utilized in Studies I-IV. a) The polypropylene reactor (Studies I and III). The dimensions of the cross-section in the schematic figure are in millimeters. The schematic figure is reproduced from the original publication [27] with permission from the Royal Society of Chemistry, b) the stainless steel reactor used in Study II. The figure is adapted from the original publication [28] with permission from Elsevier, c) the glass microreactor, with silica capillaries connected to its inlets/outlets (Study IV).

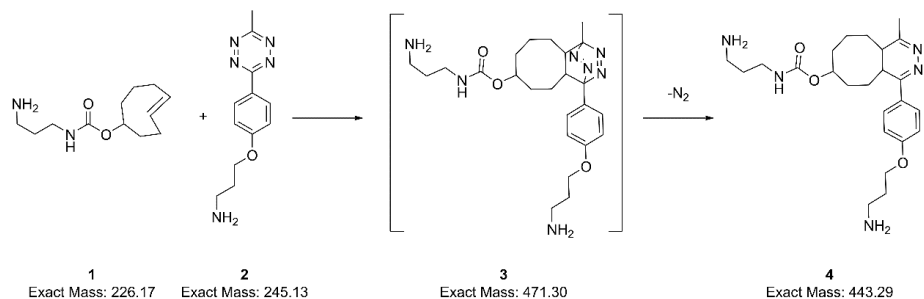
4.3.2 REACTIONS STUDIED AND EXPERIMENTAL DESIGNS

Below the reactions studied in online miniaturized reactor-MS experiments and the experimental designs are presented. Of note, complementary background experiments were typically done. These experiments e.g. consisted of direct infusion of the reactants individually and offline sampled reaction mixtures into the MS and online T-junction MS experiments (exploring a system with minimized volume to investigate whether the studied reaction occurred in the ionization process).

4.3.2.1 Inverse electron-demand Diels-Alder and subsequent retro Diels-Alder reaction (Studies I and II)

In Study I, a miniaturized polypropylene reactor was interfaced with an Agilent 6330 ion trap equipped with a capillary extension. (4*E*)-Cyclooct-4-enyl *N*-(3-aminopropyl)carbamate (**1**, abbreviated as *trans*-cyclooctene from here onwards, Scheme 3) and 3-[4-(6-methyl-1,2,4,5-tetrazin-3-yl)phenoxy]propan-1-amine (**2**, abbreviated as tetrazine from here onwards, Scheme 3), dissolved in acetonitrile:water 80:20 + 0.1 vol% formic acid-solutions in one syringe each, were infused into the microreactor (125 $\mu\text{L}/\text{min}/\text{syringe}$) during one minute to fill the reactor chamber. When the filling of the chamber was completed, infusion of reactants was stopped, and the stir bar integrated in the reactor's chamber was activated by applying a voltage of 24 V (from an external voltage supply) to a computer fan placed in the miniaturized reactor's jig. At the same time, ESI was obtained by turning on the voltage of the MS capillary to -2.5 kV, while the nano-ESI needle of the miniaturized reactor was grounded, and adjusting the position of the reactor

in front of the MS inlet. Mass spectrometric details of the experiment are presented in Table 3.

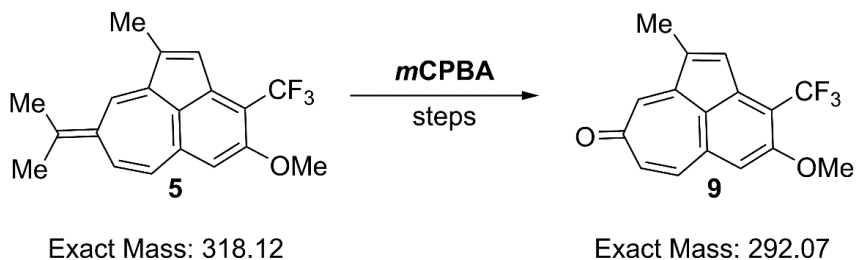


Scheme 3 The inverse electron-demand Diels-Alder and subsequent retro Diels-Alder reaction studied. *trans*-Cyclooctene (**1**) reacts with tetrazine (**2**) to form the reaction product (**3**) of the inverse electron-demand Diels-Alder reaction. The intermediate (**3**) subsequently undergoes a retro Diels-Alder reaction to form the final product (**4**).

The inverse electron-demand Diels-Alder and retro Diels-Alder reaction (Scheme 3) was also used to investigate the functionality of the stainless steel microreactor in Study II. In these experiments, *trans*-cyclooctene (**1**) and tetrazine (**2**), both dissolved in an acetonitrile:water 80:20 + 0.1 vol% formic acid-solution, were continuously infused into the microreactor with the flow rate 2.0 $\mu\text{L}/\text{min}/\text{syringe}$. The MS settings employed in these experiments are listed in Table 3. The distance between the tip of the reactor and the capillary extension of the MS was 0.5-1 cm in the experiments. In order to achieve ESI, an external high voltage (HV) supply, set at +5 kV in the presented experiment, was used, while the voltage of the MS capillary was -3 kV. This gave an HV current of 240 nA, a capillary MS current of about 130 nA and MS end plate current of about 70 nA in the experiment presented in Figure 6 (Ch.5.1.1).

4.3.2.2 *meta*-Chloroperoxybenzoic acid oxidation of heptafulvenes to tropones (Study III)

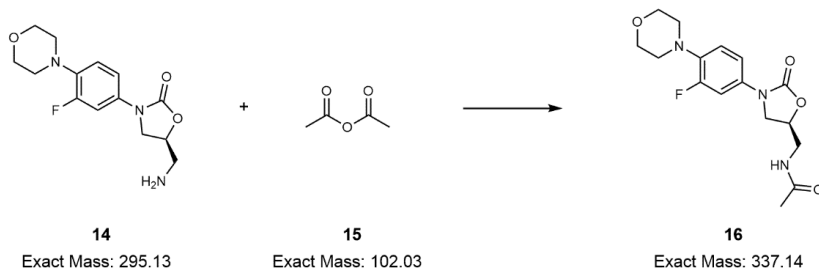
The polypropylene reactor (Figure 4a) was coupled to the Agilent 6330 ion trap in a manner identical to the one described in Study I (Ch. 4.3.2.1) to examine the *m*CPBA oxidation of heptafulvenes to tropones (Scheme 4). The MS details for investigating the reaction are presented in Table 3. In the oxidation study, *m*CPBA was contained in one syringe, while the other syringe contained the heptafulvene 8-isopropylidene-4-methoxy-1-methyl-3-trifluoromethyl-8*H*-benzo[*cd*]azulene (**5**). Both reactants were dissolved in acetonitrile + 0.1 vol% formic acid.



Scheme 4 The *m*CPBA oxidation of heptafulvene **5** into tropone **9**.

4.3.2.3 Acetylation reaction (Study IV)

In the online synthesis of linezolid (**16**, Scheme 5), the outlet of the microreactor (inlet/outlet d in Figure 4c) was coupled to a commercial ESI source, mounted on an Agilent 6330 ion trap, with fused silica capillaries. In addition to the MS settings listed in Table 3, nitrogen gas was used as nebulizing gas with a pressure of 15 psi. Samples of (5*S*)-5-(aminomethyl)-3-[3-fluoro-4-(4-morpholinyl)phenyl]-1,3-oxazolidin-2-one (linezolid-related compound C, **14**) and acetic anhydride (**15**) were prepared in acetonitrile and placed in separate syringes. The syringes were placed in a syringe pump and coupled to fused silica capillaries, which were attached to inlets (a and b in Figure 4c) of the microreactor. The samples were continuously infused into the microreactor, using flow rates of 4.0 $\mu\text{L}/\text{min}/\text{reagent}$, 1.6 $\mu\text{L}/\text{min}/\text{reagent}$, and 750 nL/min/reagent.



Scheme 5 Synthesis of the antibiotic drug linezolid (**16**) by acetylation of linezolid-related compound C (**14**) with acetic anhydride (**15**).

4.4 COMPUTATIONAL DETAILS

The software Gaussian^[137] was used for the DFT study of the reaction mechanism of the oxidation of a heptafulvene to its corresponding tropone (Study III), employing the hybrid functional set Mo6-2X^[138] and the basis set 6-311++G(d,p)^[139,140]. Based on Mo6-2X being benchmarked to give good results for investigations of organic compounds and reactions^[141], and 6-311++G(d,p) being documented to be suitable for hydrocarbon systems^[142],

this combined method was deemed to be adequate for the system investigated in Study III. Of note, heptafulvenes resembling the one investigated in Study III were investigated by Aumüller and Yli-Kauhahuoma previously, and they concluded that a functional set being a precursor (MO5-2X) of the one used in our study, employed together with the same basis set as used in Study III, gave good results for these compounds.^[143,144] All calculations were carried out in the singlet ground state. In order to resemble the solvent conditions used in the MS experiments (acetonitrile + 0.1 vol% formic acid), all calculations used a polarizable continuum model (PCM) using the integral equation formalism variant (IEFPCM) solvent model (meaning that a cavity of the specified solvent is simulated around the studied species) with pre-defined parameters for acetonitrile. Vibrational frequencies of all optimized structures were calculated, giving no imaginary frequency for stationary structures, and exactly one imaginary frequency for transition states. Regarding the (de-)protonation steps, no explicit transition states were calculated, and protons were implicitly assumed to originate from *meta*-chlorobenzoic acid. All energies discussed in Ch. 5.1.2 refer to Gibbs free energies (kcal/mol), unless explicitly noted otherwise.

4.5 MOLECULARLY IMPRINTED POLYMERS

4.5.1 PREPARATION OF MOLECULARLY IMPRINTED POLYMERS

The MIP films were synthesized on silicon dioxide-coated quartz crystal resonators, which had been prepared according to a washing and silane deposition procedure (described in Study V). Thus, polymer films both with and without polystyrene (PS) beads and porogen were prepared. When preparing polymers with PS beads, 30 μ L of PS beads in water suspension was deposited on a silanized area of the quartz crystal resonator, and the water of the suspension was evaporated by placing the resonator chip in a desiccator. After this, 1 μ L of pre-polymerization solution (which had been prepared on ice and had been purged with nitrogen gas for 10 min) was deposited on top of the PS beads or directly on the silanized area of the quartz crystal resonator. In total, nine different polymer systems with the specifications presented in Table 5 were prepared.

Table 5 Specifications of the polymer systems deposited on quartz crystal resonators.

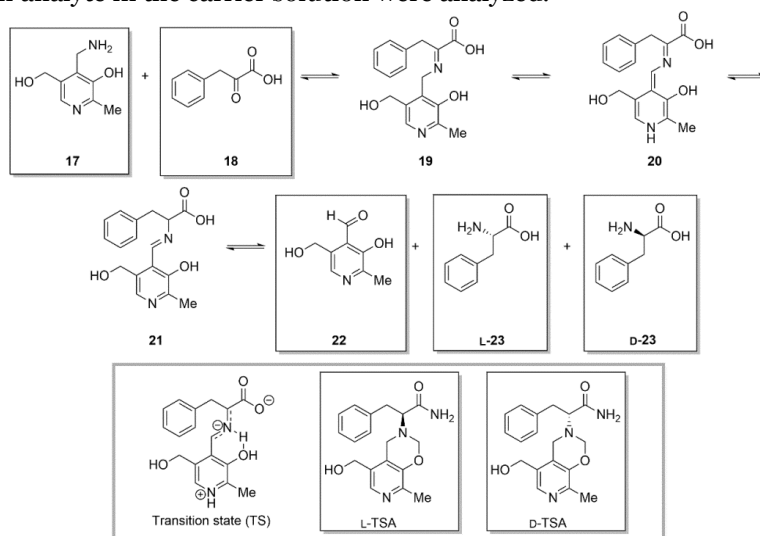
Polymer system	Molecular template	Sacrificial template	Functional monomer	Crosslinker	Initiator	Porogen
P1	-	PS beads	MAA (47.6 μ mol)	EGDMA (0.22 mmol)	AIBN (7.9 μ mol)	<i>n</i> -heptane
P2	-	-				<i>n</i> -heptane
P3	-	PS beads				-
P4	L-TSA	PS beads				<i>n</i> -heptane
P5	L-TSA					<i>n</i> -heptane
P6	L-TSA	PS beads				
P7	D-TSA	PS beads				<i>n</i> -heptane
P8	-	-				-
P9	L-TSA	-				-

A cover glass was placed on top of the pre-polymerization mixture, and the quartz crystal resonator, with the deposited pre-polymerization mixture, was placed under UV irradiation for 2 h for polymerization. After complete polymerization, the cover glass was removed, and the resonators were rinsed in a series of solvents, as detailed in Study V. Most notably, all resonators were rinsed in toluene to remove possible enclosed PS beads, and a 5 mM solution of NaOH in water to extract the (for polymers P4-7 and P9) enclosed TSA from the polymer matrix.

In addition to the polymers synthesized on quartz crystal resonators summarized in Table 5, identical series of polymers were synthesized on borosilicate glass slides (for FTIR spectroscopy experiments), and silicon slides (for SEM experiments). With the exception that two layers of 30 μ L PS bead suspension were deposited on the borosilicate glass and silicon slides (the first layer was allowed to dry before the second layer was added), the method for deposition of PS beads, composition of the pre-polymerization mixtures, and polymerization procedure for the borosilicate glass and silicon slides were identical to the ones described above for the quartz crystal resonators. Also the washing steps carried out after completed polymerization (described in Study V) for the borosilicate glass and silicon slides were identical to the ones carried out with the quartz crystal resonators, with the exception that the borosilicate glass slides on which polymer systems with PS beads (systems P1, P3, P4, P6, and P7) were deposited were washed in ethanol immediately after completed polymerization. FTIR spectra were acquired for these systems, and then the slides were washed in the same solvents as the quartz crystal resonators (including toluene, which dissolved the PS beads). The rationale behind this was to detect FTIR signals of PS in the polymer matrix, to obtain a proof that PS indeed had become enclosed in the polymers. To further support that the scheme of including PS beads in the polymers – to form pores when extracted out – worked, SEM experiments were conducted to characterize the visual appearance of the polymers after washing with all solvents (including toluene).

4.5.2 QUARTZ CRYSTAL MICROBALANCE EXPERIMENTS

The quartz crystal resonators, with the various polymer films deposited on them, were placed in measurement jigs and inserted into an Attana Cell 200 quartz crystal microbalance (QCM) instrument after being subjected to the wash procedure briefly described in the previous section. The instrument was operated under flow injection analysis (FIA) conditions, and an integrated peristaltic pump of the instrument continuously pumped a 1:1 solution of methanol:0.1 M sodium acetate in water (pH 7) with a flow rate of 50 $\mu\text{L}/\text{min}$ as the carrier solvent. All experiments were conducted at 20°C. No analyte injections were done until the system had stabilized, which was defined as a resonant frequency change of ≤ 0.5 Hz over 300 s when pumping only the carrier solution. When the system was considered to be stable, 75 μL of the analyte, dissolved in the carrier solution, was injected manually into the QCM using a gas tight syringe. Each analyte was injected at least three times for each polymer system. The analytes studied in the QCM experiments are depicted within gray framed boxes in Scheme 6. Samples of 1, 5, 10, 20, 30, and 50 mM of each analyte in the carrier solution were analyzed.



Scheme 6 The synthesis of the physiologically important amino acid phenylalanine (**23**) from pyridoxamine (**17**) and phenylpyruvic acid (**18**). The design of TSAs was originally described by Andrews *et al.*^[145]. Compounds used as analytes in the quartz crystal microbalance experiments are indicated by gray framed boxes.

5 RESULTS AND DISCUSSION

The main results obtained in the research are described below. Details can be found in Publications I-V. Firstly, the advances in coupling the miniaturized devices online to MS are described in Ch. 5.1. Presented alongside are the MS results and the (DFT) reaction mechanism studies. This topic is concluded by a comparison of the utilized devices' suitability for coupling to MS for reaction monitoring (Ch. 5.2). Next, the developed MIP systems are characterized with respect to their physicochemical properties and affinity for the TSA used (Ch. 5.3).

5.1 COUPLING OF MINIATURIZED DEVICES TO MASS SPECTROMETRY AND REACTION MECHANISM STUDIES

Three chemical reactions were studied by coupling miniaturized reactors to MS detection. A summary of results of these studies is presented in this chapter. Details of each study are given in the respective publication.

5.1.1 A 3D PRINTED MINIATURIZED POLYPROPYLENE REACTOR AND STAINLESS STEEL REACTOR FOR ONLINE STUDY OF AN INVERSE ELECTRON-DEMAND DIELS-ALDER AND RETRO DIELS-ALDER REACTION

By interfacing the polypropylene reactor (Figure 4a) and the stainless steel reactor (Figure 4b) with ESI-MS, the conversion of *trans*-cyclooctene (**1**) and tetrazine (**2**) into the Diels-Alder reaction product **4** (Scheme 3) was possible to monitor (Figure 5 and Figure 6, respectively). The identity of all ions discussed in this section is proposed based on the behavior of the extracted ion profiles (EIPs) of the reaction species as a function of the reaction time (Figure 5), MSⁿ analyses, and offline accurate MS measurements.

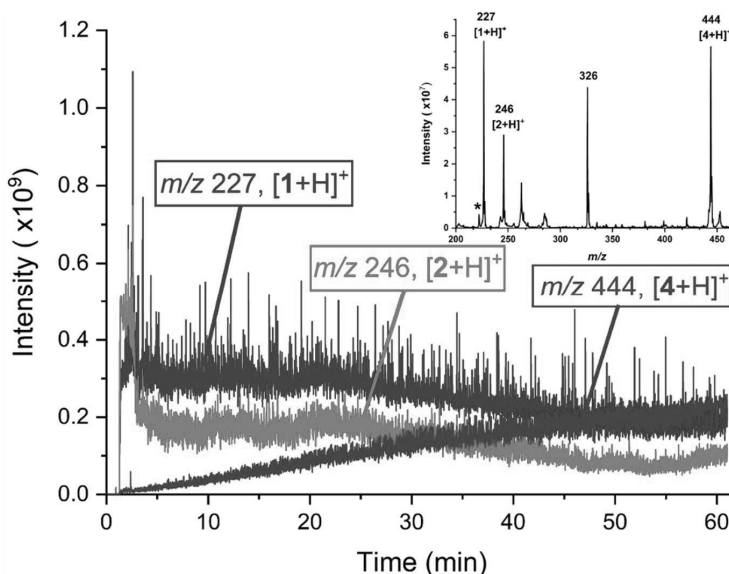


Figure 5 Extracted ion profiles recorded during the online experiment with the polypropylene reactor coupled to a mass spectrometer. The inset shows a mass spectrum, obtained by averaging the total ion current over 60–61 min. * denotes the doubly charged ion $[4+2H]^{2+}$ at m/z 222. Figures adapted from the original publication [27] with permission from the Royal Society of Chemistry.

Interfacing the polypropylene reactor to ESI-MS was, thanks to the integrated nano-ESI needle of the reactor, quite effortless. As shown in Figure 5, the reactants *trans*-cyclooctene ($[1+H]^+$) and tetrazine ($[2+H]^+$) are present as protonated molecules, at m/z 227 and m/z 246, respectively. As the reaction time progresses, the intensity of these ions decreases, while the intensity of the reaction cycloadduct, seen as a protonated molecule ($[4+H]^+$, at m/z 444), increases.

However, coupling of the stainless steel reactor to MS was more challenging than the corresponding procedure with the polypropylene reactor: it was observed that, together with the manually sharpened ESI tip, a droplet on the reactor tip was needed to obtain ESI. This strategy seemed to work satisfactorily to obtain stable ion currents. The relative standard deviations (RSDs) of the currents of the extracted ion profiles of m/z 227 ($[1+H]^+$) and m/z 246 ($[2+H]^+$) from 39.0 min to the end of the acquisition (Figure 6a) were 7.4% and 3.4%, respectively, which indicates a good stability of the obtained ESI. However, the RSD for the ion current of m/z 222.6 ($[4+2H]^{2+}$) during the same time frame was larger, 32%. This can partly be explained by the signal's lower intensity. The RSD values obtained with the stainless steel microreactor are similar to those of the total ion current reported for a commercial ESI tip made of fused silica and a microchip electrospray device, which were 9.8% and 2.1%, respectively^[146].

The events shown in Figure 6a are the following: During 0–16 min the background solution (acetonitrile:water 80:20 + 0.1 vol% formic acid) is infused through both of the reactor's inlets, and experimental conditions

(distance between reactor tip and MS inlet, voltage of HV supply, and size of the droplet at the tip of the reactor) are being optimized to obtain stable ESI. At $t=16$ min, the syringes are exchanged to syringes containing *trans*-cyclooctene (**1**, Scheme 3) and tetrazine (**2**, Scheme 3) in an acetonitrile:water 80:20 + 0.1 vol% formic acid-solution, respectively.

At about 12 min after the syringe exchange (correlating well with the experimentally measured as well as the calculated volume of the reactor, approximately 50 μL , and a total flow through the reactor of 4 $\mu\text{L}/\text{min}$), the EIPs of m/z 227 ($[\mathbf{1}+\text{H}]^+$), m/z 246 ($[\mathbf{2}+\text{H}]^+$), and m/z 222.6 ($[\mathbf{4}+2\text{H}]^{2+}$) start to increase. These three ions are also present in the mass spectrum in Figure 6b and were also observed when conducting the inverse electron-demand Diels-Alder reaction and retro Diels-Alder reaction in the polypropylene reactor (Figure 5).

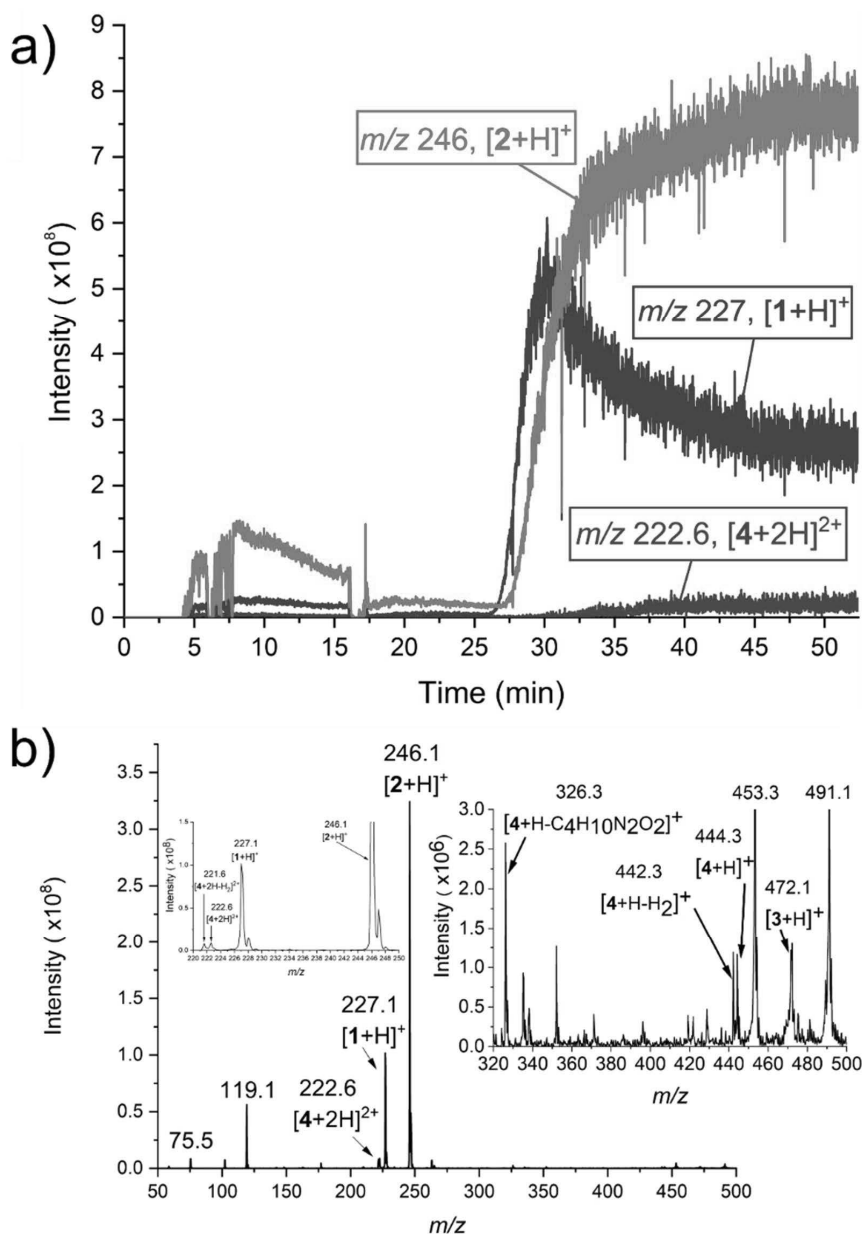


Figure 6 Results obtained when conducting the inverse electron-demand Diels-Alder reaction and retro Diels-Alder reaction in a stainless steel reactor coupled online to ESI-MS. a) Extracted ion profiles of m/z 227 ($[1+H]^+$), m/z 246 ($[2+H]^+$), and m/z 222.6 ($[4+2H]^{2+}$), b) An ESI-mass spectrum, obtained by averaging the total ion current recorded in the experiment over 51-52 min. The inset to the left is zoomed in at the mass-to-charge range m/z 220-250, while the inset to the right is zoomed in at the mass-to-charge range m/z 320-500. Figure adapted from the original publication [1]^[28] with permission from Elsevier.

5.1.1.1 Identification of reaction-related ions

As seen from the spectra in the insets of Figure 5 and Figure 6b, some ions were, in addition to the protonated reactants *trans*-cyclooctene and tetrazine at m/z 227 and m/z 246, respectively, observed both when coupling the polypropylene reactor and the stainless steel reactor to ESI-MS. These ions are: m/z 222 (in the experiments with the polypropylene reactor found at m/z 222.3 and 222.5, but reported as m/z 222, in the experiments with the stainless steel reactor found at m/z 222.6, due to differences in calibration and day-to-day variance of the ion trap), m/z 326, and m/z 444. The ion at m/z 472 was only observed in the stainless steel reactor-ESI-MS study. Of note, the ions at m/z 221 (found at m/z 221.6 in the stainless steel reactor experiments) and m/z 442 were observed with very low relative intensity (not marked in the mass spectrum in the inset of Figure 5) in the polypropylene reactor study, but with higher relative intensity in the stainless steel reactor experiment (Figure 6b, right inset). The ions at m/z 75 and m/z 119 were only observed in the stainless steel reactor study (Study II). It is not possible to say whether these ions were present in Study I since the measured mass range did not go this low. However, as these ions were formed in MS/MS analysis of the precursor ion m/z 227 ($[\mathbf{1}+\text{H}]^+$) in both Studies I and II, the ions m/z 75 and m/z 119 in Figure 6b are proposed to be fragments of $[\mathbf{1}+\text{H}]^+$, being formed in the ionization process.

The retro Diels-Alder reaction product was observed both as a protonated molecule, $[\mathbf{4}+\text{H}]^+$, at m/z 444, and as a doubly charged ion, $[\mathbf{4}+2\text{H}]^{2+}$, at m/z 222 both when conducting the reaction in the polypropylene reactor, as well as in the stainless steel reactor (here $[\mathbf{4}+2\text{H}]^{2+}$ was observed at m/z 222.6). MS^n spectra and fragmentation schemes that support the proposed identities of these ions are presented in Figure 7 and Figure 8, respectively.

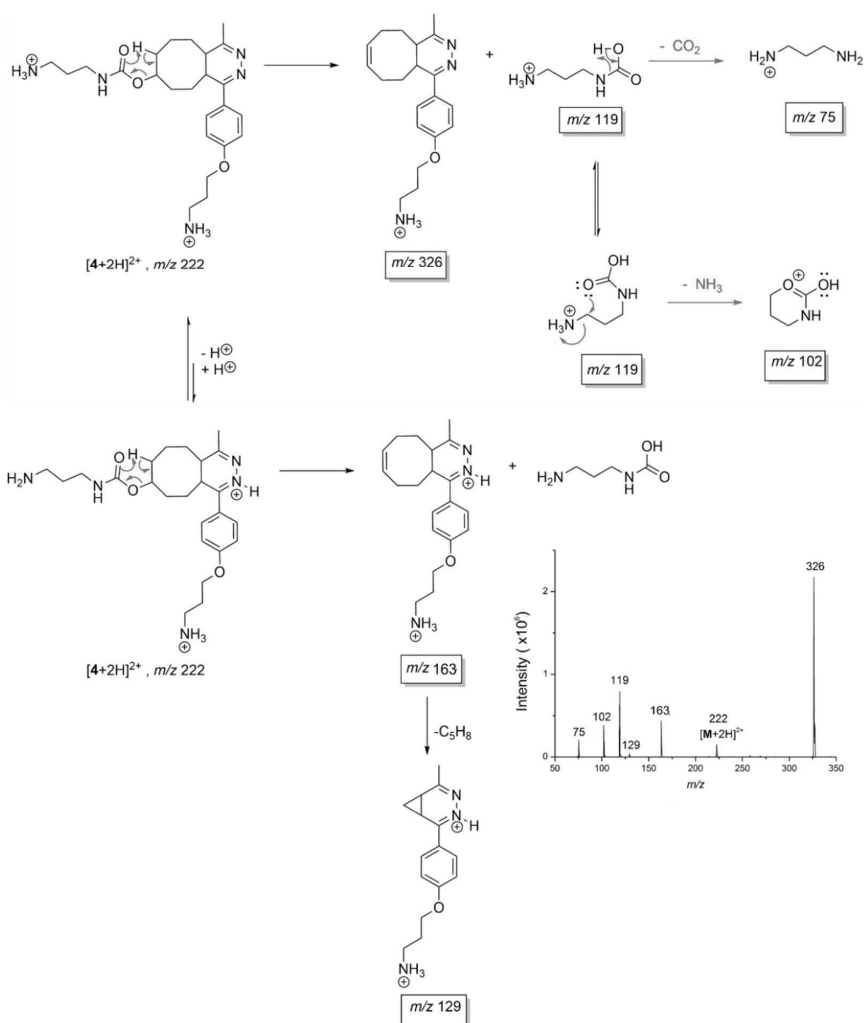


Figure 7 Proposed fragmentation scheme of the precursor ion m/z 222. A MS/MS spectrum of the precursor ion m/z 222 is shown in the inset. $M = 4$. Figure adapted with correction from the original publication [27] with permission from the Royal Society of Chemistry.

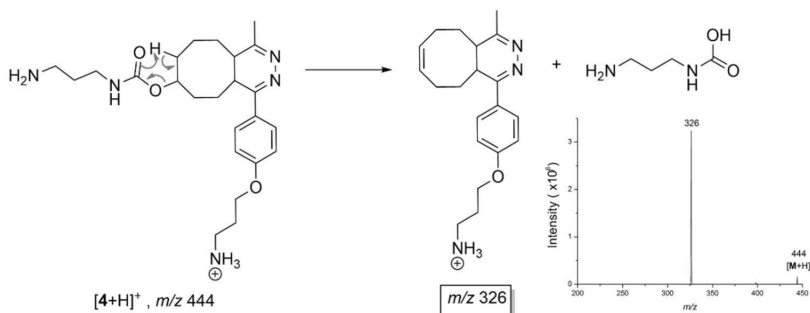


Figure 8 Proposed fragmentation scheme of the precursor ion m/z 444. A MS/MS spectrum of the precursor ion m/z 444 is shown in the inset. $M = 4$. Figure adapted from the original publication [27] with permission from the Royal Society of Chemistry.

An additional ion, proposed to be reaction-related, present in the insets of Figure 5 and Figure 6b is the ion at m/z 326. In addition to being present in the reaction mixture (mass spectrum in inset in Figure 5 and Figure 6b), m/z 326 was formed as a fragment when subjecting the precursor ions m/z 222 and m/z 444 to tandem MS analysis (Figure 7 and Figure 8). Based on this, the ion at m/z 326 in the insets of Figure 5 and Figure 6b is proposed to be a fragment of the reaction product, **4**, being formed in the ionization process. This is further supported by similarity between MSⁿ spectra obtained from three different experiments: 1) when fragmenting the precursor ion m/z 326 present in the reaction mixture (MS/MS analysis), 2) MS³ analysis of the precursor ion m/z 326 formed in MS² analysis of the precursor ion m/z 222, and 3) MS³ analysis of the precursor ion m/z 326 formed in MS² analysis of the precursor ion m/z 444 (Figure 9). The similarity of the shape of the EIPs of m/z 222 and 326 with the EIP of m/z 444 (data shown in Studies I and II) further supports that these ions are related. MSⁿ spectra and fragmentation schemes to support the proposed identities of the ions m/z 222, 326, and 444 seen in the mass spectrum in the insets of Figure 5 and Figure 6b are presented in Figure 7-9.

When coupling the stainless steel reactor to ESI-MS, an ion at m/z 472 was also observed (Figure 6b, right inset). This ion likely corresponds to the protonated reaction product of the inverse electron-demand Diels-Alder reaction, [**3**+H]⁺ (Scheme 3). This is supported by the fact that the shape of the EIP of this ion follows that of m/z 222.6 (assigned as [**4**+2H]²⁺) and m/z 444 ([**4**+H]⁺) (data shown in Study II), and the product ions formed in tandem MS analysis of this precursor ion (Figure 10).

Interpretation of the product ion mass spectrum obtained when fragmenting the precursor ion m/z 472 (Figure 10a) is limited due to its low quality; only identification of the four largest mass peaks (m/z 241, 326, 354, and 454) was attempted. For the product ions m/z 326, 354, and 454, fragmentation routes (Figure 10b-d) based on the structure assumed for the cycloadduct product **3** of the inverse electron-demand Diels-Alder reaction were proposed. These product ions are proposed to be formed by the loss of N₂+C₄H₁₀N₂O₂ (mass: 146), C₄H₁₀N₂O₂ (mass: 118), and H₂O (mass: 18) moieties, respectively. For the ion m/z 241, no fragmentation schemes based on the structure of the product **3** could be drawn. Based on this, this ion in the product ion mass spectrum could originate from a background ion having the same m/z as the protonated cycloadduct **3**, or alternatively, it has a structure that does not correspond to that of the presumed cycloadduct **3**.

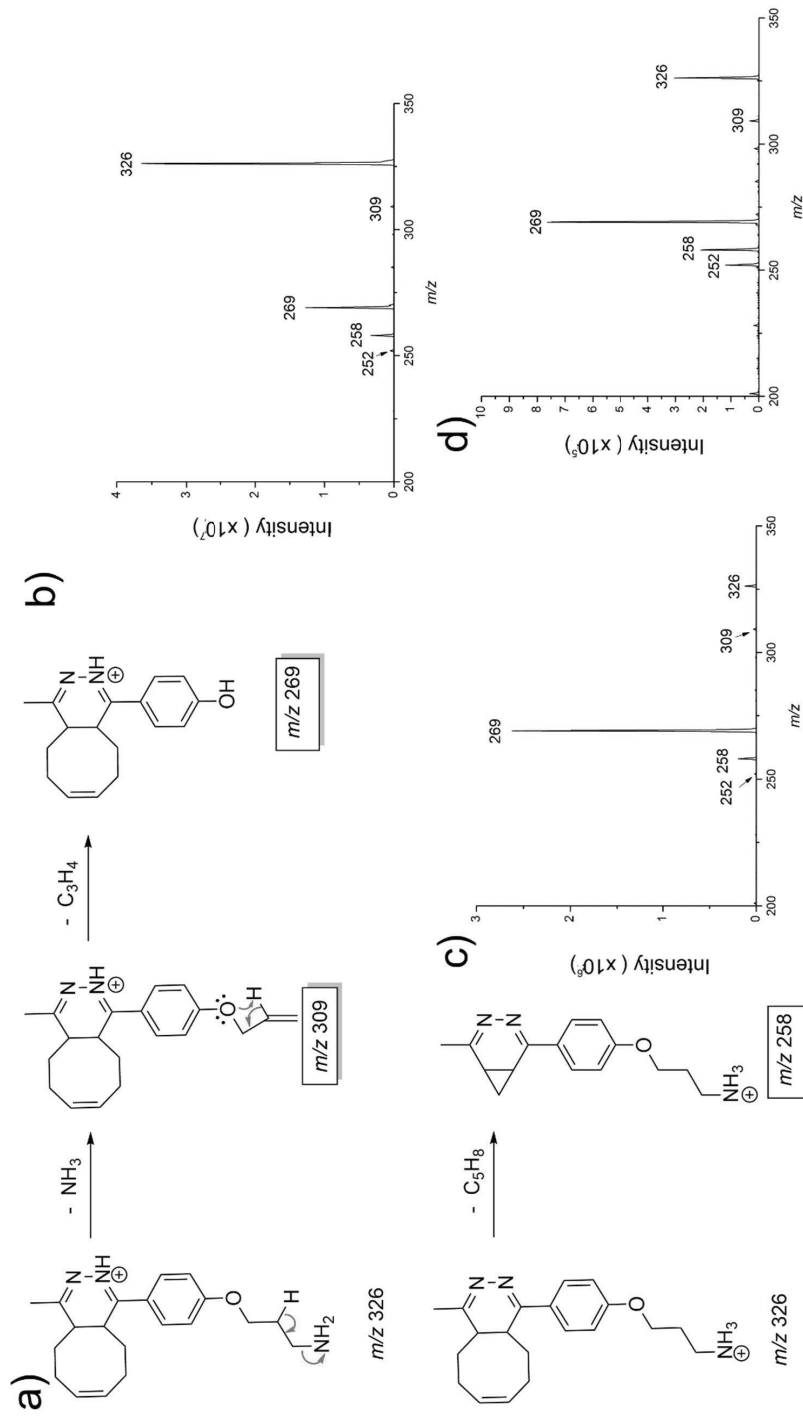


Figure 9 a) Proposed fragmentation scheme of the precursor ion m/z 326, b) MS/MS spectrum obtained when fragmenting the precursor ion m/z 326 present in the reaction mixture, c) MS³ spectrum obtained by isolating and fragmenting the ion m/z 326 from the MS² measurement of the precursor ion m/z 444 (present in the reaction mixture), d) MS³ spectrum obtained by isolating and fragmenting the ion m/z 326 from the MS² measurement of the precursor ion m/z 222 (present in the reaction mixture). Figures adapted from the original publication [27] with permission from the Royal Society of Chemistry.

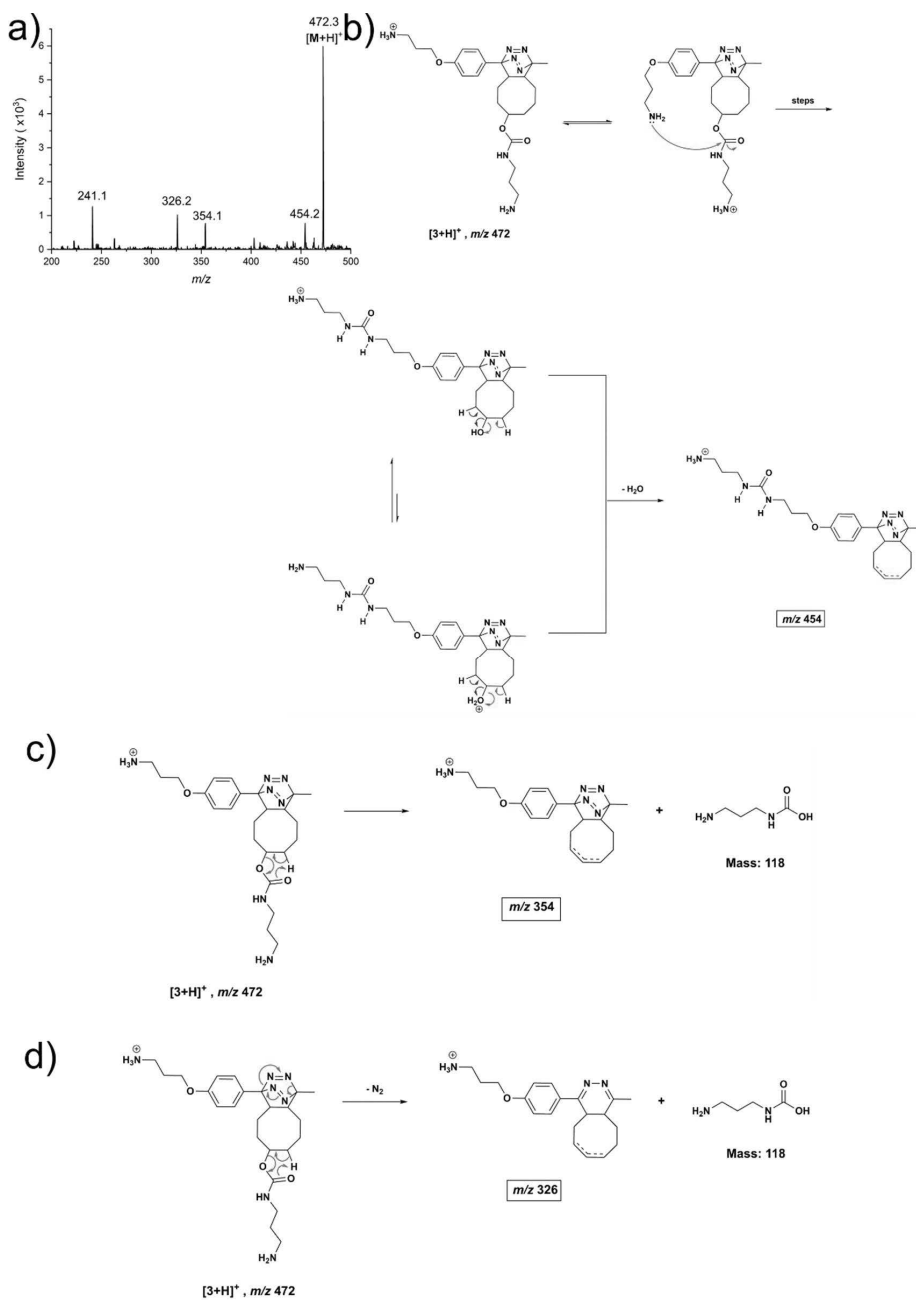


Figure 10 Investigation of the identity of the precursor ion m/z 472. a) MS/MS mass spectrum obtained when fragmenting the precursor ion m/z 472 with the fragmentation amplitude 0.3 V. $M = 3$, b) proposed fragmentation scheme for the formation of the product ion m/z 454, c) proposed fragmentation scheme for the formation of the product ion m/z 354, d) proposed fragmentation scheme for the formation of the product ion m/z 326. Figures adapted from the publication [II^{\[28\]}](#) with permission from Elsevier.

Another interesting ion seen in the right inset of the mass spectrum in Figure 6b is the ion at m/z 442. This ion could be formed in the ionization process, due to nominal loss of H_2 from $[4+H]^+$ or **4**. It is known that this kind of electrochemical reactions can occur in ESI^[96]. Support for the identity of the ion at m/z 442 further comes from the observation of an ion at m/z 221.6 (Figure 6b, left inset), whose EIP over the course of the reaction follows that of m/z 442 (data presented in Study II). As tandem MS analysis of the precursor ion m/z 442 produces fragments that are two mass units smaller than the ones obtained when fragmenting the precursor ion m/z 444, this supports the identity $[4+H-H_2]^+$ for the ion at m/z 442 (Figure 11). Similarly, as tandem MS analysis of the precursor ion m/z 221.6 yields fragments that are identical to or one mass unit smaller for ions identified as doubly charged ions, and two mass units smaller for ions identified as singly charged ions than is the case when fragmenting the precursor ion m/z 222.6, this suggests the identity $[4+2H-H_2]^{2+}$ for the ion at m/z 221.6 (Figure 11).

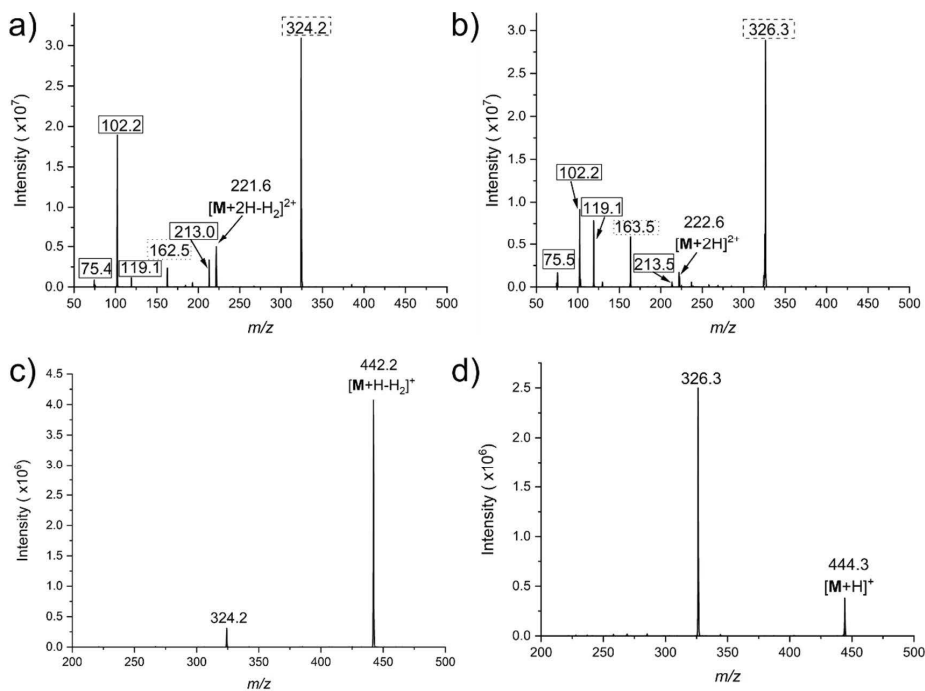


Figure 11 MS/MS spectra obtained when subjecting the precursor ions a) m/z 221.6, b) m/z 222.6, c) m/z 442, and d) m/z 444 to MS/MS analysis, using the same fragmentation amplitudes in a and b, and c and d, respectively. $M = 4$ in all spectra. The m/z values identical in (a) and (b) are marked with solid frames, the m/z value that is one unit larger in (b) than in (a) is marked with a dotted frame, and the m/z value that is 2 units larger in (b) than in (a) is marked with a lined frame. Figures adapted from the original publication II^[28] with permission from Elsevier.

5.1.2 A 3D PRINTED MINIATURIZED POLYPROPYLENE REACTOR FOR ONLINE STUDY OF THE *meta*-CHLOROPEROXYBENZOIC ACID OXIDATION OF A HEPTAFLUVENE INTO A TROPONE AND COMPLEMENTARY DENSITY FUNCTIONAL THEORY INVESTIGATIONS

The miniaturized polypropylene reactor was coupled to an ion trap as described above in Ch. 5.1.1. After the reactor was filled with the reactant solutions (heptafulvene **5** and *m*CPBA), at $t = 1$ min, the stir bar of the reactor was activated and optimization of the position of the reactor in front of the capillary extension of the MS was started. After approximately 2.5 min, ESI is achieved, as can be seen from the appearance of EIPs related to the reaction ions in Figure 12a. In Figure 12b, an averaged mass spectrum of the reaction mixture, at the end of the experiment, is shown. The most interesting ions present in this mass spectrum (Figure 12b) are m/z 293, 319, 335, and 351 (Scheme 7). The ion at m/z 293 was identified as the protonated tropone reaction product $[\mathbf{9}+\text{H}]^+$ (a MS/MS spectrum and fragmentation scheme to support this claim are shown in Figure 13), m/z 319 as the protonated heptafulvene starting material **5**, $[\mathbf{5}+\text{H}]^+$, and m/z 335 as the first intermediate of the reaction of heptafulvene **5** to tropone **9**, $[\mathbf{6}+\text{H}]^+$ or $[\mathbf{13}]^+$. For the ion at m/z 351, three structures ($[\mathbf{8}]^+$, $[\mathbf{12}+\text{H}]^+$, and $[\mathbf{S1}]^+$, Scheme 7) were investigated computationally. The EIPs in Figure 12a also indicate the presence of some oxidized species of **5** (m/z 319), especially m/z 335, but also m/z 351 and m/z 293, already at the start of the experiment. As LC-MS and NMR analysis of **5** indicated it to be pure, the presence of these species is attributed to that the analytes may have been oxidized in the ESI process^[96].

Using the experimentally observed ions and their EIP's behavior over the time of the experiment as a basis, nine alternative reaction pathways were proposed (Scheme 7, Figure 14, and Table 6). All investigated reaction pathways are discussed in detail in Study III. Here, however, only the reaction pathway with the lowest potential energy profile is discussed in detail. This is the blue reaction pathway in Scheme 7, the energy diagram (Figure 14), and Table 6. The structures depicted in black are part of all of the reaction pathways investigated (except for **9**-acetone and **9**, which are not part of the turquoise endocyclic Criegee rearrangement pathway).

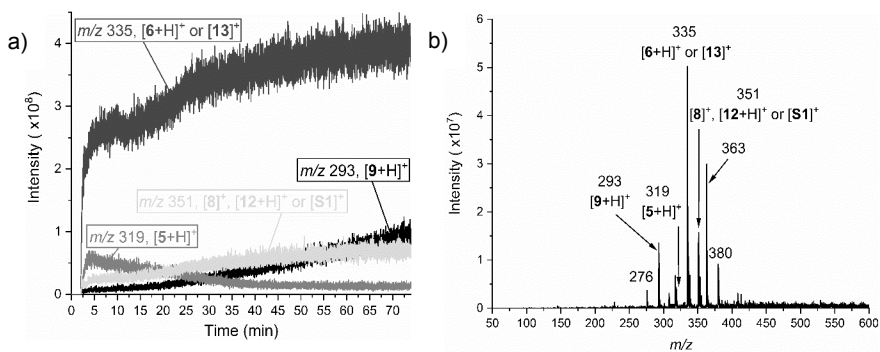


Figure 12 a) Extracted ion profiles of mass-to-charge ratio m/z 319 ([5+H]⁺), m/z 335 ([6+H]⁺ or [13]⁺), m/z 351 ([8]⁺, [12+H]⁺ or [S1]⁺), and m/z 293 ([9+H]⁺) obtained during the online reaction experiment. b) An averaged mass spectrum of the reaction mixture at 71–72 min. Figures adapted from the original publication III[29] with permission from the American Chemical Society.

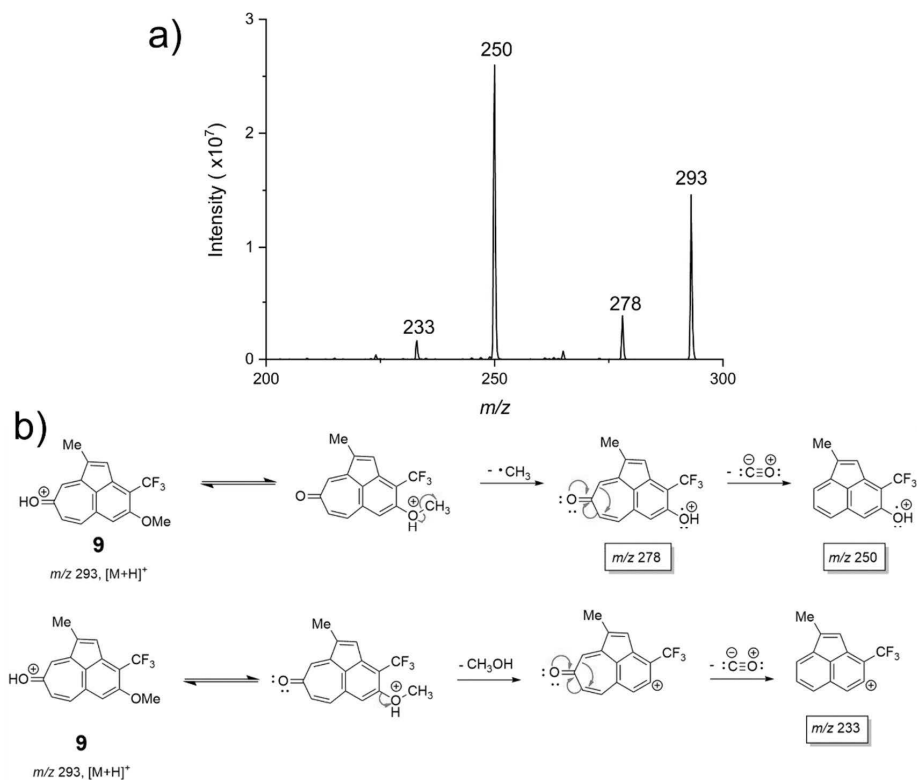
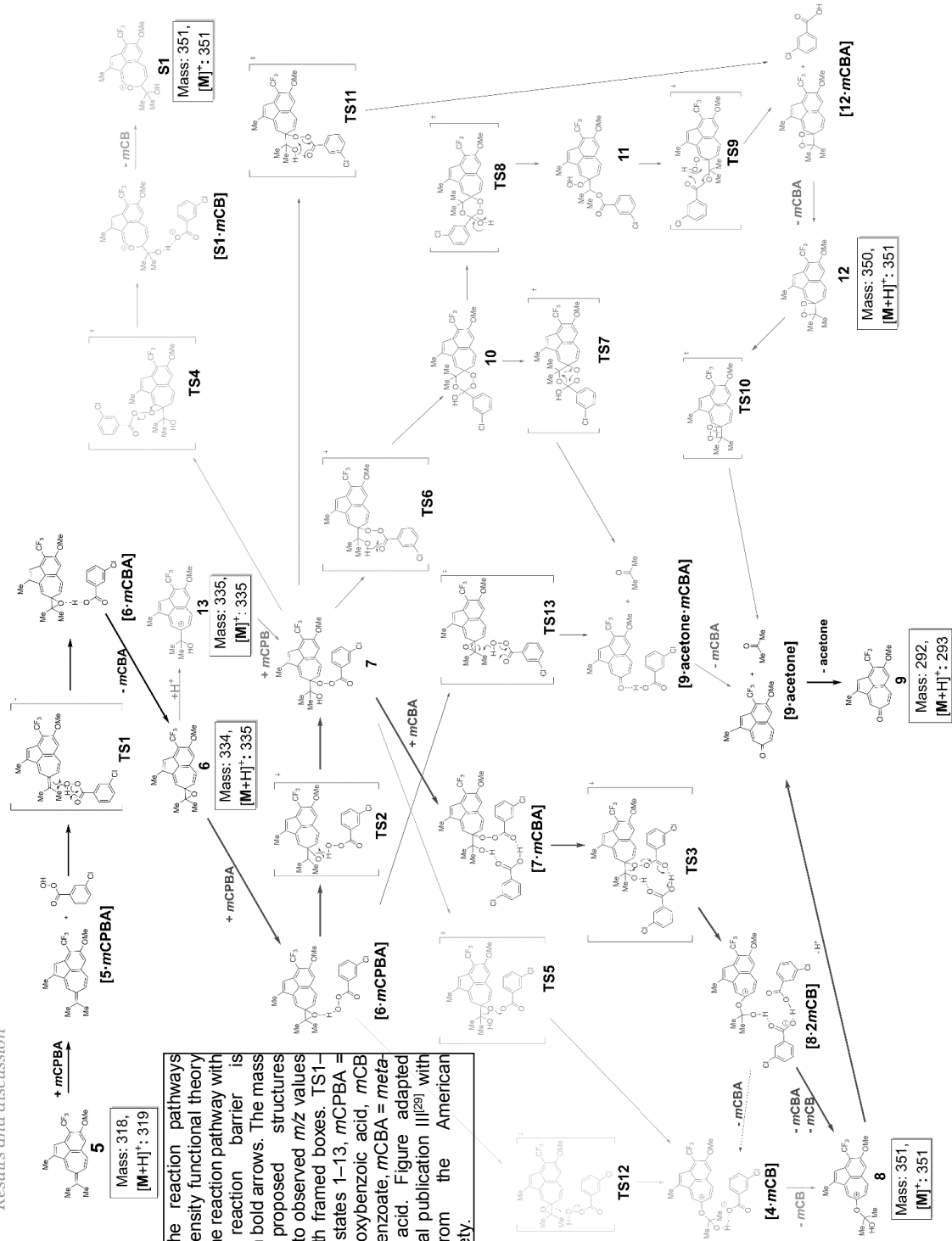


Figure 13 a) MS/MS spectrum of the precursor ion m/z 293, and b) proposed fragmentation scheme of the precursor ion m/z 293. Figures adapted from the original publication III[29] with permission from the American Chemical Society.



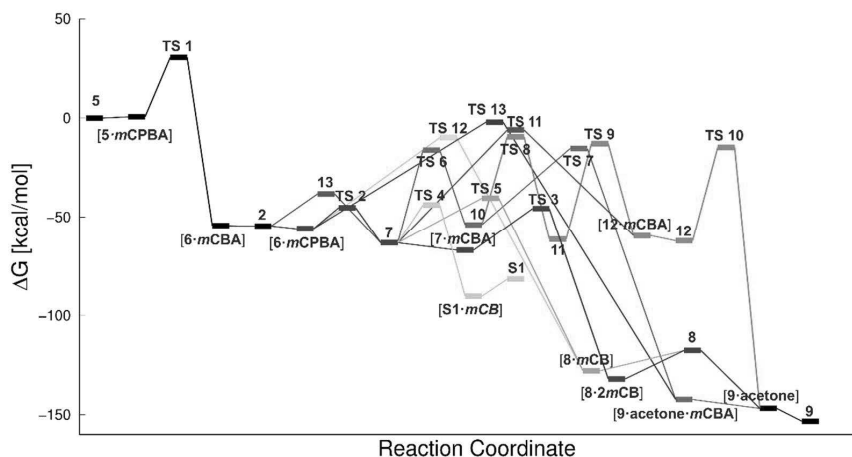


Figure 14 A summary of the Gibbs free energies of each mechanistic step. The colors of the plots correspond to the respective colors of the structures proposed in Scheme 7. TS1–13 = transition states 1–13, *mCPBA* = *meta*-chloroperoxybenzoic acid, *mCB* = *meta*-chlorobenzoate, *mCBA* = *meta*-chlorobenzoic acid. Figure adapted from the original publication III^[29] with permission from the American Chemical Society.

Table 6 An overview of the reaction pathways investigated by density functional theory (Scheme 7). The pathways are listed according to sequentially higher energy. All reaction pathways start with **5**, [**5·mCPBA**], **TS1**, [**6·mCBA**], and **6**, and merge to [**9·acetone**] and **9**. TS1–13 = transition states 1–13, *mCPBA* = *meta*-chloroperoxybenzoic acid, *mCB* = *meta*-chlorobenzoate, *mCBA* = *meta*-chlorobenzoic acid.

Reaction pathway	Pathway color	Species included in the pathway, other than the shared ones
Acid-catalyzed exocyclic Criegee rearrangement	Blue	[6·mCPBA], TS2 , 7 , [7·mCBA], TS3 , [8·2mCB], 8
Endocyclic Criegee rearrangement*	Turquoise	[6·mCPBA], TS2 , 7 , TS4 , [S1·mCB], S1
Non-acid-catalyzed exocyclic Criegee rearrangement	Orange	[6·mCPBA], TS2 , 7 , TS5 , [8·mCB], 8
1,2,4-Trioxane cycloreversion	Dark green	[6·mCPBA], TS2 , 7 , TS6 , 10 , TS7 , [10·acetone·mCBA]
1,2-Dioxetane formation	Pink	[6·mCPBA], TS2 , 7 , TS6 , 10 , TS8 , 11 , TS9 , [12·mCBA], 12 , TS10
Peroxide metathesis	Purple	[6·mCPBA], TS2 , 7 , TS11 , [12·mCBA], 12 , TS10
Tropylium formation	Red	13 , 7 , [7·mCBA], TS3 , [8·2mCB], 8
Oxidative epoxide opening	Light green	[6·mCPBA], TS12 , [8·mCB], 8
Concerted reaction	Brown	[6·mCPBA], TS13 , [9·acetone·mCBA]

* This reaction pathway does not merge to [**9·acetone**] and **9**.

The first step of all pathways is the *m*CPBA epoxidation of the exocyclic carbon-carbon double bond of heptafulvene **5**, forming compound **6**, via transition state **TS1**. In its protonated form (**[6+H]⁺/[13]⁺**), this epoxide can be observed as an ion with *m/z* 335. Following the acid-catalyzed exocyclic Criegee rearrangement pathway, a bimolecular nucleophilic substitution (S_N2) reaction with concerted proton transfer between the epoxide oxygen of **6** and the peroxy-carboxyl moiety of a second equivalent of *m*CPBA next occurs (**TS2**), forming intermediate **7**.

Intermediate **7** can then undergo a rearrangement catalyzed by *meta*-chlorobenzoic acid (**TS3**), forming **[8·2mCB]**. Dissociation of *meta*-chlorobenzoate (*m*CB) and *meta*-chlorobenzoic acid (*m*CBA) produces **8**, which has a positive charge delocalized over the tropylium ring system. This ion corresponds to *m/z* 351. Finally, **8** can undergo barrierless dissociation into the tropone product (**9**) and the by-product acetone.

As mentioned above, three structures were investigated for the ion observed at *m/z* 351, namely the reaction intermediates **[8]⁺** and **[12+H]⁺** and the reaction by-product **[S1]⁺**. In a previous study, a reaction related to the one investigated here (using the 4-hydroxy analogue of heptafulvene **5** as starting material) was studied offline using micropillar array ESI-MS^[41]. There, the ion corresponding to *m/z* 351 was suggested to be a reaction by-product. The observation that the EIP of *m/z* 351 appears to stabilize over time in the present study (Figure 12a) indicates, however, this ion to be a reaction intermediate. Furthermore, the fragmentation pattern of the precursor ion *m/z* 351 matches both potential reaction intermediate structures **[8]⁺** and **[12+H]⁺** (Figure 15). Finally, as the blue acid-catalyzed exocyclic Criegee rearrangement has the lowest overall energy barrier (Figure 14), this suggests the ion at *m/z* 351 to be a reaction intermediate with the structure **[8]⁺** (Scheme 7). Overall, the oxidation of **5** to **9** could be summarized to follow a Hock-like mechanism^[147], which is characterized by hydroperoxides with substituents having delocalized electrons.

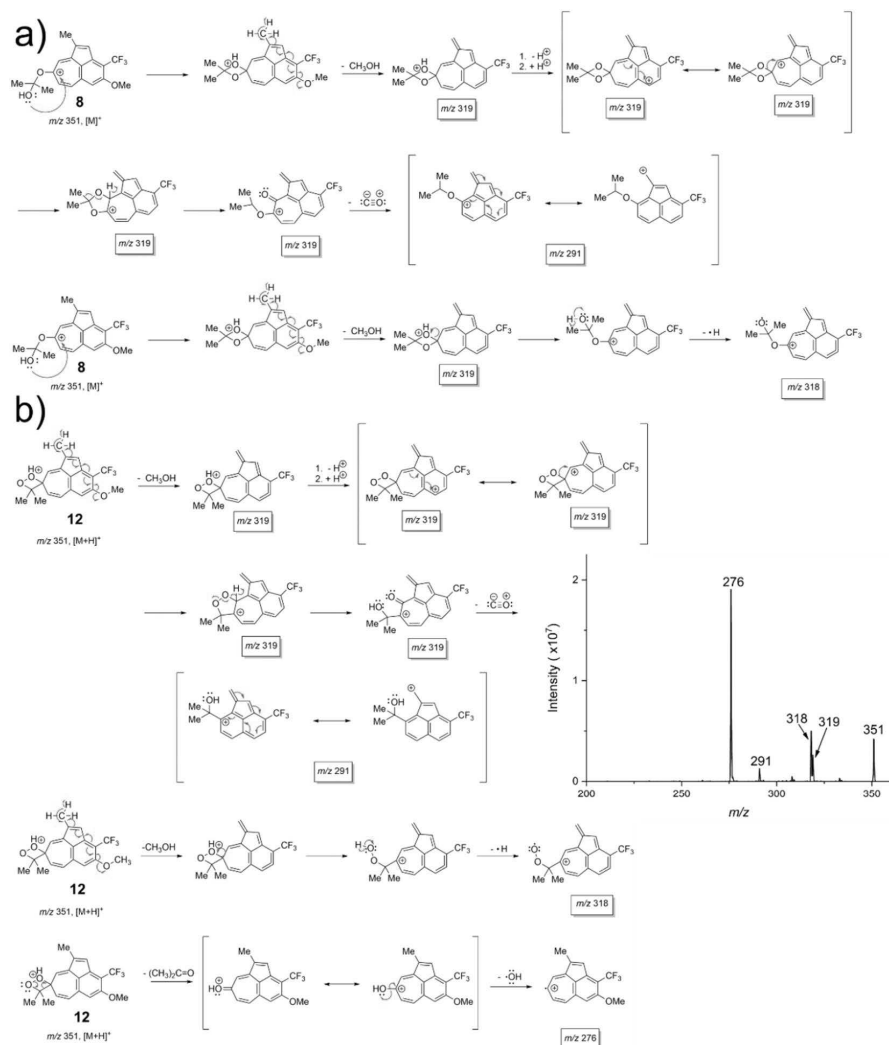


Figure 15 Proposed fragmentation scheme of the precursor ion m/z 351. The structures shown in (a) assume the precursor ion structure $[8]^+$ for m/z 351, while the structures shown in (b) assume the precursor ion structure $[12+\text{H}]^+$ for m/z 351. A MS/MS spectrum, obtained by isolating and fragmenting the precursor ion m/z 351 is shown in the inset. Figures adapted from the original publication III^[29] with permission from the American Chemical Society.

5.1.3 A 3D PRINTED MINIATURIZED GLASS REACTOR FOR ONLINE STUDY OF AN ACETYLATION REACTION

Here, the miniaturized reactor (Figure 4c) was coupled directly to a commercial ESI source. This was done by connecting the outflow of the reactor to a commercial ion source through silica capillaries, glued to the outlet of the reactor. (5*S*)-5-(Aminomethyl)-3-[3-fluoro-4-(4-morpholinyl)phenyl]-1,3-oxazolidin-2-one (**14**, Scheme 5), dissolved in acetonitrile, was infused through inlet a (Figure 4c), and acetic anhydride (**15**, Scheme 5), dissolved in

acetonitrile, was infused through inlet b (Figure 4c) for online analysis of an acetylation reaction, namely the last step in the synthesis of the drug linezolid (Scheme 5). The data presented in Figure 16 are from an experiment in which the initial reagent flow rate of 4 $\mu\text{L}/\text{min}$ per reagent (total flow 8 $\mu\text{L}/\text{min}$) was decreased in two steps, first to 1.6 $\mu\text{L}/\text{min}$ per reagent (total flow 3.2 $\mu\text{L}/\text{min}$) and then down to 750 nL/min per reagent (total flow rate 1.5 $\mu\text{L}/\text{min}$). Mass spectra using the total reagent infusion flow rate 8 $\mu\text{L}/\text{min}$ and 1.5 $\mu\text{L}/\text{min}$ are presented in Figure 16a and Figure 16b, respectively. The mass spectra in Figure 16 show protonated molecules of both reagent **14** and the final product **16** at m/z 296 and m/z 338, respectively. Additional reaction-related ions present in the mass spectra in Figure 16 include the ions m/z 241, a fragment of m/z 296 formed in the ionization process; m/z 360, $[\mathbf{16}+\text{Na}]^+$; m/z 633, $[\mathbf{14}+\mathbf{16}+\text{H}]^+$; and m/z 675, $[\mathbf{16}+\mathbf{16}+\text{H}]^+$. The mass spectra presented in Figure 16 indicate that the intensity of the protonated linezolid reaction product $[\mathbf{16}+\text{H}]^+$ (m/z 338), increases in relation to the protonated reagent $[\mathbf{14}+\text{H}]^+$ (m/z 296), as the reaction time increases, as a consequence of the decreased reagent infusion flow rate. Offline APCI-MS experiments (data shown in Publication IV) support this observation. MSⁿ mass spectra and tentative fragmentation routes for the precursor ion m/z 338 are presented in Figure 17. The product ions observed in Figure 17 agree with previously reported m/z ratios^[148] for the same precursor ion. Additionally, the fact that the product ion mass spectra displayed in Figure 17 agree with product ion mass spectra obtained when fragmenting the corresponding precursor ion (m/z 338) in samples of pure linezolid (data shown in Publication IV) further support the identity of m/z 338 ($[\mathbf{16}+\text{H}]^+$) in the reaction mixture mass spectra (Figure 16). Finally, good correlation between the MS/MS mass spectrum of the precursor ion m/z 296 ($[\mathbf{14}+\text{H}]^+$) measured for the ion observed in the reaction solution and the MS³ spectrum of the precursor ion m/z 296 formed as a fragment of the precursor ion m/z 338 ($[\mathbf{16}+\text{H}]^+$, data shown in Study IV) further substantiates the interpretation of the identities of these ions seen in the reaction mixture mass spectrum.

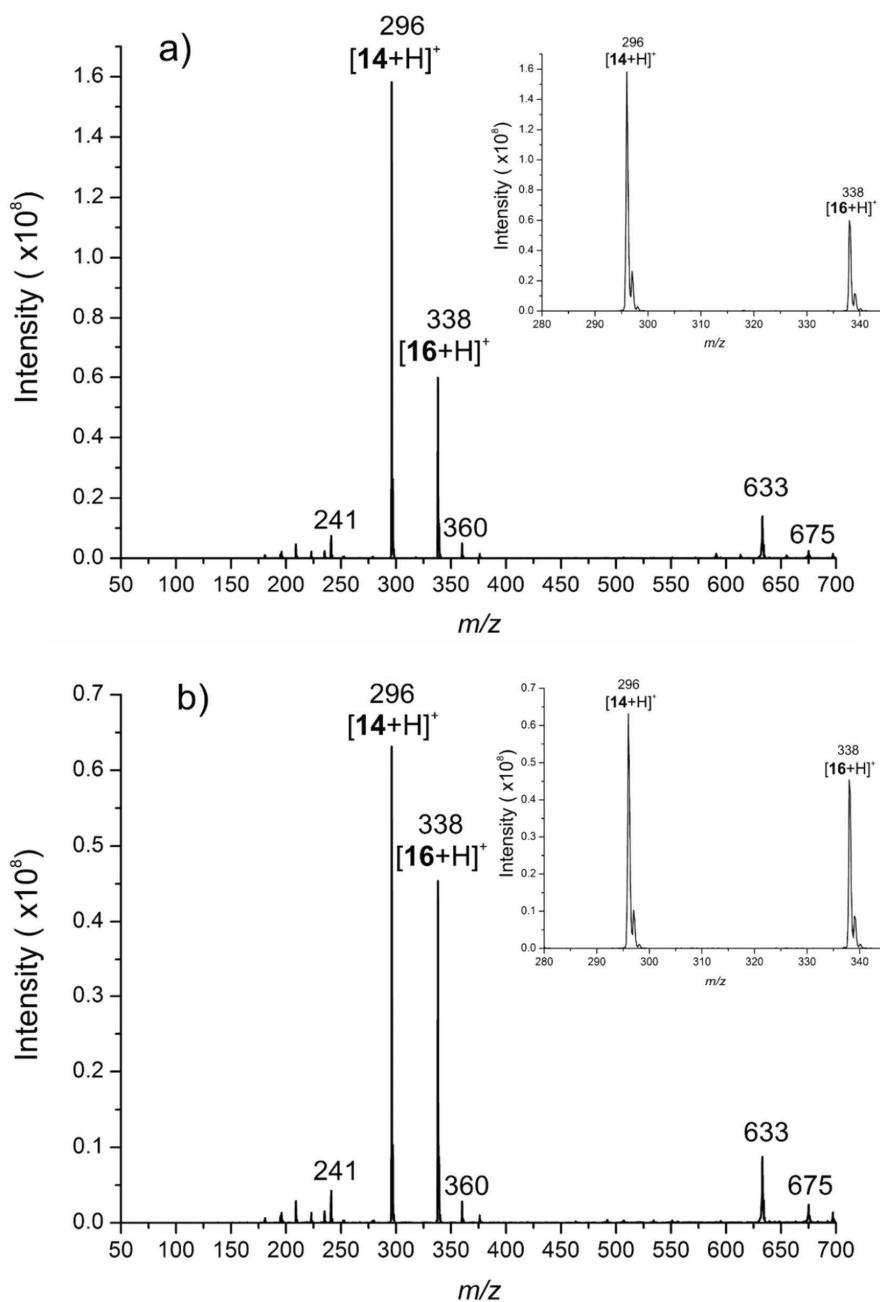


Figure 16 Mass spectra averaged over 1 min at the reactant infusion flow rate (a) 4 $\mu\text{L}/\text{min}$ per reactant (total flow 8 $\mu\text{L}/\text{min}$), and (b) 750 nL/min per reactant (total flow 1.5 $\mu\text{L}/\text{min}$). The insets display the same spectra as the full m/z scan range spectra, but only in the m/z range where the analytes of interest ($[14+H]^+$ at m/z 296 and $[16+H]^+$ at m/z 338) are present. Figure adapted from the original publication IV^[30] with permission from the Royal Society of Chemistry.

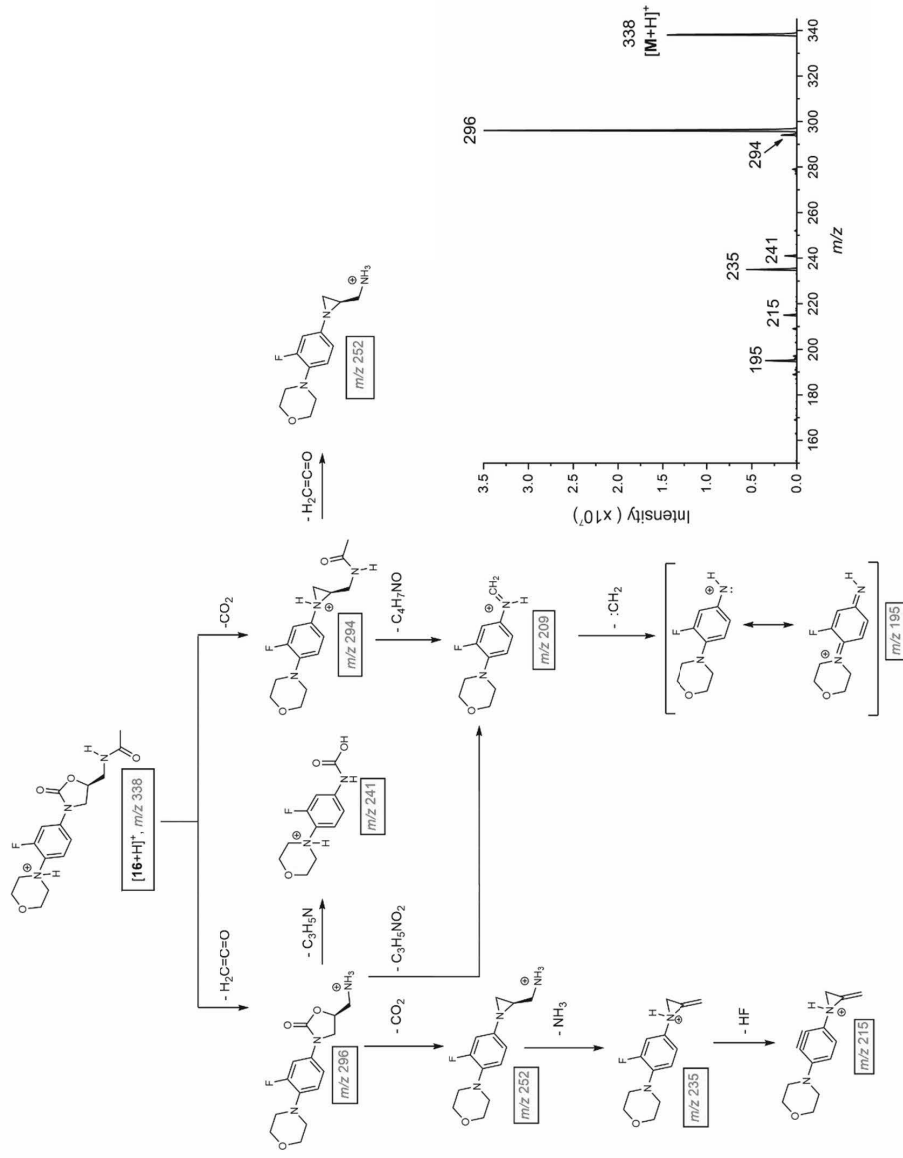


Figure 17 Proposed fragmentation routes of the protonated final product linezolid, m/z 338. MS/MS spectrum obtained when fragmenting the precursor ion m/z 338 with the fragmentation amplitude 0.35 V is shown in the inset. M = 16. Figure adapted from the original publication IV^[30] with permission from the Royal Society of Chemistry.

5.2 COMPARISON OF MINIATURIZED REACTORS AND THEIR SUITABILITY FOR COUPLING TO MASS SPECTROMETRY FOR REACTION MONITORING

In this thesis, reactors obtained through the following three different additive fabrication techniques were used: fused deposition modeling (FDM), laser additive manufacturing (LAM), and 3D printing of melted glass. As already demonstrated in Ch. 5.1, where the coupling of the reactors to MS is discussed, the various fabrication techniques and materials, and, as a consequence, the produced devices gave rise to varying challenges for online coupling to MS for studying reactions. Namely, the reactor used in Studies I and III, which was fabricated from polypropylene by fused deposition modeling, exhibited quite poor printing resolution, resulting in rough reactor surfaces (Figure 18a). It is well-known that FDM yields only relatively poor printing resolution (the obtainable resolution is at best 10 μm) compared with other 3D printing techniques^[149], resulting in the fabricated objects typically having relatively rough surfaces^[150]. This a limitation in, for example, analytical and synthetic chemistry applications, as it may lead to memory effects. Furthermore, microchannels fabricated by FDM typically have dimensions of a few hundred micrometers^[150].

Also the reactor channel of the microreactor used in Study II was of low printing resolution (Figure 18b). The reason for this was that the stainless steel powder used to fabricate the device had a relatively large diameter (median 31 μm) as well as a large variation in the range of particle diameter (20–50 μm), which naturally impacted the smoothness of the structures produced. The rough reactor channel walls of the stainless steel reactor may have resulted in absorption of analytes to the reactor walls, providing a plausible explanation for the detection of reactants when infusing the background solution (Figure 6a, 0–16 min), as well as for the variance in time from injection of analytes until MS detection of the related ions in Study II. Non-uniform filling of the mixing chamber of the stainless steel reactor, consisting of parallel channels (Figure 4b), may also have contributed to the latter. The adsorption of compounds to the reactor walls might be alleviated by fabrication of smoother reactor surfaces, which should be attainable by optimizing the LAM process and use of stainless steel powder with smaller particle size, or by coating the reactor channel walls with, for example, a silica-based material^[151].

In contrast, it is easily seen that the surface of the channel of the glass reactor used in the online reaction monitoring in Study IV is smooth (Figure 18c), except that there is undulation of the reactor channel wall, which most likely is due to the glass layer thickness.

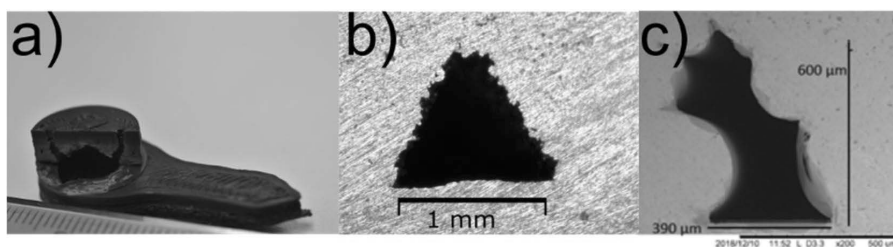


Figure 18 Inner surfaces of the used reactors. a) A photograph of the polypropylene reactor, used in Studies I and III. At the bottom of the picture, the millimeter scale of a ruler is shown to give an estimate of the dimensions, b) an optical micrograph of the stainless steel reactor, used in Study II (figure reproduced from the original publication II^[28] with permission from Elsevier), and c) a SEM picture of the reactor used in Study IV (figure reproduced from the original publication IV^[30] with permission from the Royal Society of Chemistry).

These visual observations were supported by measurements of the root mean square (RMS) roughness of the glass reactor (Study IV), and a reference device for the stainless steel reactor that was fabricated using the same LAM method and apparatus (Study II). A stylus profilometer was used for performing these measurements. The RMS of the reference device for the reactor in Study II was measured in a previous work^[152] to be $R_q = 16.4 \mu\text{m}$. On the other hand, the surfaces of the devices presented in Study IV were smooth – when scanning the outer glass surface of a device over $400 \mu\text{m}$ at 10 different spots, the average roughness, R_a , and RMS roughness, R_q , were 47 nm (standard deviation 17 nm) and 58 nm (standard deviation 22 nm), respectively. For the reactor used in Studies I and III, no investigation of the roughness of the reactor surface was done. However, the estimated surface area to volume ratio of the polypropylene reactor (used in Studies I and III) is approximately four times smaller than that of the stainless steel reactor (used in Study II), and about ten times smaller than the estimated surface area to volume ratio of the glass reactor (used in Study IV). Due to this, the roughness of the surface of the reactor used in Studies I and III is likely of less impact on the online monitoring results than in the experiments presented in Studies II and IV (see Figure 4 for presentations of the reactor designs).

Integration of the reactors with MS detection was successful in all cases. However, the different reactors posed various levels of challenges. In the case of Studies I and III, the process of obtaining ESI-MS was relatively straightforward thanks to the nano-ESI needle integrated at the reactor outlet. This was also the case in Study IV, where the outflow of the reactor was conducted to a commercial ESI-MS source by a silica capillary. In the case of Study II, integration of ESI-MS with the reactor was also achieved. However, this was more challenging than was the case for the reactors used in Studies I, III, and IV due to the need to combine the manually sharpened reactor tip with a droplet at the tip to obtain ESI. This use of a droplet at the reactor tip resulted in a volume increase, additional to the reactor channel, which could not be precisely controlled. It is thus not possible to discriminate between reactions occurring in the reactor channel, in the solvent droplet at the reactor tip, and in the ESI process. The fabrication of a better defined reactor channel exit hole

might eliminate the need for a droplet at the tip of the reactor, and thus, the related limitations.

Occurrence of reactions proposed to take place in the ESI process was, however, also observed when the inverse electron-demand Diels-Alder and retro Diels-Alder reaction was studied in Study I (here, however, the species proposed to be formed in the ESI process were only observed to a relatively small extent) and in Study III, where oxidized species of the reactant **5** were observed when analyzing it alone with ESI-MS. This highlights the importance of controlling the purity of analytes with several analytical methods, e.g. LC-MS, NMR spectroscopy, and thin-layer chromatography (TLC), to take measures to minimize occurrence of reactions in the ionization process (if not desired), as well as to conduct experiments exploring whether reactions to be studied occur in the reactor or at other sites (e.g. in the ionization process) of the system.

5.3 DEVELOPMENT OF MOLECULARLY IMPRINTED POLYMERS FOR ENANTIOSELECTIVE TRANSAMINATION

The nine MIP systems prepared (Table 5) were characterized with respect to their physical (SEM imaging) and chemical (FTIR experiments) characteristics, as well as their recognition properties (investigated by FIA-QCM analysis) with regard to compounds related to the transamination reaction (Scheme 6).

Presence of long-range ordered interconnected networks of pores (Figure 19) replicating the layers of sacrificial self-assembled polystyrene (PS) beads were confirmed by SEM analysis. The well-ordered pores seen in Figure 19a and Figure 19c indicate that the integrity of the polymer-PS bead assemblies mainly remain intact throughout the polymerization process. As expected, the polymer films prepared in the absence of PS beads (P2, P5, P8, and P9, Table 5) lacked macroporous structures. A SEM image of P5, being representative of the polymer structure of all polymers prepared in the absence of PS beads, is shown in Figure 19b. Comparison of the SEM images of P4, prepared using the porogen *n*-heptane and PS beads, and P6, using no porogen, revealed that P6 resulted in a polymer network that was moderately more regularly structured (Figure 19c compared with Figure 19a). This is likely due to more intimate connections arising between the PS beads and the functional monomers in the latter.

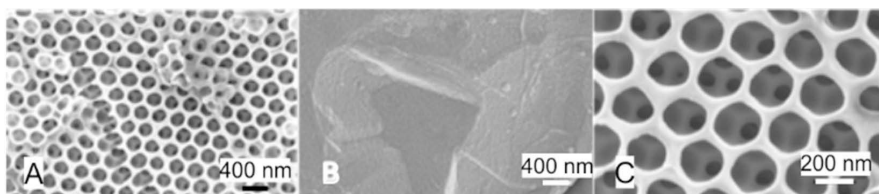


Figure 19 SEM images of polymer systems imprinted with L-TSA, prepared in a) the presence of polystyrene beads and the porogen *n*-heptane (P4), b) the presence of *n*-heptane, but the absence of polystyrene beads (P5), and c) the presence of polystyrene beads, but the absence of *n*-heptane (P6). Figures adapted from the original publication V⁽¹⁵³⁾ with permission from the Royal Society of Chemistry.

An important objective of studying the polymers with FTIR was to confirm the inclusion of PS beads in them (polymer systems P1, P3, P4, P6, and P7) before the toluene wash, and the absence of the beads after extraction with toluene. In terms of bands expected to arise from the components included in all polymer films prepared (i.e. from the functional monomer and crosslinker), bands $\nu\text{C}=\text{O}$ (1710 cm^{-1}), $\delta\text{C}-\text{H}$ (1455 cm^{-1}), $\nu\text{C}-\text{O}$ (1250 and 1145 cm^{-1}), $\rho\text{C}-\text{H}$ (750 cm^{-1}), and $\nu\text{C}-\text{H}$ (2920 cm^{-1}) were present (Figure 20a). This observation supports that both the presence and the removal of PS beads do not have a significant impact on the chemical properties of the MIPs. The absence of PS beads after toluene extraction is indicated by disappearance of bands associated with PS, especially overtones found at $1800\text{-}2000\text{ cm}^{-1}$ after this washing step (Figure 20b, section marked with boxes).

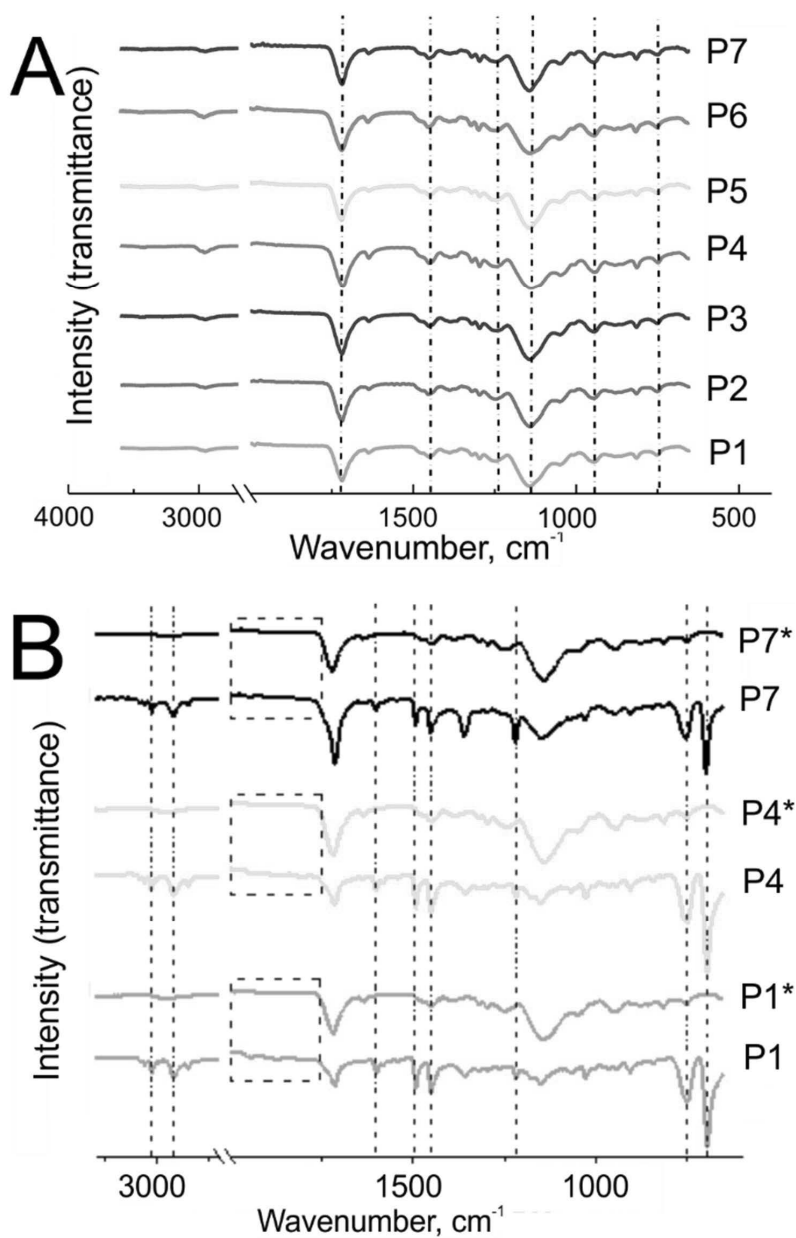


Figure 20 a) FTIR spectra of the polymer systems P1-P7 after wash with ethanol, toluene, and a 5 mM solution of NaOH in water. The interesting bands are marked: $\rho\text{C-H}$ (750 and 900 cm^{-1}), $\nu\text{C-O}$ (1145 and 1250 cm^{-1}), $\alpha\text{C-H}$ (1455 cm^{-1}), and $\nu\text{C=O}$ (1710 cm^{-1}), b) FTIR spectra of the polymer systems P1, P4, and P7 before and after (*) washing in toluene to remove polystyrene beads. The bands characteristic for polystyrene are marked: $\rho\text{C-H}$ (696 and 752 cm^{-1}), δ (C-H) (1216 cm^{-1}), $\nu\text{C=C}$ (1449, 1492 and 1602 cm^{-1}), and $\nu\text{C-H}$ (2922 and 3025 cm^{-1}). Overtones characteristic for polystyrene, at 1800-2000 cm^{-1} , are highlighted within the boxes. Figures adapted from the original publication $V^{[153]}$ with permission from the Royal Society of Chemistry.

Next, the recognition properties of the polymer-coated resonators were explored by FIA-QCM analysis (Figure 21). First, the polymers' recognition of L-TSA and D-TSA was investigated by injecting various concentrations of these analytes, dissolved in a 1:1 solution of methanol:0.1 M solution of sodium acetate in H₂O (pH 7.0) on the systems. In these experiments, we observed that the polymer film P4, imprinted with L-TSA and prepared in the presence of PS beads and *n*-heptane, showed a clear selectivity for L-TSA over its enantiomer, while no significant enantioselectivity was observed in the case of the non-imprinted P1. To support this hypothesis, the polymer P7, which used D-TSA as a template and was prepared with the porogen *n*-heptane and sacrificial bead scaffold, proved to exhibit selectivity for the D-TSA over L-TSA – the opposite selectivity behavior to that observed for P4. The importance of the PS sacrificial bead scaffold, and even the presence of porogen, on the capacity and enantioselectivity of the polymers was clear in comparing the imprinted and non-imprinted polymers prepared in the absence of the bead scaffold, P2 and P5, or the porogen, P3 and P6. For these polymers, no significant template enantioselectivity was observed. This highlights the synergistic impact of the porogen and sacrificial bead scaffold-induced interconnected pores on access to template-selective binding sites. Polymer films containing neither porogen nor sacrificial PS beads (zero polymers P8 and P9) demonstrated low levels of binding and sensitivity for the TSAs relative to system P4, which reveals the expected lack of accessible sites. These results further substantiated the effectivity of combining the PS beads and porogen for creating accessible binding sites for template binding.

Finally, the selectivity of the polymer films towards the reactants and products for transamination reaction (Scheme 6) was assayed. The TSAs showed stronger binding for all of the systems. This is probably due to the fact that they, compared with the other analytes, have a greater number of functional groups and two aromatic rings, which are able to contribute to both the TSA-selective and non-specific binding through a combination of electrostatic and hydrophobic binding interactions. The other analytes showed lower non-specific binding. It is worth noting that phenylpyruvic acid exhibited a higher degree of selectivity for the hyperporous TSA-imprinted polymers, P4 and P7, than for the other polymers. This suggests that phenylpyruvic acid accesses the binding domains arising from the TSA's aromatic rings, which is an advantageous process in the aqueous rebinding media. The selectivity behavior of the polymers observed in Study V generally agrees with the selectivity data previously reported for the corresponding bulk polymers prepared in the absence of PS beads, using the porogen chloroform^[23].

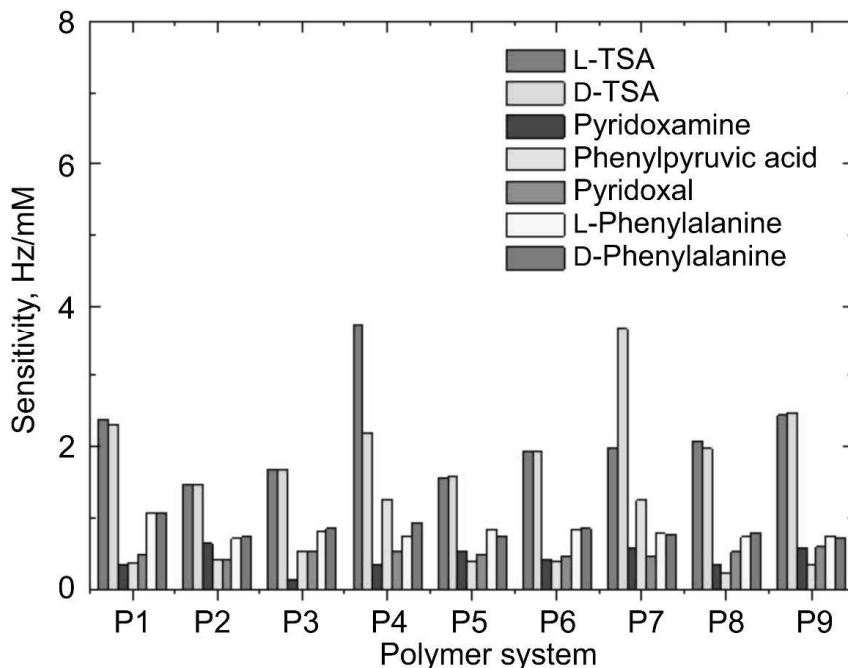


Figure 21 Histogram of sensitivity of polymer systems P1-P9 (Table 5) obtained from the slope of the FIA calibration plots upon injection of various analytes. Figures adapted from the original publication V^[153] with permission from the Royal Society of Chemistry.

6 SUMMARY, ASSESSMENT OF LIMITATIONS, AND OUTLOOK

The research behind this thesis had three goals: 1) coupling of miniaturized devices to MS for reaction monitoring and evaluation of the experimental setup, 2) reaction mechanism investigation combining online MS and DFT, and 3) preparation and investigation of MIP systems for enantioselective transamination reaction.

Three different miniaturized devices, fabricated by additive manufacturing, were coupled to MS for reaction monitoring. As demonstrated in Ch. 5.1-5.2 above, the experimental systems developed, consisting of a miniaturized device and MS, work sufficiently for online analysis of reactions. However, the results simultaneously highlight that this field of research is still under development; as discussed in Ch. 5.2, the manufacturing techniques were not always ideal for fabricating miniaturized devices for online coupling to MS for reaction studies (particularly evident in the case of the stainless steel reactor used in Study II). However, as the main method for fabricating miniaturized fluidic devices traditionally has been “subtractive fabrication” (in contrast to additive), which has to be carried out in clean rooms^[128], the availability of miniaturized fluidic devices has hitherto been limited due to restricted access to clean rooms, high fabrication cost, and typically a requirement for highly trained personnel. The fabrication method used for producing the miniaturized devices in Studies I-IV, additive fabrication, addresses all of these points, providing relatively inexpensive and rapid means for fabricating miniaturized fluidic devices, using technology that typically is easily accessible and generally requires less user training than subtractive manufacturing. Furthermore, as 3D printing enables a much faster testing cycle and prototyping than subtractive techniques,^[154] this allows rapid testing of several different device designs and the correction of possible design flaws for the next fabrication cycle. Furthermore, as the fabrication cycle of additive manufacturing is considerably cheaper than the cycle of subtractive manufacturing,^[155] it is economically justified to use the 3D printed systems as disposable devices, which may eliminate the limitations connected to memory effects (especially observed in Study II). In conclusion, the microreactors presented in Studies I-IV represent clear progress relative to the established techniques (namely subtractive fabrication) in terms of accessibility and simplicity of fabrication.

When coupling the miniaturized devices to MS for reaction monitoring, it was observed that it was challenging to find concentration ranges suitable for analysis. The concentration ranges used in the online reaction experiments in this thesis are relatively high (tens to hundreds of μM) compared with typical MS conditions (typically a few nM- μM , although concentrations as low as fM have been detected with MS for certain analytes^[156]). This, on one hand,

resulted in a high degree of contamination of the MS (which necessitated frequent MS cleaning) and the miniaturized devices used, and might also have contributed to memory effects in cases where miniaturized devices with rough inner surfaces were used (see discussion in Ch. 5.2). Also, high analyte concentrations can, especially in ESI, result in ion suppression.^[91] As ESI was the ionization technique used in all online reaction studies presented in this thesis, it would have been beneficial to rule out this possibility by e.g. additional reaction studies with a different ionization technique or by evaluating the signal-concentration relationship of specific ions in separate offline experiments^[157]. The later measurements are not that easy to perform since pure reference compounds of all the reaction constituents would be needed^[91]. However, it has been shown that the main cause of ion suppression is a change of the solution properties of the spray droplets (typically caused by the presence of non-volatile or less volatile analytes).^[158] As the analytes studied in each reaction in Studies I-IV had similar properties, this should have decreased the likelihood of changes of the solution properties of the spray droplets, and thus, the risk of ion suppression.

On the other hand, the reactant concentrations used were already rather low compared with typical synthetic chemistry conditions, which limited the reactions that could be studied using the time frame dictated by the volume of the reactors and the reactant infusion flow rate at which stable electrospray could be obtained (as, generally, lower concentrations lead to lower reaction rates^[159]). Of note, the concentrations of reactants used in Studies I-IV were similar or slightly lower than those found in other published studies using reactors coupled online to ESI-MS (Table 1)^[31,46,59–61,63,65,68,70,72–79]. This indicates that finding concentration ranges suitable from both synthesis and detector points of view in reaction time frames accessible with miniaturized devices is a general challenge when working with miniaturized devices coupled online to MS. A documented strategy to enable combination of higher analyte concentrations in the miniaturized device, while only allowing limited amounts of analytes to reach the detector include e.g. connecting the outlet of the reactor to a T-junction infusing a diluting solvent that mixes with the outflow of the reactor before it reaches the detector, as employed by e.g. Mathieson *et al.*^[31]. Future developments of miniaturized devices that may help to overcome the high concentrations of reactants could focus on a number of strategies, including:

- Integration of a dilution functionality in the reactor system, aiming to dilute the reactant solution before it reaches the detector.
- Addition of features to optimize the reaction conditions for the studied reaction such as heating, cooling, improved mixing, or catalysis features in the reactor. Optimization of the reaction conditions may enable lower concentrations of reactants to be used without compromising the yield or rate of the reaction.
- Fabrication of reactors with larger reactor volume and/or use of a decreased reactant infusion flow rate. Both these strategies bring longer

reaction times, which may make it possible to decrease the reactant concentrations and still obtain significant progress of the reaction within the defined time frame.

In addition to the above-proposed developments of miniaturized systems for online coupling to MS, the use of a robust MS, dedicated only to reaction studies could make it more acceptable to use reactant solutions of higher concentrations.

The reactions studied in Studies I, II, and IV were of proof-of-concept type, to test the suitability of the fabricated reactor for combination with MS for reaction monitoring. This aligns the results presented here well with most works already published in this field^[1] (Table 1). When it comes to studying novel reaction mechanisms with MS, this has not typically been done using microreactors, but rather by containing the reaction mixture in a syringe for continuous infusion into the MS, or by offline sampling^[14], or by use of T-junctions coupled to MS^[51–56]. However, in Study III, the focus was to a greater extent on investigating the mechanism of a chemical reaction, rather than establishing a new experimental setup. As the experimental investigations in Study III, furthermore, were combined with theoretical (DFT) studies, the concept of using miniaturized reactors coupled online to MS for reaction mechanisms was further developed – at the time of writing, no reports of the combination of miniaturized reactor-coupled MS and computational chemistry for reaction mechanism studies has been published.

When it comes to MIPs, the work presented in this thesis is of rather fundamental nature. Specifically, techniques and systems previously established, namely the use of MIPs imprinted with the transition state analogue L-TSA or D-TSA to steer the enantioselectivity of a transamination reaction (Scheme 6)^[23], and inclusion of PS beads to obtain a MIP system with ordered pores^[160], were applied and combined for the first time. The developed porous MIP systems (P4 and P7, Table 5) were shown to be selective with respect to the employed TSA. Furthermore, the synthesis of the polymers on top of PS beads, which left behind regular pores in the polymers when extracted, means that these systems would be suitable for introduction into miniaturized devices, for which active site density and mass transfer are crucial.

In summary, the 3D printed miniaturized devices interfaced with MS presented here highlight the feasibility of this set-up for monitoring reaction mechanisms online. However, it is clear that this field is still under development both regarding the suitability of the 3D printed devices for this objective and considering the reaction conditions that are applicable for online-MS analysis. Due to characteristics of the ionization technique used in all online-MS experiments, it would be interesting in the future to complement the experiments presented herein with investigations using other ionization techniques, mass analyzers, and possibly even other detection (e.g. online with MS) techniques. In any case, the work presented here demonstrates significant advances in the use of miniaturized devices coupled online to MS for reaction

studies, and especially combining this approach with DFT for reaction studies is an entirely novel concept. Also the application of MIPs in enantioselective synthesis is advanced by the work presented in this thesis. Based on the results presented here, especially the possibility to combine miniaturized reactors and MIPs in the future is promising.

REFERENCES

- [1] A. Ray, T. Bristow, C. Whitmore, J. Mosely, *Mass Spectrom. Rev.* **2018**, *37*, 565–579.
- [2] P. Watts, C. Wiles, *Chem. Commun.* **2007**, 443–467.
- [3] K. Jähnisch, V. Hessel, H. Löwe, M. Baerns, *Angew. Chem., Int. Ed.* **2004**, *43*, 406–446.
- [4] M. Brivio, W. Verboom, D. N. Reinhoudt, *Lab Chip* **2006**, *6*, 329–344.
- [5] R. L. Hartman, K. F. Jensen, *Lab Chip* **2009**, *9*, 2495–2507.
- [6] R. Porta, M. Benaglia, A. Puglisi, *Org. Process Res. Dev.* **2016**, *20*, 2–25.
- [7] P. Watts, S. J. Haswell, *Drug Discovery Today* **2003**, *8*, 586–593.
- [8] A. Gioiello, *Chim. Oggi* **2017**, *35*, 8–10.
- [9] G. Nys, M. Fillet, *J. Pharm. Biomed. Anal.* **2018**, *159*, 348–362.
- [10] D. Fabris, *Mass Spectrom. Rev.* **2005**, *24*, 30–54.
- [11] G. L. Glish, R. W. Vachet, *Nat. Rev. Drug Discovery* **2003**, *2*, 140–150.
- [12] H. Awad, M. M. Khamis, A. El-Aneed, *Appl. Spectrosc. Rev.* **2015**, *50*, 158–175.
- [13] M. Haapala, L. Luosujärvi, V. Saarela, T. Kotiaho, R. A. Ketola, S. Franssila, R. Kostiaainen, *Anal. Chem.* **2007**, *79*, 4994–4999.
- [14] L. S. Santos, *Reactive Intermediates: MS Investigations in Solution*, Wiley-VCH Verlag GmbH & Co. KGaA, Weinheim, **2009**.
- [15] J. P. McMullen, K. F. Jensen, *Annual Rev. Anal. Chem.* **2010**, *3*, 19–42.
- [16] J. H. Kim, A. R. Scialli, *Toxicol. Sci.* **2011**, *122*, 1–6.
- [17] B. Tóth, G. Horvai, in *Molecular Imprinting*, Springer-Verlag, Berlin Heidelberg, **2012**, pp. 267–306.
- [18] K. Polborn, K. Severin, *Chem. Eur. J.* **2000**, *6*, 4604–4611.
- [19] H. Zhang, T. Piacham, M. Drew, M. Patek, K. Mosbach, L. Ye, *J. Am. Chem. Soc.* **2006**, *128*, 4178–4179.
- [20] S. Nakai, H. Sunayama, Y. Kitayama, M. Nishijima, T. Wada, Y. Inoue, T. Takeuchi, *Langmuir* **2017**, *33*, 2103–2108.
- [21] G. Wulff, J. Vietmeier, *Macromol. Chem.* **1989**, *190*, 1727–1735.
- [22] B. Sellergren, K. J. Shea, *Tetrahedron: Asymmetry* **1994**, *5*, 1403–1406.
- [23] J. Svenson, N. Zheng, I. A. Nicholls, *J. Am. Chem. Soc.* **2004**, *126*, 8554–8560.
- [24] J. Hedin-Dahlström, S. Shoravi, S. Wikman, I. A. Nicholls, *Tetrahedron: Asymmetry* **2004**, *15*, 2431–2436.
- [25] J. V. Beach, K. J. Shea, *J. Am. Chem. Soc.* **1994**, *116*, 379–380.
- [26] J. Heilmann, W. F. Maier, *Angew. Chem., Int. Ed.* **1994**, *33*, 471–473.
- [27] G. Scotti, S. M. E. Nilsson, M. Haapala, P. Pöhö, G. Boije af Gennäs, J. Yli-Kauhaluoma, T. Kotiaho, *React. Chem. Eng.* **2017**, *2*, 299–303.
- [28] G. Scotti, S. M. E. Nilsson, V.-P. Matilainen, M. Haapala, G. Boije af Gennäs, J. Yli-Kauhaluoma, A. Salminen, T. Kotiaho, *Heliyon* **2019**, *5*, e02002.
- [29] S. M. E. Nilsson, H. Henschel, G. Scotti, M. Haapala, A. Kiriazis, G. Boije af Gennäs, T. Kotiaho, J. Yli-Kauhaluoma, *J. Org. Chem.* **2019**, *84*, 13975–13982.
- [30] E. Gal-Or, Y. Gershoni, G. Scotti, S. M. E. Nilsson, J. Saarinen, V. Jokinen, C. J. Strachan, G. Boije af Gennäs, J. Yli-Kauhaluoma, T. Kotiaho, *Anal. Methods* **2019**, *11*, 1802–1810.
- [31] J. S. Mathieson, M. H. Rosnes, V. Sans, P. J. Kitson, L. Cronin, *Beilstein J. Nanotechnol.* **2013**, *4*, 285–291.
- [32] K. C. Nicolaou, S. A. Snyder, T. Montagnon, G. Vassilikogiannakis, *Angew. Chem., Int. Ed.* **2002**, *41*, 1668–1698.
- [33] A. Whiting, C. M. Windsor, *Tetrahedron* **1998**, *54*, 6035–6050.
- [34] F. Liu, R. S. Paton, S. Kim, Y. Liang, K. N. Houk, *J. Am. Chem. Soc.* **2013**, *135*, 15642–15649.
- [35] Y. Nakagawa, K. Tayama, *Chem.-Biol. Interact.* **1998**, *116*, 45–60.

- [36] A. Kiriazis, R. L. Vahakoski, N. M. Santio, R. Arnaudova, S. K. Eerola, E.-M. Rainio, I. B. Aumüller, J. Yli-Kauhaluoma, P. J. Koskinen, *PLoS One* **2013**, *8*, e55409.
- [37] T. J. Trust, K. H. Bartlett, *Antimicrob. Agents Chemother.* **1975**, *8*, 381–383.
- [38] M. R. Barbachyn, D. S. Toops, D. A. Ulanowicz, K. C. Grega, S. J. Brickner, C. W. Ford, G. E. Zurenko, J. C. Hamel, R. D. Schaadt, D. Stapert, et al., *Bioorg. Med. Chem. Lett.* **1996**, *6*, 1003–1008.
- [39] M. J. Donlin, A. Zunica, A. Lipnicky, A. K. Garimallaprabhakaran, A. J. Berkowitz, A. Grigoryan, M. J. Meyers, J. E. Tavis, R. P. Murelli, *Antimicrob. Agents Chemother.* **2017**, *61*, e02574-16.
- [40] I. B. Aumüller, J. Yli-Kauhaluoma, *Org. Lett.* **2009**, *11*, 5363–5365.
- [41] T. Nissilä, N. Backman, M. Kolmonen, A. Leinonen, A. Kiriazis, J. Yli-Kauhaluoma, L. Sainiemi, R. Kostiaainen, S. Franssila, R. A. Ketola, *Int. J. Mass Spectrom.* **2012**, *310*, 65–71.
- [42] S. J. Brickner, M. R. Barbachyn, D. K. Hutchinson, P. R. Manninen, *J. Med. Chem.* **2008**, *51*, 1981–1990.
- [43] S. M. R. Hashemian, T. Farhadi, M. Ganjparvar, *Drug. Des., Devel. Ther.* **2018**, *12*, 1759–1767.
- [44] X. Wang, L. Yi, N. Mukhitov, A. M. Schrell, R. Dhumpa, M. G. Roper, *J. Chromatogr. A* **2015**, *0*, 98–116.
- [45] R. M. Bain, C. J. Pulliam, R. G. Cooks, *Chem. Sci.* **2014**, *6*, 397–401.
- [46] C. E. Falcone, Z. Jaman, M. Wleklinski, A. Koswara, D. H. Thompson, R. G. Cooks, *Analyst* **2017**, *142*, 2836–2845.
- [47] E. Y. Basova, F. Foret, *Analyst* **2014**, *140*, 22–38.
- [48] A. De Simone, M. Naldi, M. Bartolini, L. Davani, V. Andrisano, *Chromatographia* **2019**, *82*, 425–441.
- [49] J. Lee, S. A. Soper, K. K. Murray, *J. Mass Spectrom.* **2009**, *44*, 579–593.
- [50] F. T. G. van den Brink, W. Olthuis, A. van den Berg, M. Odijk, *TrAC, Trends Anal. Chem.* **2015**, *70*, 40–49.
- [51] S. Meyer, J. O. Metzger, *Anal. Bioanal. Chem.* **2003**, *377*, 1108–1114.
- [52] S. Meyer, R. Koch, J. O. Metzger, *Angew. Chem., Int. Ed.* **2003**, *42*, 4700–4703.
- [53] S. Fürmeier, J. O. Metzger, *J. Am. Chem. Soc.* **2004**, *126*, 14485–14492.
- [54] L. S. Santos, J. O. Metzger, *Angew. Chem., Int. Ed.* **2006**, *45*, 977–981.
- [55] C. Marquez, J. O. Metzger, *Chem. Commun.* **2006**, *0*, 1539–1541.
- [56] B. V. Silva, F. A. Violante, A. C. Pinto, L. S. Santos, *Rapid Commun. Mass Spectrom.* **2011**, *25*, 423–428.
- [57] D. L. Browne, S. Wright, B. J. Deadman, S. Dunnage, I. R. Baxendale, R. M. Turner, S. V. Ley, *Rapid Commun. Mass Spectrom.* **2012**, *26*, 1999–2010.
- [58] N. Holmes, G. R. Akien, R. J. D. Savage, C. Stanetty, I. R. Baxendale, A. J. Blacker, B. A. Taylor, R. L. Woodward, R. E. Meadows, R. A. Bourne, *React. Chem. Eng.* **2016**, *1*, 96–100.
- [59] J. Appun, M. Boomhoff, P. Hoffmeyer, I. Kallweit, M. Pahl, D. Belder, C. Schneider, *Angew. Chem., Int. Ed.* **2017**, *56*, 6758–6761.
- [60] M. Brivio, A. Liesener, R. E. Oosterbroek, W. Verboom, U. Karst, A. van den Berg, D. N. Reinhoudt, *Anal. Chem.* **2005**, *77*, 6852–6856.
- [61] J. J. Heiland, R. Warias, C. Lotter, L. Mauritz, P. J. W. Fuchs, S. Ohla, K. Zeitler, D. Belder, *Lab Chip* **2017**, *17*, 76–81.
- [62] J. W. Sam, X.-J. Tang, R. S. Magliozzo, J. Peisach, *J. Am. Chem. Soc.* **1995**, *117*, 1012–1018.
- [63] M. C. Mitchell, V. Spikmans, A. Manz, A. J. de Mello, *J. Chem. Soc., Perkin Trans. 1* **2001**, 514–518.
- [64] J. Brum, P. Dell’Orco, S. Lapka, K. Muske, J. Sisko, *Rapid Commun. Mass Spectrom.* **2001**, *15*, 1548–1553.
- [65] V. Spikmans, S. J. Lane, B. Leavens, A. Manz, N. W. Smith, *Rapid Commun. Mass Spectrom.* **2002**, *16*, 1377–1388.

- [66] M. Brivio, R. H. Fokkens, W. Verboom, D. N. Reinhoudt, N. R. Tas, M. Goedbloed, A. van den Berg, *Anal. Chem.* **2002**, *74*, 3972–3976.
- [67] M. Brivio, N. R. Tas, M. H. Goedbloed, H. J. G. E. Gardeniers, W. Verboom, A. van den Berg, D. N. Reinhoudt, *Lab Chip* **2005**, *5*, 378–381.
- [68] M. Brivio, R. E. Oosterbroek, W. Verboom, A. van den Berg, D. N. Reinhoudt, *Lab Chip* **2005**, *5*, 1111–1122.
- [69] L. S. Santos, J. O. Metzger, *Rapid Commun. Mass Spectrom.* **2008**, *22*, 898–904.
- [70] S. Fritzsche, S. Ohla, P. Glaser, D. S. Giera, M. Sickert, C. Schneider, D. Belder, *Angew. Chem., Int. Ed.* **2011**, *50*, 9467–9470.
- [71] Z.-X. Zhao, H.-Y. Wang, Y.-L. Guo, *J. Mass Spectrom.* **2011**, *46*, 856–858.
- [72] A. E. Kirby, A. R. Wheeler, *Lab Chip* **2013**, *13*, 2533–2540.
- [73] J. J. Haven, J. Vandenberg, T. Junkers, *Chem. Commun.* **2015**, *51*, 4611–4614.
- [74] C. Benz, M. Boomhoff, J. Appun, C. Schneider, D. Belder, *Angew. Chem., Int. Ed.* **2015**, *54*, 2766–2770.
- [75] C. Dietze, S. Schulze, S. Ohla, K. Gilmore, P. H. Seeberger, D. Belder, *Analyst* **2016**, *141*, 5412–5416.
- [76] C. Lotter, E. Poehler, J. J. Heiland, L. Mauritz, D. Belder, *Lab Chip* **2016**, *16*, 4648–4652.
- [77] R. J. Beulig, R. Warias, J. J. Heiland, S. Ohla, K. Zeitler, D. Belder, *Lab Chip* **2017**, *17*, 1996–2002.
- [78] R. Warias, A. Zaghi, J. J. Heiland, S. K. Piendl, K. Gilmore, P. H. Seeberger, A. Massi, D. Belder, *ChemCatChem* **2018**, *10*, 5382–5385.
- [79] M. Pahl, M. Mayer, M. Schneider, D. Belder, K. R. Asmis, *Anal. Chem.* **2019**, *91*, 3199–3203.
- [80] M. Dole, L. L. Mack, R. L. Hines, R. C. Mobley, L. D. Ferguson, M. B. Alice, *J. Chem. Phys.* **1968**, *49*, 2240–2249.
- [81] J. V. Iribarne, B. A. Thomson, *J. Chem. Phys.* **1976**, *64*, 2287–2294.
- [82] J. A. Syage, S.-S. Cai, L. C. Short, *LCGC North America* **2008**, *26*, 286–296.
- [83] M. Wilm, *Mol. Cell. Proteomics* **2011**, *10*, M111.009407.
- [84] S. Banerjee, S. Mazumdar, *Int. J. Anal. Chem.* **2012**, DOI 10.1155/2012/282574.
- [85] M. N. Eberlin, *Eur. J. Mass Spectrom.* **2007**, *13*, 19–28.
- [86] E. de Hoffmann, V. Stroobant, in *Mass Spectrometry - Principles and Applications*, John Wiley & Sons, Incorporated, Chichester, **2007**, pp. 224–226.
- [87] M. Wilm, M. Mann, *Anal. Chem.* **1996**, *68*, 1–8.
- [88] A. El-Faramawy, K. W. M. Siu, B. A. Thomson, *J. Am. Soc. Mass Spectrom.* **2005**, *16*, 1702–1707.
- [89] A. E. Kirby, M. J. Jebrail, H. Yang, A. R. Wheeler, *Rapid Commun. Mass Spectrom.* **2010**, *24*, 3425–3431.
- [90] A. Schmidt, M. Karas, T. Dülcks, *J. Am. Soc. Mass Spectrom.* **2003**, *14*, 492–500.
- [91] T. M. Annesley, *Clin. Chem.* **2003**, *49*, 1041–1044.
- [92] E. de Hoffmann, V. Stroobant, in *Mass Spectrometry - Principles and Applications*, John Wiley & Sons, Incorporated, Chichester, **2007**, p. 54.
- [93] A. Kiontke, A. Oliveira-Birkmeier, A. Opitz, C. Birkemeyer, *PLoS One* **2016**, *11*, e0167502.
- [94] K. Morand, G. Talbo, M. Mann, *Rapid Commun. Mass Spectrom.* **1993**, *7*, 738–743.
- [95] M. Chen, K. D. Cook, *Anal. Chem.* **2007**, *79*, 2031–2036.
- [96] G. J. Van Berkel, V. Kertesz, *Anal. Chem.* **2007**, *79*, 5510–5520.
- [97] S. P. Pasilis, V. Kertesz, G. J. Van Berkel, *Anal. Chem.* **2008**, *80*, 1208–1214.
- [98] Y. Chai, H. Sun, J. Wan, Y. Pan, C. Sun, *Analyst* **2011**, *136*, 4667–4669.
- [99] H. Oberacher, F. Pitterl, R. Erb, S. Plattner, *Mass Spectrom. Rev.* **2015**, *34*, 64–92.
- [100] W. Koch, M. C. Holthausen, in *A Chemist's Guide to Density Functional Theory*, Wiley-VCH Verlag GmbH & Co. KGaA, Weinheim, **2001**, p. 31.
- [101] P. Hohenberg, W. Kohn, *Phys. Rev.* **1964**, *136*, B864–B871.

- [102] R. F. W. Bader, *Atoms in Molecules: A Quantum Theory*, Clarendon Press, Oxford, **1990**.
- [103] E. C. Meurer, H. Chen, L. S. Riter, R. G. Cooks, M. N. Eberlin, *J. Am. Soc. Mass Spectrom.* **2004**, *15*, 398–405.
- [104] R. G. Cooks, H. Chen, M. N. Eberlin, X. Zheng, A. Tao, *Chem. Rev.* **2006**, *106*, 188–211.
- [105] R. O. M. A. de Souza, E. T. da Penha, H. M. S. Milagre, S. J. Garden, P. M. Esteves, M. N. Eberlin, O. A. Antunes, *Chem. Eur. J.* **2009**, *15*, 9799–9804.
- [106] G. W. Amarante, M. Benassi, H. M. S. Milagre, A. A. C. Braga, F. Maseras, M. N. Eberlin, F. Coelho, *Angew. Chem., Int. Ed.* **2009**, *15*, 12460–12469.
- [107] T. S. Rodrigues, V. H. C. Silva, P. M. Lalli, H. C. B. de Oliveira, W. A. da Silva, F. Coelho, M. N. Eberlin, B. A. D. Neto, *J. Org. Chem.* **2014**, *79*, 5239–5248.
- [108] L. Dalla-Vechia, V. G. Santos, M. N. Godoi, D. Cantillo, C. O. Kappe, M. N. Eberlin, R. O. M. A. de Souza, L. S. M. Miranda, *Org. Biomol. Chem.* **2012**, *10*, 9013–9020.
- [109] V. M. Williams, J. R. Kong, B. J. Ko, Y. Mantri, J. S. Brodbelt, M.-H. Baik, M. J. Krische, *J. Am. Chem. Soc.* **2009**, *131*, 16054–16062.
- [110] U. Gellrich, A. Meißner, A. Steffani, M. Kähny, H.-J. Drexler, D. Heller, D. A. Plattner, B. Breit, *J. Am. Chem. Soc.* **2014**, *136*, 1097–1104.
- [111] G. A. Medeiros, W. A. da Silva, G. A. Bataglioni, D. A. C. Ferreira, H. C. B. de Oliveira, M. N. Eberlin, B. A. D. Neto, *Chem. Commun.* **2014**, *50*, 338–340.
- [112] H. G. O. Alvim, G. A. Bataglioni, L. M. Ramos, A. L. de Oliveira, H. C. B. de Oliveira, M. N. Eberlin, J. L. de Macedo, W. A. da Silva, B. A. D. Neto, *Tetrahedron* **2014**, *70*, 3306–3313.
- [113] X.-F. Wu, P. Anbarasan, H. Neumann, M. Beller, *Angew. Chem., Int. Ed.* **2010**, *49*, 9047–9050.
- [114] T. A. Fernandes, B. G. Vaz, A. J. M. da Silva, P. M. Esteves, M. N. Eberlin, P. R. R. Costa, *J. Braz. Chem. Soc.* **2013**, *24*, 500–506.
- [115] J. Rydfjord, F. Svensson, A. Trejos, P. J. R. Sjöberg, C. Sköld, J. Sävmarker, L. R. Odell, M. Larhed, *Chem. Eur. J.* **2013**, *19*, 13803–13810.
- [116] B. Skillinghaug, C. Sköld, J. Rydfjord, F. Svensson, M. Behrends, J. Sävmarker, P. J. R. Sjöberg, M. Larhed, *J. Org. Chem.* **2014**, *79*, 12018–12032.
- [117] M. R. dos Santos, R. Coriolano, M. N. Godoi, A. L. Monteiro, H. C. B. de Oliveira, M. N. Eberlin, B. A. D. Neto, *New J. Chem.* **2014**, *38*, 2958–2963.
- [118] M. N. Godoi, F. de Azambuja, P. D. G. Martinez, N. H. Morgon, V. G. Santos, T. Regiani, D. Lesage, H. Dossmann, R. B. Cole, M. N. Eberlin, et al., *Eur. J. Org. Chem.* **2017**, *2017*, 1794–1803.
- [119] M. J. Whitcombe, N. Kirsch, I. A. Nicholls, *J. Mol. Recognit.* **2014**, *27*, 297–401.
- [120] G. Vasapollo, R. D. Sole, L. Mergola, M. R. Lazzoi, A. Scardino, S. Scorrano, G. Mele, *Int. J. Mol. Sci.* **2011**, *12*, 5908–5945.
- [121] S. Muratsugu, M. Tada, in *Handbook of Molecularly Imprinted Polymers*, Smithers Rapra, Shropshire, **2013**, p. 246.
- [122] L. Chen, X. Wang, W. Lu, X. Wu, J. Li, *Chem. Soc. Rev.* **2016**, *45*, 2137–2211.
- [123] D. A. Spivak, *Adv. Drug Delivery Rev.* **2005**, *57*, 1779–1794.
- [124] G. K. E. Scriba, *Chromatographia* **2012**, *75*, 815–838.
- [125] S. Emir Diltemiz, R. Keçili, A. Ersöz, R. Say, *Sensors* **2017**, *17*, 454.
- [126] M. Pohanka, *Materials* **2018**, *11*, 448.
- [127] G. Sauerbrey, *Z. Physik* **1959**, *155*, 206–222.
- [128] D. I. Walsh, D. S. Kong, S. K. Murthy, P. A. Carr, *Trends Biotechnol.* **2017**, *35*, 383–392.
- [129] S. Waheed, J. M. Cabot, N. P. Macdonald, T. Lewis, R. M. Guijt, B. Paull, M. C. Breadmore, *Lab Chip* **2016**, *16*, 1993–2013.
- [130] L. Froyen, J. p. Kruth, T. Laoui, X. Wang, *Assembly Autom.* **2003**, *23*, 357–371.
- [131] H. Schleifenbaum, W. Meiners, K. Wissenbach, C. Hinke, *CIRP J. Manuf. Sci. Tech.* **2010**, *2*, 161–169.

- [132] G. Scotti, V. Matilainen, P. Kanninen, H. Piili, A. Salminen, T. Kallio, S. Franssila, *J. Power Sources* **2014**, *272*, 356–361.
- [133] W. J. Sames, F. A. List, S. Pannala, R. R. Dehoff, S. S. Babu, *Int. Mat. Rev.* **2016**, *61*, 315–360.
- [134] A. Bracha, E. Gal-Or, *WIPO, PCT/IB2018/051178 (WO 2018/163006 A1)*, **2018**.
- [135] A. Bracha, E. Gal-Or, *WIPO; PCT/IB2018/051179 (WO 2018/163007 A1)*, **2018**.
- [136] A. Bracha, E. Gal-Or, *WIPO, PCT/IB2018/051181 (WO 2018/163008 A1)*, **2018**.
- [137] M. J. Frisch, G. W. Trucks, H. B. Schlegel, G. E. Scuseria, A. Robb, J. R. Cheeseman, G. Scalmani, V. Barone, B. Mennucci, G. A. Peterson, et al., *Gaussian 09*, Gaussian, Inc., Wallingford CT, USA, **2009**.
- [138] Y. Zhao, D. G. Truhlar, *Theor. Chem. Acc.* **2008**, *120*, 215–241.
- [139] R. Krishnan, J. S. Binkley, R. Seeger, J. A. Pople, *J. Chem. Phys.* **1980**, *72*, 650–654.
- [140] T. Clark, J. Chandrasekhar, G. W. Spitznagel, P. V. R. Schleyer, *J. Comput. Chem.* **1983**, *4*, 294–301.
- [141] Y. Zhao, D. G. Truhlar, *Chem. Phys. Lett.* **2011**, *502*, 1–13.
- [142] Peverati Roberto, Truhlar Donald G., *Philos. Trans. R. Soc., A* **2014**, *372*, 20120476.
- [143] I. B. Aumüller, J. Yli-Kauhaluoma, *Theor. Chem. Acc.* **2010**, *126*, 55–73.
- [144] I. B. Aumüller, J. Yli-Kauhaluoma, *Comput. Theor. Chem.* **2011**, *964*, 40–48.
- [145] P. R. Andrews, M. Iskander, G. P. Jones, D. A. Winkler, *Eur. J. Med. Chem.* **1988**, *23*, 125–132.
- [146] G. A. Schultz, T. N. Corso, S. J. Prosser, S. Zhang, *Anal. Chem.* **2000**, *72*, 4058–4063.
- [147] I. A. Yaremenko, V. A. Vil', D. V. Demchuk, A. O. Terent'ev, *Beilstein J. Org. Chem.* **2016**, *12*, 1647–1748.
- [148] R. N. Tiwari, C. G. Bonde, *J. Liq. Chromatogr. Relat. Technol.* **2012**, *35*, 188–203.
- [149] D. Pranzo, P. Larizza, D. Filippini, G. Percoco, *Micromachines* **2018**, *9*, 374.
- [150] G. IJ. Salentijn, P. E. Oomen, M. Grajewski, E. Verpoorte, *Anal. Chem.* **2017**, *89*, 7053–7061.
- [151] N. Riboni, L. Magrini, F. Bianchi, M. Careri, A. Cappiello, *Anal. Chim. Acta* **2017**, *978*, 35–41.
- [152] G. Scotti, P. Kanninen, V.-P. Matilainen, A. Salminen, T. Kallio, *Energy* **2016**, *106*, 475–481.
- [153] S. M. E. Nilsson, S. Suriyanarayanan, S. Kathiravan, J. Yli-Kauhaluoma, T. Kotiaho, I. A. Nicholls, *RSC Adv.* **2019**, *9*, 33653–33656.
- [154] A. Bonyár, H. Sántha, B. Ring, M. Varga, J. Gábor Kovács, G. Harsányi, *Procedia Eng.* **2010**, *5*, 291–294.
- [155] D. S. Thomas, S. W. Gilbert, *Special Publication (NIST SP) - 1176* **2014**.
- [156] T. E. Angel, U. K. Aryal, S. M. Hengel, E. S. Baker, R. T. Kelly, E. W. Robinson, R. D. Smith, *Chem. Soc. Rev.* **2012**, *41*, 3912–3928.
- [157] A. Furey, M. Moriarty, V. Bane, B. Kinsella, M. Lehane, *Talanta* **2013**, *115*, 104–122.
- [158] R. King, R. Bonfiglio, C. Fernandez-Metzler, C. Miller-Stein, T. Olah, *J. Am. Soc. Spectrom.* **2000**, *11*, 942–950.
- [159] A. Cornish-Bowden, in *Fundamentals of Enzyme Kinetics*, Wiley-VCH Verlag GmbH & Co. KGaA, Berlin Heidelberg, **2012**, pp. 189–226.
- [160] S. Suriyanarayanan, L. Petrone, T. Ederth, I. A. Nicholls, *Chem. Commun.* **2013**, *49*, 5274–5276.

